Hybrid and nonlinear control of power converters

Aya Alawieh

UNIVERSITÉ PARIS SUD

Comprendre le monde, construire l'avenir®

L2S

UNIVERSITÉ PARIS-SUD

ÉCOLE DOCTORALE : Sciences et Technologies de l'Information des Télécommunications et des Systèmes (STITS)

Laboratoire de Signaux et Systèmes (L2S)

DISCIPLINE : Physique

THÈSE DE DOCTORAT

soutenue le 26/09/2012

par

Aya ALAWIEH

Hybrid and Nonlinear Control of Power Converters

Directeur de thèse :	Romeo ORTEGA	Directeur de recherche CNRS, L2S
Co-directeur de thèse :	Francoise.LAMNABHI -LAGARRIGUE	Directeur de recherche CNRS, L2S

Composition du jury :

Président du jury :	Emmanuel GODOY	Professeur, SUPELEC
Rapporteurs :	Eduardo MENDES	Professeur, INP Grenoble
	Robert GRINO	Professeur, Universitat Politècnica de Catalunya UPC
Examinateurs :	Abdelkrim BENCHAIB	Professeur associé, CNAM

Thèse préparée au :

Laboratoire des signaux et systèmes (L2S)

Ecole supérieur d'électricité (Supélec)

3 rue Joliot Curie, 91 190 Gif sur Yvette, France

Contents

Acknowlegments

I would like to express my sincere gratitude to my thesis advisor Romeo Ortega, for giving me the opportunity to develop this research subject. His wide knowledge and experience have been of great value for me. His encouraging and personal guidance have provided a good background for the present thesis.

I also want to thank my co-supervisor Francoise Lamnabhi-lagarrigue, for her help during my work in L2S.

Many thanks to the professor Roberto Grino at Universitat Politecnica Catalunya, and the professor Eduardo Mendes at INP Grenoble, for accepting to review my work as well as for participating in my jury committee. Their constructive suggestions on the thesis are really appreciated for me. I am grateful that they accepted these tasks.

I am also grateful the professor Emmanuel Godoy at Supélec, the doctor Abdelkrim Benchaib at CNAM Paris for their commitment to take part in my jury committee.

I will be always grateful of all my laboratory partners for the good moments that we shared.

My warm thanks to my family who have always supported and helped me in life.

Publications

- *Journal Papers*

  -Aya Alawieh, Harish Pillai, Romeo Ortega, Alessandro Astolfi, Eric Berthelot, "A simple robust feedback controller for voltage regulation of a boost converter in discontinuous conduction mode", submited to Control System Magazine CSM.

  -Ali Jaafar, Aya Alawieh, Romeo Ortega, Emanuel Godoy, Pierre Lefranc, "PI Stabilization of Power Converters with Partial State Measurements", IEEE Trans. Control Systems Technology, Volume: PP, Issue: 99, Page(s): 1-9.

- *Conference Papers*

  -Aya Alawieh, Harish Pillai, Romeo Ortega, Alessandro Astolfi and Eric Berthelot, "Adaptive Control of the Boost Converter in Discontinuous Conduction Mode", IFAC World Congress 2011, pp: 3310-3315, Milano, Italy.

  -Aya Alawieh, Ali Jaafar, Romeo Ortega, Emanuel Godoy, Pierre Lefranc, "Observer-Based Passive PI Stabilization of Power Converters", ACC American Control Conference 2012, pp:1448-1453, Montréal, Canada.

  -Aya Alawieh, Romeo Ortega, "Adaptive Control of the Buck-boost Converter in Discontinuous Conduction Mode", accepted at CLCA, 15th Latinamerican Control Conference 2012, Lima, Peru.

Résumé Détaillé

Introduction

Les systèmes électroniques commutés sont de plus en plus utilisés dans plusieurs domaines domestiques ou industriels: les écrans à cristaux liquides, les appareils électroménagers, l'éclairage, les ordinateurs personnels, les centrales électriques, les véhicules de transport et ainsi de suite. L'efficacité des opérations de toutes les applications dépend du travail essentiel réalisé par des systèmes électroniques à commutation, dont le comportement est déterminé par une interconnexion et un contrôle appropriés des dispositifs analogiques et numériques.

De point de vue technique, la plupart des systèmes électroniques commutés peuvent être classés comme convertisseurs de puissance. Ces systèmes peuvent être considérés comme des réseaux composés de commutateurs à semi-conducteurs, par exemple, thyristors, transistors et des diodes, ainsi que des éléments passifs, par exemple, des condensateurs, des inductances et des résistances, et des sources de courant-tension.

La classification la plus fréquente de systèmes de conversion de puissance est basée sur la forme d'onde des signaux d'entrée et de sortie, si elles sont en courant alternatif (AC) ou à courant continu (DC). Selon le caractère de la source d'entrée, ils peuvent être convertisseurs à source de tension ou convertisseurs à source de courant. En outre, les convertisseurs peuvent être de faible, moyen ou haut niveau de tension et/ou de courant.

Les systèmes à commutation jouent un rôle fondamental dans tous les environnements où la régulation, le contrôle et la conversion de l'énergie électrique est une question clé. Ces dernières années, des contraintes d'efficacité de et de qualité plus exigeantes sont imposées sur l'énergie électrique dans des applications telles que les systèmes de puissance, les véhicules de transport. Ce qui a déterminé un intérêt de nouvelles recherches dans l'étude des approches formelles pour l'analyse, la conception et le contrôle des convertisseurs de puissance. Dans ce contexte, l'analyse, la conception et le contrôle des systèmes électroniques commuté est une question clé, et l'utilisation d'outils mathématiques avancés peut être une approche efficace pour lutter contre les exigences croissantes de performance et d'efficacité.

Comme motivation de ce travail, nous considérons les convertisseurs DC-DC de puissance, en raison de leurs large gamme d'applicabilité, et leurs présence dans tous les types

de circuits électroniques, soit dans les applications industrielles (systèmes d'alimentation d'engins spatiaux, les matériels de télécommunication) ou les applications personnelles (PC, matériel de bureau, appareils électriques), et avec une gamme de puissance de quelques milliwatts, pour le téléphone portable par exemple, à des mégawatts, pour les systèmes électriques de transmission de puissance.

Le problème de la modélisation et le contrôle de ces systèmes d'électronique de puissance, c'est qu'ils ont des topologies de circuit qui intègrent des éléments en temps continu, comme des résistances, des inductances, condensateurs, et de sources de tension et de courant qui sont interfacés avec des appareils électroniques tels que les diodes et les commutateurs électroniques tels que des thyristors, des transistors MOSFET. Cela conduit à des types de systèmes hybrides qui impliquent un comportement d'un système en temps continu mélangé avec un comportement de commutation logique à temps discret. Les systèmes de contrôle traditionnels a été basée sur des modèles moyennés où l'action des commutateurs sont assimilés à des signaux continus allant dans un certain interval fermé,$[0, 1]$, en négligeant la présence d'ondulations.

Une littérature récente sur les systèmes hybrides est apparue dans la communauté de contrôle dans les dernières années [25]. Comme d'habitude dans la théorie du contrôle, l'objectif principal de la recherche s'est orientée vers le développement de méthodologies générales, surtout pour l'analyse [22] mais aussi pour la conception du contrôleur, des classes de systèmes dynamiques hybrides a motivation théorique. Pour cela, il est un vraiment besoin de développer un contrôle hybride et l'objectif de contrôle ne sera pas la stabilisation d'un point d'équilibre, mais la génération d'une orbite périodique autour d'un point de fonctionnement désiré.

Motivé par ce fait, dans la première partie de la thèse une perspective différente a été adoptée, c'est le développement d'une solution pour des exemples pratiques. Nous allons considérer un convertisseur de type boost et un convertisseur buck-boost en mode d'operation discontinue DCM, et notre principale contribution sera un algorithme de contrôle simple et robuste.

Négliger la présence des ondulations permet de reformuler le problème de regulation du convertisseur comme un problème d'équilibre classique pour qui, des techniques nonlinéaires de conception des contrôleurs, par exemple, mode de glissement et de la passivité sont directement applicables.

Développer le contrôle des systèmes non linéaires, qui intègre à un niveau fondamental la structure des systèmes physiques et fournit des solutions à des problèmes pratiques d'ingénierie, a été la motivation de plusieurs ouvrages. Une contribution principale dans ce domaine a été l'identification d'une grande classe de convertisseurs qui peuvent être stabilisées par l'intermédiaire de la régulation adaptative PI. Une procédure de concevoir

des contrôleurs linéaires proportionnel et intégral assurant la stabilité asymptotique globale pour les convertisseurs de puissance a été proposé dans [39]. La construction nécessite la mesure de l'état complet du système, qui est souvent indisponible dans la pratique.

L'objectif principal de la deuxième partie sera de montrer que l'approche I&I de [37] peut être utilisé pour concevoir un observateur asymptotiquement convergent d'ordre réduit pour une classe bien définie de convertisseurs de puissance, qui est caractérisé par une simple inégalité matricielle linéaire (LMI). Par ailleurs, nous allons prouver que l'observateur I&I peut être combiné avec le contrôleur PI en préservant les propriétés de la stabilité asymptotique globale de la boucle. La nouvelle commande est appliquée à réguler la tension du convertisseur SEPIC.

Dans ce resumé, nous allons presenter les contributions principales de la thèse:

Dans la première partie nous intéressons au problème de la régulation de la tension des convertisseurs de puissance fonctionnant dans le mode de conduction discontinue. Deux convertisseurs de puissance sont considérés: le convertisseur boost et le convertisseur buck-boost. L'objectif de commande est la génération d'une orbite périodique. Notre principale contribution est un algorithme simple et robuste qui donne des formules explicites pour les temps de commutation sans approximations. Les résultats de simulation et expérimentales qui illustrent la robustesse du système à l'incertitude des paramètres, ainsi que des comparaisons de performance avec la pratique actuelle, sont présentés.

Dans la deuxième partie une classe de convertisseurs de puissance qui peut être globalement stabilisé avec un contrôleur PI a été identifié. Par ailleurs, nous allons prouver que l'observateur I&I peut être combiné avec le contrôleur PI tout en préservant les propriétés de stabilité asymptotique globale de la boucle fermé. La classe se caractérise par une inégalité matricielle linéaire simple. Le nouveau controleur est illustré avec le convertisseur très - populaire, et difficile à controler, le SEPIC, pour lequel les résultats expérimentaux sont présentés.

Commande Hybride Robuste des Convertisseurs de Puissance DC-DC en Mode de Conduction Discontinue

Les interrupteurs idéals dans les convertisseurs de puissance sont généralement mis en oeuvre en utilisant des dispositifs semi-conducteurs unidirectionnels qui peuvent conduire à une nouveau mode de fonctionnement générique appelé *mode de conduction discontinu* (DCM). Ce mode survient lorsque l'ondulation est suffisamment grande pour provoquer la polarité du signal (courant ou tension) appliquée à l'interrupteur à inverser, en violant les hypothèses de l'irréversibilité formulées dans la réalisation de l'interrupteur. Dans les topologies de convertisseur classique le mode discontinu apparaît très souvent pour une faible charge [24].

La dynamique du convertisseur est significativement altérée dans le mode de conduction discontinu. Les techniques existantes pour l'analyse et la conception du contrôleur, notamment, les approximations de la dynamique moyenne (valable pour les commutations rapides) ou pour les petites ondulations, ne sont plus valables. Avec les approximations derniers le convertisseur peut être traité comme un système continu (éventuellement non linéaire), avec l'action des commutateurs assimilé à des signaux continus allant dans un certain interval fermé, $[0, 1]$. Négliger la présence des ondulations permet de reformuler le problème de régulation comme un problème de stabilisation classique pour lequel, plusieurs techniques non-linéaires de conception des contrôleurs, par exemple, modes glissants [29] - [33] et à base de la passivité [34] - [36], sont directement applicables. Dans la plupart de ces littératures que le mode de fonctionnement continu CCM est considéré. Une méthode de calcul des instants de temps de commutation sur la base d'énergie du convertisseur boost en fonctionnement DCM, où les ondulations sont considérés a été proposé dans [28]. Dans cette stratégie, les instants de commutation sont choisis de sorte que le changement d'énergie totale est égale à zéro. Les calculs nécessaires ne sont pas simples dans cette stratégie, et seul les résultats de simulation sont présentés.

Le convertisseur donc est un système de hybride, qui présente des comportements des systèmes à temps continu et à temps discret en meme temps. Les signes distinctifs seront comme suit:

(i) Le contrôle n'est pas un signal continu, mais directement les positions des commutateurs, qui prennent des valeurs binaires $\{0, 1\}$, et décide la commutation entre les différentes topologies du convertisseur.

(ii) En raison de considérations technologiques, l'activation des interrupteurs est soumis à un temps minimum qui doit être pris en compte.

(iii) En plus des commutations induites par les positions de commutation, il y aura les commutations forcées en raison de la violation de l'hypothèse de l'unidirectionnalité.

(iv) Comme l'ondulation ne peut être négligé, l'objectif de contrôle n'est pas la stabilisation d'un point d'équilibre, mais la génération d'une orbite périodique ("avec une amplitude minimale") autour du point de fonctionnement souhaité.

Une littérature récente sur les systèmes hybrides est apparue dans la communauté de contrôle dans les dernières années [25]. Comme d'habitude dans la théorie du contrôle, l'objectif principal de la recherche s'est orientée vers le développement de méthodologies générales, surtout pour l'analyse [22] mais aussi pour la conception du contrôleur, des classes de systèmes dynamiques hybrides à motivation théorique. Pour cela une perspective différente a été adoptée, c'est le développement d'une solution pour des exemples

pratiques. Nous allons considérer un convertisseur de type boost et un convertisseur buck-boost en mode d'operation discontinu DCM. La formulation du problème sera présenté dans la section suivante.

Modèle et formulation du problème

Deux types de convertisseurs de puissance sont considerés: le convertisseur boost et le convertisseur buck-boost donnés dans les Figs. 1.4(b), et 1.4(c).

Les circuits pour les trois topologies correspondants aux trois modes d'opération sont décrits dans les Figs. 2.1, et 2.2. Ces modes depend de la position de l'interrupteur et de la conduction de la diode diode comme décrit ci-dessous. Les états sont le courant de l'inductance x_1 et la tension du condensateur x_2. La dynamique dans les deux cas sont décrits par le modèle:

$$\dot{x} = A_i x + b_i v_{in},\ i = 1, 2, 3,$$

ou le paire (A_i, b_i) constitut la matrice du système et la matrice d'entrée, i=1,2,3 représente le mode de fonctionnement.

Dans le cas du convertisseur boost: Les paires (A_i, b_i) pour les trois topologies sont

$$\begin{aligned}
\Omega_1: \quad & A_1 = \begin{bmatrix} \frac{-r_L}{L} & \frac{-1}{L} \\ \frac{1}{C} & \frac{-1}{CR_0} \end{bmatrix},\ b_1 = \begin{bmatrix} \frac{1}{L} \\ 0 \end{bmatrix} \\
\Omega_2: \quad & A_2 = \begin{bmatrix} 0 & 0 \\ 0 & \frac{-1}{CR_0} \end{bmatrix},\ b_2 = \begin{bmatrix} 0 \\ 0 \end{bmatrix} \\
\Omega_3: \quad & A_3 = \begin{bmatrix} \frac{-r_L}{L} & 0 \\ 0 & \frac{-1}{CR_0} \end{bmatrix},\ b_3 = \begin{bmatrix} \frac{1}{L} \\ 0 \end{bmatrix}.
\end{aligned}$$

Dans la topologie Ω_3, lorsque l'interrupteur est ON, la batterie externe $v_{in} \in \mathbb{R}_+$ fournit de l'énergie magnétique a l'inductance L, tandis que l'énergie électrique du condensateur C est déchargé dans la charge, représentée ici par une résistance R_0. Lorsque l'interrupteur est OFF et la diode est ON le circuit prend la topologie Ω_1, alors l'énergie se transfert de l'inducteur au condensateur, assurant la construction de sa tension de x_2 et la réalisation de l'amplification souhaitée. La topologie Ω_2 représente le mode de conduction discontinu.

Dans le cas du convertisseur buck-boost: Les paires (A_i, b_i) pour les trois topologies sont

$$\begin{aligned}
\Omega_1: \quad & A_1 = \begin{bmatrix} \frac{-r_L}{L} & \frac{-1}{L} \\ \frac{1}{C} & \frac{-1}{CR_0} \end{bmatrix},\ b_1 = \begin{bmatrix} 0 \\ 0 \end{bmatrix} \\
\Omega_2: \quad & A_2 = \begin{bmatrix} 0 & 0 \\ 0 & \frac{-1}{CR_0} \end{bmatrix},\ b_2 = \begin{bmatrix} 0 \\ 0 \end{bmatrix} \\
\Omega_3: \quad & A_3 = \begin{bmatrix} \frac{-r_L}{L} & 0 \\ 0 & \frac{-1}{CR_0} \end{bmatrix},\ b_3 = \begin{bmatrix} \frac{1}{L} \\ 0 \end{bmatrix}.
\end{aligned}$$

Pour le convertisseur buckboost Fig.2.2, l'inductance gagne de l'énergie dans la topologie Ω_3 et le condensateur perd son énergie dans les topologies Ω_3 et Ω_2. Dans la topologie Ω_1 l'inductance fournit de l'énergie au condensateur.

Les deux systèmes évoluent dans l'ensemble $\{x_1 > 0, x_2 > 0\} =: \mathbb{R}^2_+$ pour les topologies Ω_1 et Ω_3, tandis que pour la topologie Ω_2, les trajectoires sont limitées à l'ensemble $\{x_1 = 0, x_2 > 0\}$. Une trajectoire typique dans le plan de phase $x_1 - x_2$ est montrée dans la figure Fig. 2.3, où $t_i \in \mathbb{R}_+$, $i = 1, 2, 3$, représente le temps pendant chacune des topologies.

En raison de considérations technologiques, un minimum de temps (dwell time), $t_D \in \mathbb{R}_+$, est imposé à l'interrupteur. Si t_D est grand, par rapport à la constante de temps R_0C, le courant x_1 devient nul et une transition forcée de Ω_1 à Ω_2 est induite. D'autre part, les transitions de Ω_2 à Ω_3 et de Ω_3 à Ω_1, déterminées par la position de l'interrupteur, sont décidées par le contrôleur. Bien sûr, ces temps de transition de commutation doivent respecter la contrainte de temps minimale.

Compte tenu de t_1 — le temps qu'il faut pour le courant pour passer à zéro — le concepteur doit décider les temps de commutation t_2 et t_3, qui devraient satisfaire la contrainte sur le temps

$$t_3 \geq t_D, \quad t_1 + t_2 \geq t_D.$$

L'objectif du contrôle est de générer un cycle limite attractif (de période $t_1 + t_2 + t_3$) contenu dans la bande

$$x_2(t) \in [x_2^* - \epsilon_1, x_2^* + \epsilon_2],$$

où $x_2^* \in \mathbb{R}_+$ est la valeur moyenne souhaitée pour x_2 et — pour réduire au minimum l'ondulation de la tension — les constantes $\epsilon_i \in \mathbb{R}_+$ sont aussi petits que possible. Bien que la gamme des valeurs de $x_1(t)$ n'est pas la principale préoccupation, pour des raisons pratiques, ce courant est également limité à une borne supérieure $x_1(t) \leq x_1^M$.

Algorithme de commande

Les calculs dans la section 2.3 conduisent à l'algorithme de contrôle suivant:
Step 1. Fixer un point $(x_1^0, x_2^0) \in \mathbb{R}^2_+$, tel que t_3 donné par:

$$t_3 = -\frac{L}{r_L} \ln \left(1 - \frac{r_L x_1^0}{v_{in}}\right).$$

vérifie $t_3 \geq t_D$ et $x_2^0 < x_2^*$.
Step 2. A l'instant $t_0 \geq 0$ quand $x(t_0) = (x_1^0, x_2^0)$ activer le passage de $u = 0$ à $u = 1$.
Step 3. Attendre (en mode Ω_1) jusqu'à $x_1(t) = 0$ et mesurer x_2^1 correspondant.
Step 4. Calculer $t_2 + t_3$. Si $t_2 > 0$ aller à l'étape 5, sinon definir $t_2 := t_D - t_1$, puis passer à l'étape 5.
Step 5. Attendre (en mode Ω_2) pour un temps t_2 et activer le passage de $u = 1$ a $u = 0$.

Step 6. Attendre (en mode Ω_3) pour un temps t_3 et mesurer l'état, soit (x_1^0, x_2^0). Vérifier si, pour la nouvelle valeur (x_1^0, x_2^0), $t_3 \geq t_D$ et $x_2^0 < x_2^*$. Si oui, aller à l'étape 2, sinon attendre pour un temps plus long jusqu'à ce que l'état est conforme aux contraintes, puis attribuer la nouvelle valeur t_3 et passer à l'étape 2.

Comme indiqué dans l'introduction, en fonctionnement normal, le circuit fonctionne dans le DCM, d'où à l'étape 3 $t_2 > 0$. En outre, il est clair que, dans des conditions idéales, lorsque les paramètres sont exactement connues et il n'ya pas de perturbations, le point de (x_1^0, x_2^0) obtenu à l'étape 6 coïncide avec le point initial. Toutefois, en pratique il y aura un écart, d'où la nécessité de recalculer les temps de commutation en fonction des mesures.

Cet algorithme peut être robustifié vis à vis les incertitudes dans les constantes de temps. Ce calcul est presenté dans la section 2.4

L'utilité du système de contrôle proposé a été évaluée par des simulations numériques et des éxperimentations. Les résultats sont présentés respectivement dans les sections: 2.5 et 2.6.

Stabilisation des Convertisseurs de Puissance par PI avec des Mesures Partielles de l'État

Les controleurs se basant sur la passivité ont été très efficaces pour les convertisseurs de puissance. Mais, pour générer la sortie pourlaquelle la passivité incrémentielle est établie [39], la mesure complète de l'état est généralement requise. Pour des raisons économiques et technologiques, il est souhaitable d'éviter la nécessité d'avoir de capteurs dans les convertisseurs de puissance, et donc détendre l'hypothèse d'une mesure de l'état.

La principale contribution de cette partie est de montrer que l'approche de l'immersion et l'invariance (I&I) de [37] peut etre utilisée pour concevoir un observateur à ordre réduit asymptotiquement convergent pour une classe définie de convertisseurs de puissance, qui se caractérise par une inégalité matricielle linéaire simple (LMI). Par ailleurs, l'observateur I&I peut etre combiné avec le controleur PI proposé dans [39] préservant les propriétés GAS de la boucle fermée. Le nouveau controleur est appliqué pour réguler la tension du convertisseur très - populaire, et difficile à controler, le SEPIC, pour lequel les résultats expérimentaux sont présentés.

Conception de l'observateur

Nous considérons la classe de convertisseurs de puissance commutés avec des condensateurs et des inductances linéaires, décris dans la forme hamiltonienne

$$\dot{x} = \left(J_0 + \sum_{i=1}^{m} J_i u_i - R \right) \nabla H(x) + E \tag{1}$$

où $x \in \mathbb{R}^n$, composée des flux des inducteurs et des charges des condensateurs, est l'état du convertisseur, $u \in \mathbb{R}^m$ désigne le rapport cyclique, l'énergie totale stockée dans les inductances et les condensateurs est

$$H(x) = \frac{1}{2} x^\top Q x, \quad Q = Q^\top > 0, \tag{2}$$

$\nabla = \frac{\partial}{\partial x}$, $J_i = -J_i^\top \in \mathbb{R}^{n\times n}$, $i \in \{0\} \bigcup \bar{m} := \{1, \ldots, m\}$ sont les matrices d'interconnections, $R \in \mathbb{R}^{n\times n}$, $R = R^\top \geq 0$ est la matrice de dissipation, et le vecteur $E \in \mathbb{R}^n$ contient les sources de tension et courants externes.

Le problème d'observateur d'état est formulé comme suit. Supposons

$$y_m = Cx \in \mathbb{R}^p,$$

avec $p < n$ et $C \in \mathbb{R}^{p\times n}$ rang plein, est disponible pour la mesure. Pour reconstruire l'état x on definit une matrice $S \in \mathbb{R}^{(n-p)\times n}$ telle que la matrice carrée

$$T := \begin{bmatrix} S \\ C \end{bmatrix} \in \mathbb{R}^{n\times n} \tag{3}$$

est de rang plein et on considère le changement de coordonnées

$$\begin{bmatrix} \eta \\ y_m \end{bmatrix} = Tx.$$

Le problème est alors de produire une estimation pour le vecteur $\eta \in \mathbb{R}^{n-p}$, $\hat{\eta} \in \mathbb{R}^{n-p}$, pour définir l'état observé comme

$$\hat{x} := T^{-1} \begin{bmatrix} \hat{\eta} \\ y_m \end{bmatrix} = \begin{bmatrix} D_1 & D_2 \end{bmatrix} \begin{bmatrix} \hat{\eta} \\ y_m \end{bmatrix}, \tag{4}$$

où, pour une référence future, on a introduit les matrices $D_1 \in \mathbb{R}^{n\times(n-p)}$ and $D_2 \in \mathbb{R}^{n\times p}$.

Une classe de convertisseurs de puissance pour laquelle le problème d'observation est résolu est caractérisée par le LMI qui suit

Hypothèse 1. *Etant donné*

$$J_0, \cdots, J_m, R, Q \in \mathbb{R}^{n\times n},$$

$$S \in \mathbb{R}^{(n-p)\times n},\ D_1 \in \mathbb{R}^{n\times(n-p)}, \quad C \in \mathbb{R}^{p\times n}.$$

On definit

$$\begin{aligned} F_0 &:= S(J_0 - R)QD_1 \\ F_i &:= SJ_iQD_1, \quad i \in \bar{m} \\ G_0 &:= C(J_0 - R)QD_1 \\ G_i &:= CJ_iQD_1, \quad i \in \bar{m}. \end{aligned} \tag{5}$$

Il existe

$$Z \in \mathbb{R}^{(n-p)\times p}, \quad P = P^\top \in \mathbb{R}^{(n-p)\times(n-p)}$$

solution des LMI suivantes

$$\begin{aligned} P &> 0 \\ sym\{PF_0 + ZG_0\} &< 0 \\ sym\{PF_i + ZG_i\} &= 0,\ i \in \bar{m}, \end{aligned} \tag{6}$$

où sym$\{\cdot\}$ *désigne la partie symétrique.*

Proposition 1. *Considérons le convertisseur de puissance* (1), (2) *vérifiant l'hypothèse 1. Définissons*

$$\begin{aligned} A &: \mathbb{R}^m \to \mathbb{R}^{n\times n} \\ A(u) &:= (J_0 - R)Q + \sum_{i=1}^{m} J_i Q u_i, \end{aligned} \tag{7}$$

avec $u := col(u_1, \ldots, u_m)$*. l'observateur I&I a dimension* $(n-p)$

$$\begin{aligned} \dot{\xi} &= (S + \Gamma C)[A(u)((D_2 - D_1\Gamma)y_m + D_1\xi) + E] \\ \hat{\eta} &= \xi - \Gamma y_m \end{aligned} \tag{8}$$

où

$$\Gamma = P^{-1}Z \in \mathbb{R}^{(n-p)\times p} \tag{9}$$

avec P *et* Z *la solution des LMI, assure la convergence exponentielle globale de l'erreur d'observation. Pour toutes les conditions initiales* $x(0) \in \mathbb{R}^n, \xi(0) \in \mathbb{R}^{n-p}$*, et tout* $u(t)$*, il existe* $\alpha, k \in \mathbb{R}_+$ *tel que*

$$|\hat{\eta}(t) - \eta(t)| \leq ke^{-\alpha t}|\hat{\eta}(0) - \eta(0)|,$$

pour tout $t \geq 0$*, où* $|\cdot|$ *est la norme euclidienne.*

La preuve de cette proposition est donné dans la section 3.1.

Controlleur PI à retour de sortie GAS

Dans cette section, nous proposons d'utiliser l'observateur I&I de la section précédente, avec le controleur PI du [39], préservant la GAS de la boucle fermé. Afin de simplifier notre présentation (une légère variation) des principaux résultats rapportés dans le chapitre 1 sont d'abord rappelés ci-dessous.

Proposition 2. *Considérons un convertisseur de puissance décrit par (1). Soit $x^\star \in \mathbb{R}^n$ un point d'équilibre admissible, alors, il satisfait*

$$0 = \left(J_0 + \sum_{i=1}^{m} J_i u_i^* - R \right) Q x^\star + E, \tag{10}$$

pour certains $u^\star \in \mathbb{R}^m$. On definit l'entrée incrémentale

$$\tilde{u} := u - u^\star,$$

et le signal de sortie

$$y = \mathcal{C} x,$$

avec

$$\mathcal{C} := - \begin{bmatrix} (x^\star)^\top Q J_1 Q \\ \vdots \\ (x^\star)^\top Q J_m Q \end{bmatrix} \in \mathbb{R}^{m \times n}. \tag{11}$$

1. *L'application $\tilde{u} \to y$ est passive. Plus précisément, le système vérifie l'inégalité de dissipation*

$$\dot{H} \leq y^\top \tilde{u}, \tag{12}$$

avec la fonction de stockage

$$\begin{aligned} H &: \mathbb{R}^n \to \mathbb{R}_+ \\ H(\tilde{x}) &= \frac{1}{2} \tilde{x}^\top Q \tilde{x}, \end{aligned} \tag{13}$$

ou $\tilde{x} := x - x^\star$.

2. *Le convertisseur de puissance en boucle fermée avec le régulateur PI*

$$\begin{aligned} \dot{w} &= y \\ u &= -K_p y - K_i w, \end{aligned} \tag{14}$$

avec $K_p = K_p^\top > 0, K_i = K_i^\top > 0$ assure que l'équilibre

$$(x, w) = (x^\star, -K_i^{-1} u^\star),$$

est GAS si y est detectable. *Autrement dit, si pour toute solution $(x(t), w(t))$ de la boucle fermée du système, l'implication suivante est vraie:*

$$y(t) \equiv 0 \quad \Rightarrow \quad \lim_{t \to \infty} x(t) = x^\star, \lim_{t \to \infty} w(t) = -K_i^{-1} u^\star. \tag{15}$$

Nous sommes en mesure de présenter le résultat principal de cette section.

Proposition 3. *Considérons un convertisseur de puissance décrit par (1), vérifiant l'hypothèse 1, avec un état d'équilibre $x^\star$ et une entrée correspondante $u^\star$. Supposons* (15) *de la proposition détient. le controlleur PI avec l'observateur*

$$\begin{aligned} \dot{w} &= \mathcal{C}\hat{x} \\ u &= -K_p\mathcal{C}\hat{x} - K_i w \end{aligned} \tag{16}$$

où $\hat{x}$ est l'estimation de l'état généré par l'intermédiaire (4), (7), (8) *and* (9), *assure que l'équilibre*

$$(x, w, z) = (x^\star, -K_i^{-1}u^\star, 0)$$

est GAS.

La preuve de cette proposition est également fourni dans la section 3.3.

Application au SEPIC

Le SEPIC est un des convertisseur de puissance qui a trouvé une large application dans l'industrie parce qu'il est relativement simple et peut fonctionner aussi bien en mode elevateur et abaisseur [49]. En dépit de sa similitude avec le convertisseur Cuk bien connu, il est largement reconnu que la conception d'un controleur pour obtenir un comportement de haute performance est un problème majeur ouvert.

En supposant qu'il est en mode de conduction continue, son modèle moyen, peut etre exprimé sous forme hamiltonienne (1) avec $n = 4$ et les définitions

$$x = \mathrm{col}(\phi_1, \phi_2, q_1, q_2),\ E = \mathrm{col}(V_{in}, 0, 0, 0)$$

$$R = \mathrm{diag}\left\{r_{L_1}, r_{L_2}, 0, \frac{1}{r}\right\}$$

$$Q = \mathrm{diag}\left\{\frac{1}{L_1}, \frac{1}{L_2}, \frac{1}{C_1}, \frac{1}{C_2}\right\}$$

$$J_0 = \begin{bmatrix} 0 & 0 & -1 & -1 \\ 0 & 0 & 0 & 1 \\ 1 & 0 & 0 & 0 \\ 1 & -1 & 0 & 0 \end{bmatrix}$$

$$J_1 = \begin{bmatrix} 0 & 0 & 1 & 1 \\ 0 & 0 & -1 & -1 \\ -1 & 1 & 0 & 0 \\ -1 & 1 & 0 & 0 \end{bmatrix}$$

ou ϕ_i sont les flux dans les inducteurs L_i, q_i les charges dans les condensateurs C_i, u est l'indice de modulation, V_{in} est la tension d'alimentation constante directe, L_i, C_i, r_{L_i}, sont les paramètres SEPIC et r est la résistance de charge.

L'objectif du controle est la régulation de la tension de sortie à une valeur donnée constante $V^\star$, *i.e.*, la régulation de la charge x_4 pour une référence souhaitée $x_4^\star > 0$ où $C_2 V^\star = x_4^\star$. Il est supposé que la seule variable disponible pour la mesure est la tension de sortie, parsuite $p = 1$, et

$$C = (0\ 0\ 0\ 1).$$

La proposition ci-dessous qui — par la proposition 1 établit l'existence d'un observateur I&I GAS. L' application directe de la proposition prouve alors qu'un controleur PI par retour de sortie rend le SEPIC GAS.

Proposition 4. *Fixons $P_{13} > 0$ et posons*

$$P_{22} = \frac{1}{r_{L_2}} P_{13} + K \tag{17}$$

$$P_{33} = (r_{L_2} + \frac{L_2}{C_1 r_{L_2}}) P_{13} + \frac{L_2}{C_1} K. \tag{18}$$

Il existe $K_{min} > 0$ tel que, pour tous $K \geq K_{min}$ les matrices

$$P = \begin{bmatrix} \frac{L_2}{L_1} P_{22} & 0 & P_{13} \\ 0 & P_{22} & P_{13} \\ P_{13} & P_{13} & P_{33} \end{bmatrix}$$

et

$$Z = \begin{bmatrix} -P_{13} \\ -P_{13} \\ L_2(\frac{P_{22}}{C_1} - \frac{P_{33}}{L_1}) \end{bmatrix}.$$

sont solutions des LMI de l'Hypothèse 1 pour le modèle du SEPIC. Par ailleurs, K devrait satisfaire les deux conditions suivantes:

$$\frac{1}{4 r_{L_2}^3 C_1} \frac{L_2^4}{L_1} K^2 + (\frac{1}{2 r_{L_2}} \frac{L_2}{L_1} + \frac{1}{r_{L_2}^3 C_1} \frac{L_2^3}{L_1}) K P_{13} + (\frac{1}{r_{L_2} L_1} + \frac{1}{r_{L_2}^3 C_1} \frac{L_2^2}{L_1} - \frac{1}{r_{L_2}} \frac{L_2}{L_1} - \frac{1}{r_{L_2}}) P_{13}^2 > 0. \tag{19}$$

$$\frac{r_{L_1}}{r_{L_2}} \frac{L_2^2}{L_1^2} K^2 + (2 \frac{r_{L_1}}{r_{L_2}} \frac{L_2}{L_1^2} - \frac{r_{L_1}^2}{L_1^2} \frac{C_1}{2}) P_{13} K - \frac{1}{L_2^2} P_{13}^2 > 0. \tag{20}$$

Ces conditions sont obtenues après une démonstration détaillée expliquée dans le chapitre 3. Comme les coefficients de K^2 sur les cotés droite de (19) et (20) sont positifs, il est clair que, pour tout P_{13} choisi, il existe $K > 0$ telles que les deux inégalités sont satisfaites. Le nouveau controleur est illustré avec le convertisseur SEPIC, pour lequel les simulations et les résultats expérimentaux sont présentés dans la section 3.5.

Introduction

Switched electronic systems are used in a huge number of everyday domestic and industrial utilities: liquid crystal displays, home appliances, lighting, personal computers, power plants, transportation vehicles and so on. Efficient operations of all such applications depend on the essential " hidden work" done by switched electronic systems, whose behaviour is determined by a suitable interconnection and control of analog and digital devices.

From the engineering point of view, most switched electronic systems can be classified as power converters. These systems can be viewed as networks composed of semiconductor switches, e.g., thyristors, transistors and diodes, along with passive elements, e.g., inductors capacitors and resistors, and current-voltage sources.

The most common classification of power conversion systems is based on the waveform of the input and output signals, in the case whether they are alternating current (AC) or direct current (DC), thus: DC to DC, DC to AC, AC to DC and AC to AC. Depending on the character of the input source, they may be voltage-source converters or current-source converters. Moreover, converters may be of low, medium or high voltage and/or current level.

Switched systems play a fundamental role in all those environments where regulation, control and conversion of the electrical energy is a key issue. In recent years, continuously more demanding efficiency and quality constraints are imposed on the electrical energy in applications such as electrical drives, power systems and transportation vehicles. This has determined a new research interest in the study of formal approaches for the analysis, design and control of power converters. In this context the analysis, design and control of switched electronic systems is a key issue, and the use of advanced mathematical tools can be an effective approach for tackling increasing requirements in performance and efficiency.

As a motivation of this work, we consider the DC-DC power converters, due to there wide range of applicability, and presence in all kind of electronic circuits, from industrial applications (spacecraft power systems, DC motor drives, telecommunication equipment) to personal applications (PCs, office equipment, electrical appliance, and with a power range from milliwatts, mobile phone, for example, to megawatts, in electric power transmission systems.

The problem of modeling and control of these power electronics systems is that they have circuit topologies that include continuous time elements like resistors, inductors, capacitors, and voltage and current sources that are interfaced with electronic devices like diodes, and electronic switches such as thyristors, transistors, and MOSFETs. This leads to hybrid system types that involve continuous-time system behavior mixed with discrete-time logic switching behavior. Traditional control schemes was based on averaged models where the action of the switches are assimilated to continuous signals ranging in some closed interval, *e.g.*, $[0, 1]$, then neglecting the presence of ripples. A burgeoning literature on hybrid systems has emerged in the control community in the last few years [25]. As usual in control theory, the main thrust of the research has been towards the development of general methodologies, mainly for analysis [22] but also for controller design, of classes of theoretically motivated, hybrid dynamical systems. That is, there is a truly need to develop hybrid control, and the control objective will be not the stabilization of an equilibrium point but the generation of a periodic orbit around a desired operating point. Motivated by this fact, in the first part of the thesis a different perspective was adopted, namely the development of a solution for a specific example of practical relevance. We will consider a boost and a buck-boost converter operating in DCM, and our main contribution will be a simple robust control algorithm.

Neglecting the presence of the ripple permits to recast the converter regulation as a classical equilibrium problem for which, by now standard, nonlinear controller design techniques, e.g. sliding mode and passivity based are directly applicable.

Developing control of nonlinear systems that incorporates at a fundamental level the systems physical structure and provides solutions to practical engineering problems, was the motivation of several works. A main contribution in this domain was the identification of a large class of converters that can be stabilized via adaptive PI control . A procedure to design globally asymptotically stabilizing linear proportional plus integral controllers for switched power converters was proposed in [39]. The construction requires the measurement of the full state of the system which is often unavailable in practice. The main objective of the second part will be to show that the I&I approach of [37] can be used to design an asymptotically convergent reduced order observer for a well–defined class of power converters, which is characterized by a simple linear matrix inequality (LMI). Moreover, we will prove that the I&I observer can be combined with the PI controller preserving the GAS properties of the closed–loop. The new (certainty–equivalent) controller is applied to regulate the voltage of the widely–popular, and difficult to control, single–ended primary inductor converter (SEPIC).

This thesis is composed of three chapters:

The first chapter presents some background materials, concepts and results. We begin first with an introduction about switching power converters, then the different conduction modes: the continuous and discontinuous conduction modes of power converters. The results of stabilization via adaptive PI control of a large class of converters using the key property of passivity of the nonlinear incremental model, and the procedure to design the globally asymptotically stabilizing controllers for these converters are then presented. After a brief introduction where the main ideas of immersion and invariance are illustrated, then the design principle of observers for general nonlinear systems provided by $I\&I$ are given.

In chapter 2 we are interested in the problem of voltage regulation of power converters operating in discontinuous conducting mode. Two power converters are considered: the boost converter and the buck-boost converter. The system does not admit a (continuous–time) average model approximation, hence is a *bona fide* hybrid system where the control objective is the generation of a periodic orbit and the actuator commands are switching times. Our main contribution is a simple robust algorithm that gives explicit formulas for the switching times without approximations. Simulation and experimental results that illustrate the robustness of the scheme to parameter uncertainty, as well as performance comparisons with current practice, are presented.

In chapter 3 a class of power converters that can be globally stabilized with an output–feedback PI controller has been identified. Moreover, we will prove that the I&I observer can be combined with the PI controller preserving the GAS properties of the closed–loop. The class is characterized by a simple linear matrix inequality. The new controller is illustrated with the widely–popular, and difficult to control, single–ended primary inductor converter, for which simulation and experimental results are presented.

Chapter 1

Preliminaries

Contents

In this chapter some background materials, concepts and results are presented.

We begin first with an introduction about switching power converters, providing the different topologies from a circuit theory perspective, then the different conduction modes: the continuous and discontinuous conduction modes of power converters. In this section the DC-DC power converters that will be considered in this thesis are presented.

The results of stabilization via adaptive PI control of a large class of converters using the key property of passivity of the nonlinear incremental model, and the procedure to design the globally asymptotically stabilizing controllers for these converters are then presented in the next section.

After a brief introduction where the main ideas of immersion and invariance are illustrated, then the design principle of observers for general nonlinear systems provided by $I\&I$ are given.

1.1 Switching Power converters

Switching power converters are in existence for almost five decades. They control the flow of power between two systems by changing the character of electrical energy: from direct current to alternating current, from one voltage level to another voltage, or in some other way. The most common classification of power conversion systems is based on the waveform of the input and output signals, in the case whether they are alternating current (AC) or direct current (DC), thus: DC to DC, DC to AC, AC to DC and AC to AC [1], [2]. Depending on the character of the input source, they may be the family of voltage-source converters or the less-known family of current-source converters. Moreover, converters may be of low, medium or high voltage and/or current level. Another sort of classification may be performed according to the size of the output signal obtained from the input signal; if the converter accomplishes a lower output signal it is well known as step-down, and if it obtains a larger signal, it is known as step-up.

DC-DC power converters, with which this thesis is concerned, forms a major chunk of these systems. They have recently aroused the interest in the current market due to there wide range of applicability.

This section provides first from a circuit theory perspective, how fundamental converters are derived, how they are related, and how they can be integrated to result in more complicated types of converters. Then the two modes of conduction of power converters: the continuous and discontinuous conduction mode are explained.

1.1.1 Minimum configurable switching storage structures

Switching power conversion encompasses two types of conversions, namely voltage conversion and current conversion. Power converters which electronically convert an energy source of one voltage level to another voltage level are known as voltage converters. In this respect, current converters are power electronics that convert an energy source from one current level to another current level [3]. The basic mechanism of performing an ideally lossless voltage or current conversion involves the rapid repeated connection and disconnection of the voltage or current source to an appropriate storage device, namely an inductor or capacitor, in a controlled manner via electronic switches, such that the energy is transferred at the appropriate voltage or current level before being released to the output load in the desired form. In configuring such power converters, it is important that the voltage sources are never connected directly to a capacitor and the current sources are never connected directly to an inductor. From a theoretical viewpoint, there are two simplest configurable switching storage structures possible, namely a star-connected two-switch inductor cell and a delta-connected two-switch capacitor cell. We will next give a discussion on these storage cells and how they are configured to give the various possible types of power converters [4], [6], [7].

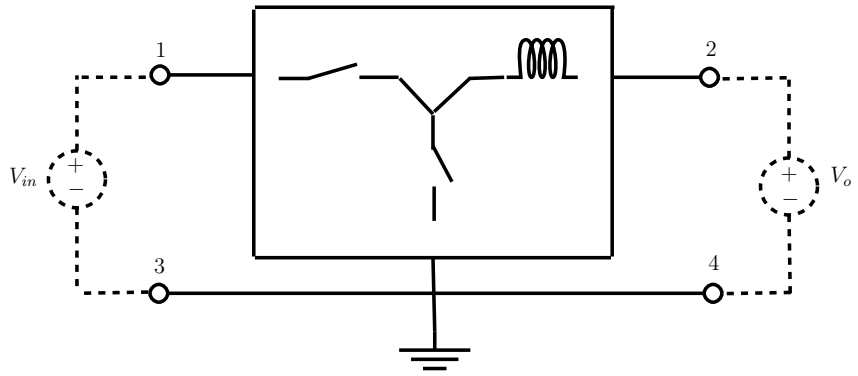

Figure 1.1: DC-DC voltage converter using the switching-inductor cell.

1.1.1.1 Switching-inductor cell

The switching-inductor cell comprises a storage inductor and two switches arranged in a star connection as depicted in Fig. 1.1. Since current flowing through an inductor must be continuous and cannot become zero instantaneously, the two switches must be designed to operate complementarily such a closed-circuit continuous path will always exist for the flow of the inductor current. For this reason, this switching-inductor cell represents the minimum configurable switching inductor structure possible. To qualify for a lossless conversion process, the switching-inductor cell must be implemented with an input voltage source together with an output voltage sink, which forms the basis for a voltage-to-voltage converter.

As illustrated in Fig. 1.2, there are three possible ways of configuring the switching-inductor cell while still maintaining the star-connection structure. Each can be realized by swapping the positions of any two of the three circuit elements. For proper operation of such a configuration with its input source and output sink, there should be no instance when the two switches are concurrently turned on. This will cause a direct short circuit of either the source, the sink, or the source with the sink for the respective configurations given in Fig. 1.2. Additionally, when there is current flowing in the inductor, there should be no instance when both the switches are simultaneously turned off.

By replacing the voltage sink in Fig. 1.1 with a more realistic and practical circuit representation in the form of a resistor-capacitor sink as illustrated in Fig. 1.3, and by considering the three possible configurations of the switching-inductor cell given in Fig. 1.2, three fundamental types of voltage converters can be obtained. They are the voltage buck, boost, and buck-boost converters, which represent the fundamental topologies of the voltage converters. The schematics of these converters are given in Fig. 1.4 . For economical reasons, one of the two switches is replaced by a diode. The primary difference between the topologies is that each converter has a different voltage conversion ratio M such that $M(D) = \frac{V_o}{V_{in}}$, where D is the duty cycle and is a function of the turn-on time

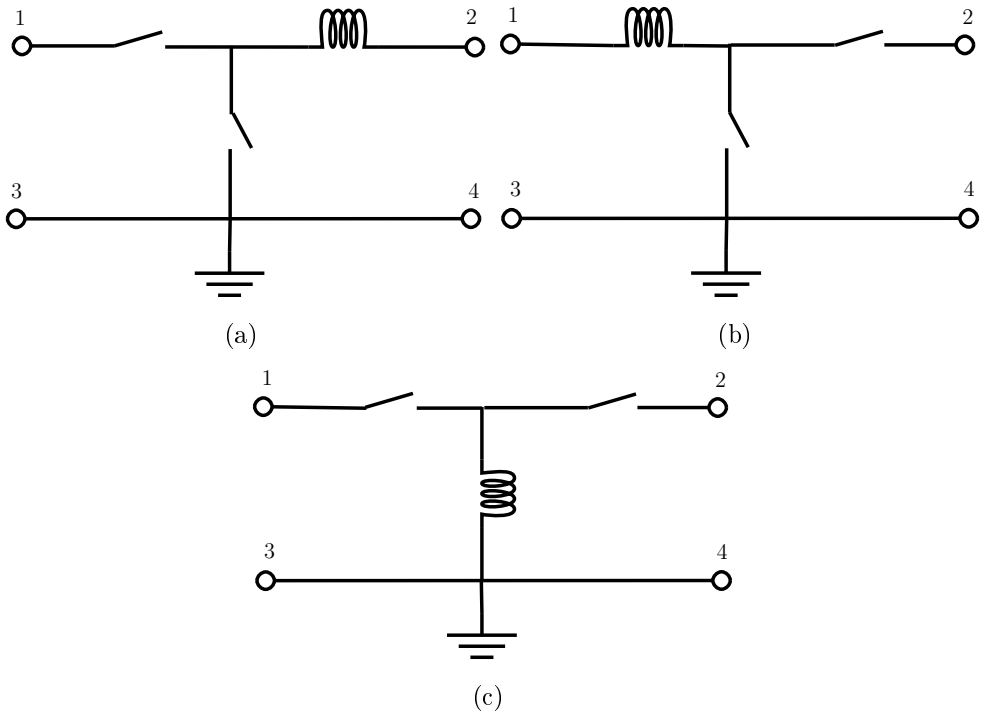

Figure 1.2: The three possible configurations of the switching-inductor cell. (a) Structure 1, (b) Structure 2, (c) Structure 3.

T_{on} and the period T which is the sum of turn-on and turn-off time periods, $T_{on} + T_{off}$, of the active switch S, i.e. $D = \frac{T_{on}}{(T_{on}+T_{off})}$.

For example, the voltage conversion ratios $M(D)$ for the respective converters when they are operating in the continuous inductor conduction mode (current flow of the inductor never falls to zero) are:

- Voltage buck converter:
$$\frac{V_o}{V_{in}} = D \tag{1.1}$$
- Voltage boost converter:
$$\frac{V_o}{V_{in}} = \frac{1}{1-D} \tag{1.2}$$
- Voltage buck-boost converter:
$$\frac{V_o}{V_{in}} = \frac{D}{1-D} \tag{1.3}$$

From these equations, one can expect since the duty ratio is confined as $0 < D < 1$, the voltage buck converter can only produce an output voltage smaller than the input voltage, i.e. $V_o < V_{in}$; a voltage boost converter can only produce an output voltage bigger than the input voltage, i.e. $V_o > V_{in}$; whereas a voltage buck-boost converter will have $V_o < V_{in}$ when $0 < D < 0.5$ and $V_o > V_{in}$ when $0.5 < D < 1$. In the case of discontinuous inductor

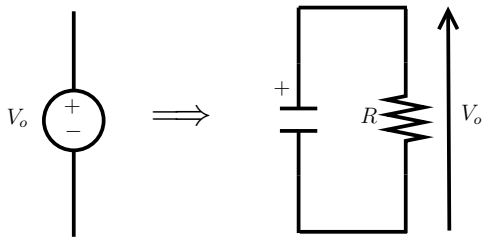

Figure 1.3: Voltage sink replaced by resistor-capacitor sink.

conduction mode, the converters inherit a different set of conversion ratios (given later in section 1.1.3). Nevertheless, their properties of stepping up or stepping down voltage levels remain the same regardless of the conduction mode.

1.1.1.2 Switching-capacitor cell

The switching-capacitor cell comprises a storage capacitor and two switches arranged in a delta connection as depicted in Fig. 1.5. The voltage of a capacitor has to be maintained continuous and cannot become zero instantaneously. The presence of the two switches is important in the sence that they must be synchronised to operate complementarily to ensure that there is no circumstance that the capacitor has a direct short circuit. This gives the minimum configurable switching-capacitor cell must be implemented with an input current source and an output current sink. This forms the basis for the current-to-current converters.

As illustrated in Fig. 1.6, there are three possible ways of configuring the switching-capacitor cell while still maintaining the delta-connection structure. Each can be realised by swapping the positions of any two of three circuit elements. For proper operation of such a configuration with its input source and output sink, there should be no instance when the two switches are concurrently turned off. This will cause a direct open circuit of either the source (in case (a)) or the sink (in case (b)), or a short circuit between the current source and the current sink (in case (c)) for the respective configurations given in Fig. 1.6. Additionally, when there is stored charge in the capacitor, there should be no instance when both the switches are simultaneously turned on, thus avoiding a capacitor short circuit.

By considering the three possible configurations of the switching-capacitor cell given in Fig. 1.6, three fundamental types of current converters can be obtained. They are the current buck, boost, and buck-boost converters, which are in reality the dual counterparts of the voltage converters given in Fig. 1.4. These converters represent the fundamental topologies in the family of current converters. The schematics of these converters are given in fig. 1.7. For economical reasons, one of the two switches can be replaced by a diode. Here each of these topologies possesses a different current conversion ratio M, such

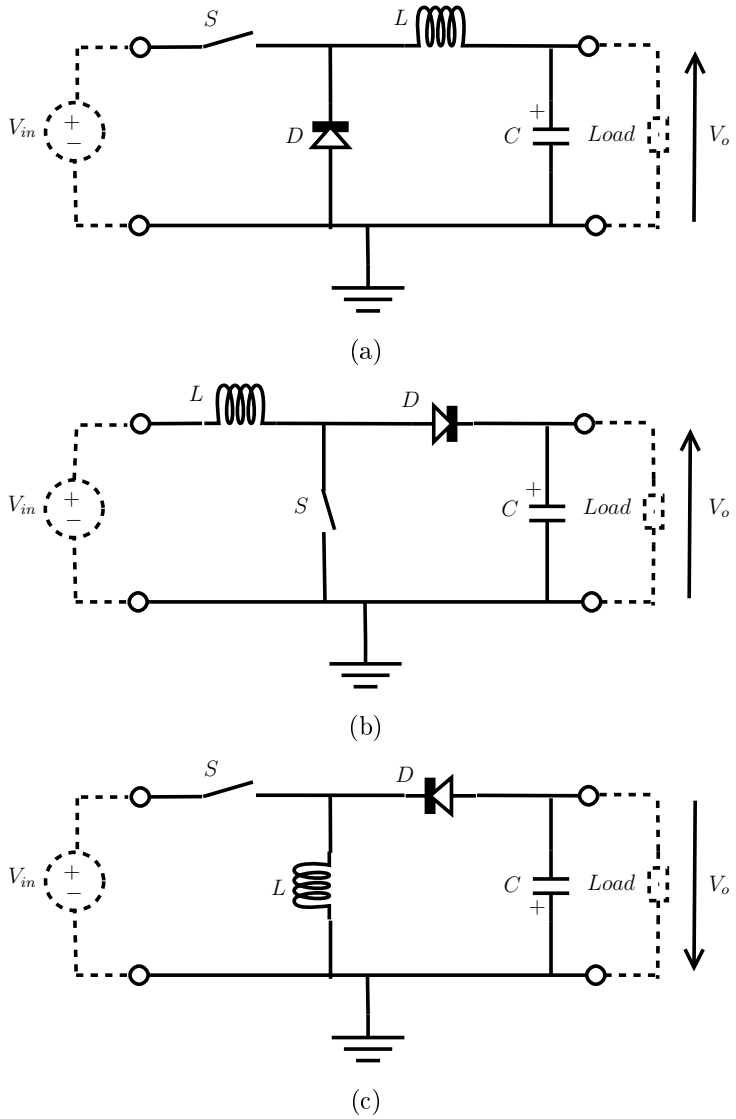

Figure 1.4: The three fundamental DC-DC voltage converters. (a) Voltage buck converter, (b) Voltage boost converter, (c) Voltage buck-boost converter.

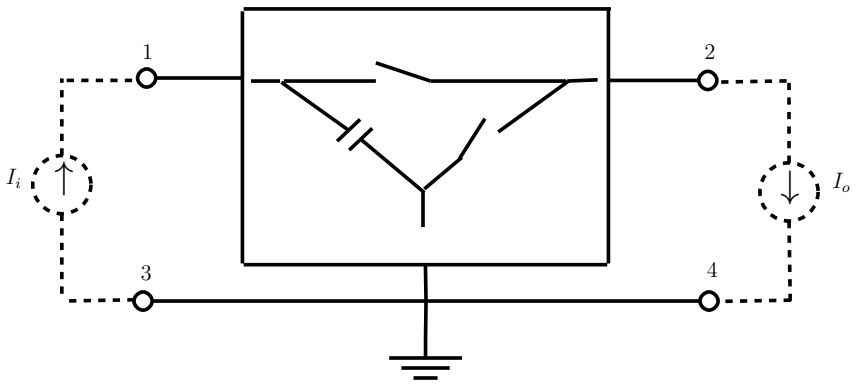

Figure 1.5: DC-DC current converter using the switching-capacitor cell.

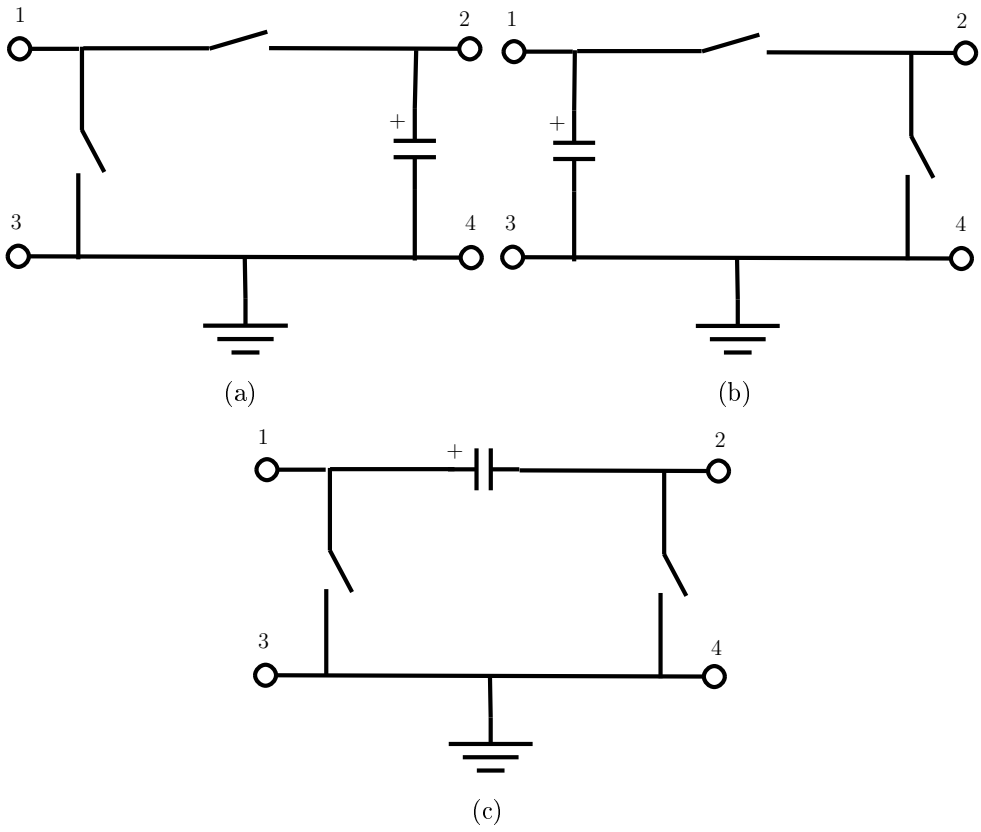

Figure 1.6: The three possible configurations of the switching-capacitor cell. (a) Structure 1, (b) Structure 2, (c) Structure 3.

that $M(D^{'}) = \frac{I_o}{I_i}$, where $D^{'} = 1 - D$ and $D = \frac{T_{on}}{(T_{on}+T_{off})}$ represents the duty cycle of S.

The current conversion ratios $M(D^{'})$ for the respective converters when they are operating in the continous voltage conduction mode (voltage of the capacitor never falls to zero) are:

- Current buck converter:
$$\frac{I_o}{I_i} = D^{'} \tag{1.4}$$
- Current boost converter:
$$\frac{I_o}{I_i} = \frac{1}{1 - D^{'}} \tag{1.5}$$
- Current buck-boost converter:
$$\frac{I_o}{I_i} = \frac{D^{'}}{1 - D^{'}} \tag{1.6}$$

It is clear from the equations that for a buck current converter, the output current is always smaller than its input, i.e. $I_o < I_i$; for the current boost converter, output current is always bigger than the input current, i.e. $I_o > I_i$; and for the current buck-boost converter, $I_o < I_i$ when $0 < D^{'} < 0.5$ and $I_o > I_i$ when $0.5 < D^{'} < 1$.

1.1.1.3 Duality of voltage and current converters

The family of current converters are basically the dual counterparts of the voltage converters. So far, we have demonstrated the formulation of these converters from basic circuit rules and framework of a switching-inductor cell and a switching-capacitor cell. Interestingly, using the principle of circuit duality, it is possible to extract the same family of current converters from the voltage converters, and conversely, the family of voltage converters from the current converters.

1.1.1.4 Practical current DC-DC converters

While the reported family of current DC-DC converters in Fig. 1.7 are theoretically feasible, in reality, it is uncommon that practical current source and current sink are available. Hence, a more practical scenario would be to replace the current sources and current sinks with their circuit equivalent of voltage sources and sinks, which are respectively shown in Fig. 1.8. This will result in an interesting family of current buck, boost and buck-boost converters that are based on voltage sources and sinks, as depicted in Fig. 1.9. Note that the derived converters possesses two inductors and two capacitors and they must be operated only in the continuous inductor conduction mode such that the currents of both the inductors are always continuous(to preserve the original property of a current source and current sink). The presented current buck and boost converters and their modified versions, as illustrated in Figs. 1.7, 1.9 are relatively unknown topologies which may

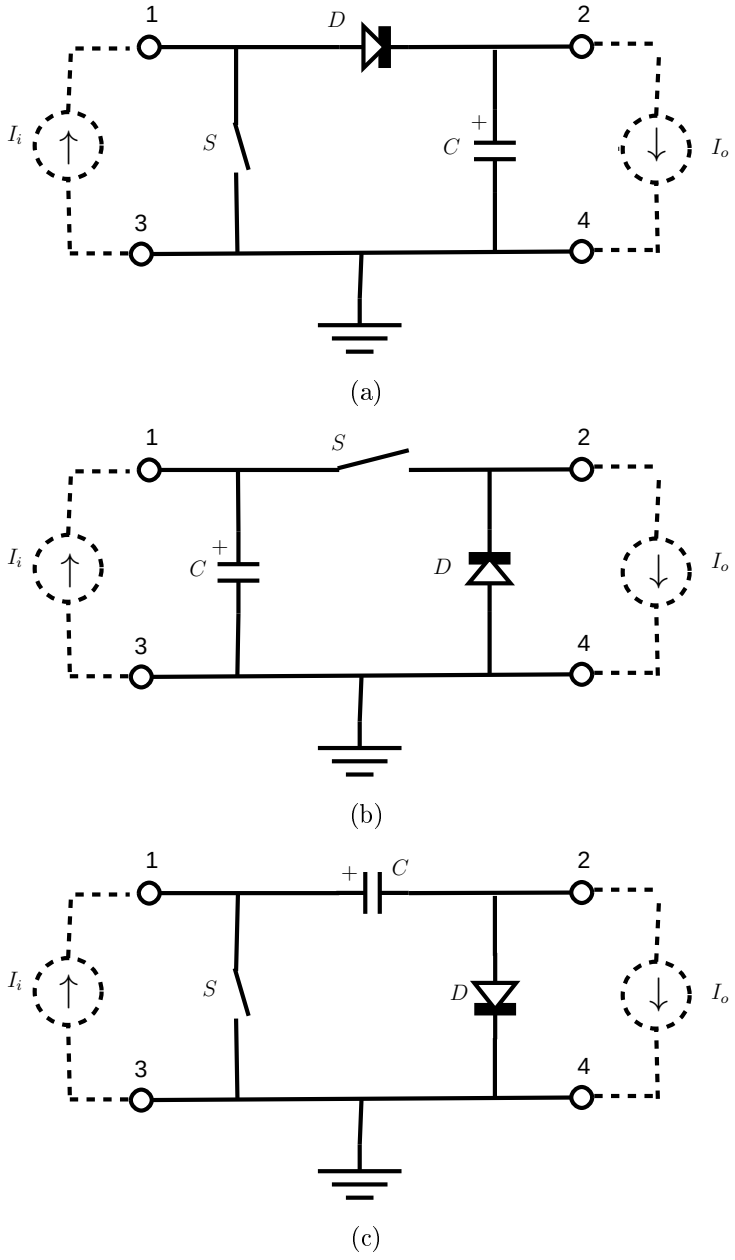

Figure 1.7: The three fundamental DC-DC current converters. (a) Current buck converter, (b) Current boost converter, (c) Current buck-boost converter.

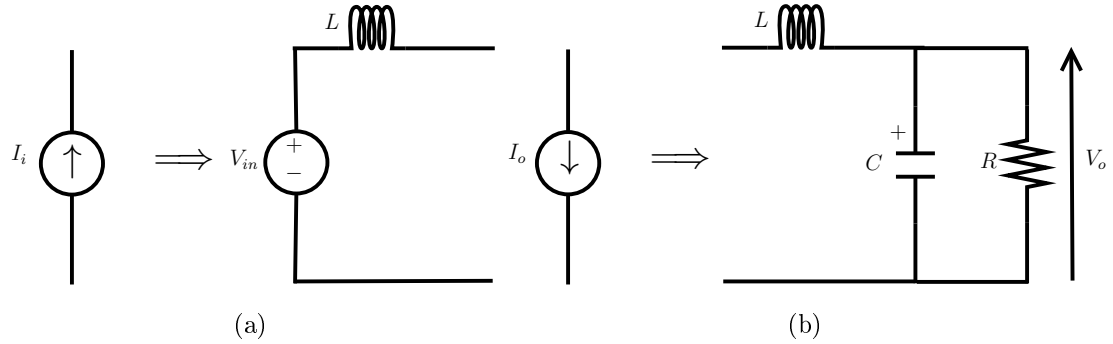

Figure 1.8: (a) Current source replaced by an equivalent of voltage source and series inductor and (b) Current sink replaced by a resistor-capacitor sink and series inductor.

be interesting for new emerging applications. Coincidentally, the modified buck-boost converter given in Fig. 1.9(c) happens to be the well known Cuk converter.

1.1.2 Fourth-order converters

The Cuk, SEPIC, and zeta converters are a family of fairly interesting fourth-order converters that were introduced in 1980s [5]. They have been classified as fourth order converters for the reason that each of these converters comprises four independent storage elements involving two inductors and two capacitors that are inter-actively configured with the voltage source and sink via a switch and a diode.

From a topological viewpoint, fourth-order converters have twice the number of storage elements and are more complicated than the fundamental voltage buck, boost, and buck-boost converters, which are primarily second-order converters. Nevertheless, the fourth-order converters possess unique features which renders them preferential in certain applications over the second-order converters.

Next we will illustrate how this family of fourth-order converters can be obtained from a two-inductor-two-switch circuit cutset.

1.1.2.1 Two-inductor-two-switch circuit cutset

Based on the two-inductor-two-switch cutset, the family of fourth-order converters can be portrayed in the generic structure as depicted in Fig. 1.10. In this diagram, the four boxes in dotted lines which are labeled as 1_A, 1_B, 2_A, and 2_B represent either an inductor or a switch.

The structure itself is known as the two-inductor-two-switch circuit cutset. To ensure that there will be no short-circuit operation of the voltage source and voltage sink, the cutset must be configured such that if component 1_A is a switch, then the component 1_B must be an inductor, and vice versa. Likewise, if component 2_A is a switch, then

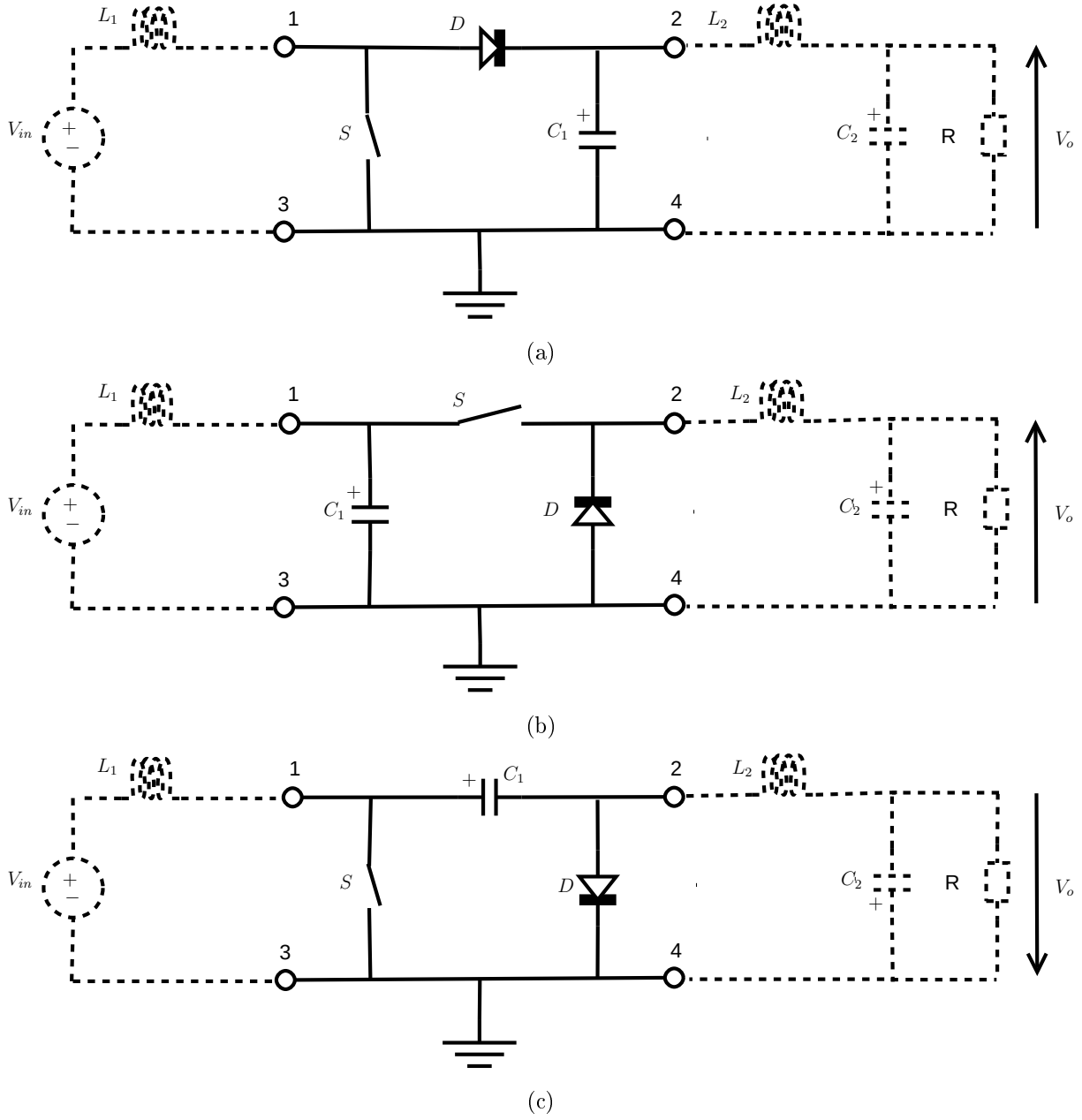

Figure 1.9: The three fundamental DC-DC current converters with their input current sources and output current sinks replaced by equivalent viltage source and sink circuits. (a) Modified current buck converter, (b) Modified current boost converter, (c) Modified current buck-boost converter.

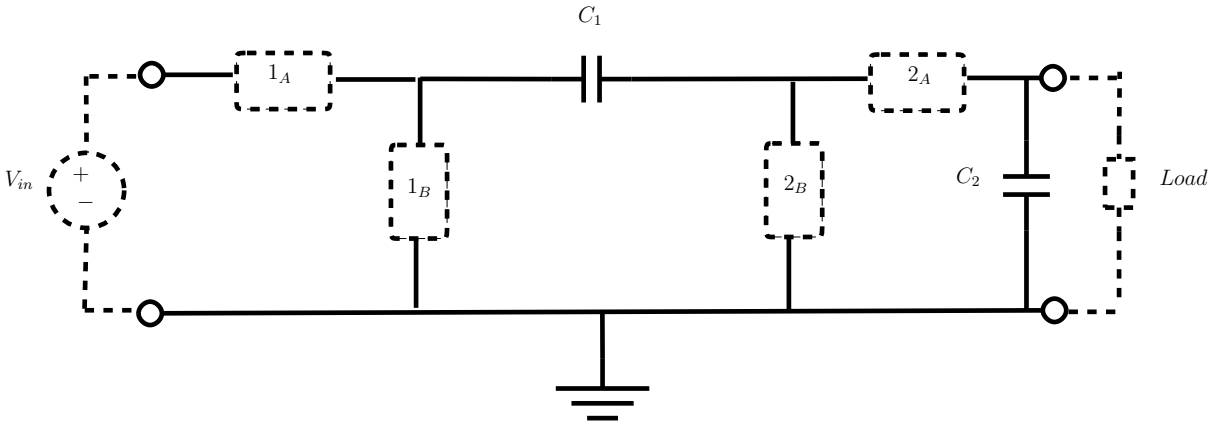

Figure 1.10: Generic fourth-order converter with two-inductor-two-switch cutset.

component 2_B must be an inductor, and vice versa. With these constraints, there exist only four possible configurations in this two-inductor-two-switch cutset. One of these possible configurations is: 1_A is an inductor, 1_B is a switch, 2_A is an inductor, and 2_B is a diode. This makes the Cuk converter given in Fig. 1.11(a). A second configuration is to assign 1_A as inductor, 1_B as a switch, 2_A as an inductor, and 2_B as a diode. This gives the SEPIC converter, which is shown in Fig. 1.11(b). The third configuration is to assign 1_A as a switch, 1_B as an inductor, 2_A as an inductor, and 2_B as a diode, to give what is known as the zeta converter, as depicted in Fig. 1.11(c).

For all the three topologies, the voltage conversion ratios $M(D)$ for the continuous inductor conduction mode are exactly that of a buck-boost converter, i.e.

$$\frac{V_o}{V_{in}} = \frac{D}{1-D} \tag{1.7}$$

The difference between these converters and the voltage buck-boost converter is that for the latter, both the input current and the output current are non-pulsating. For the SEPIC converter, the input current is non-pulsating but the output current is pulsating. For the zeta converter, the input current is pulsating but the output current is non-pulsating.

1.1.3 Continuous and discontinuous conduction mode

When the ideal switches of a dc-dc converter are implemented using current-unidirectional and/or voltage-unidirectional semiconductor switches, one or more new modes of operation known as discontinuous conduction modes (DCM) can occur. The discontinuous conduction mode arises when the switching ripple in an inductor current or capacitor voltage is large enough to cause the polarity of the applied switch current or voltage to reverse, such that the current- or voltage-unidirectional assumptions made in realizing the switch with semiconductor devices are violated. The DCM is commonly observed in dc-dc

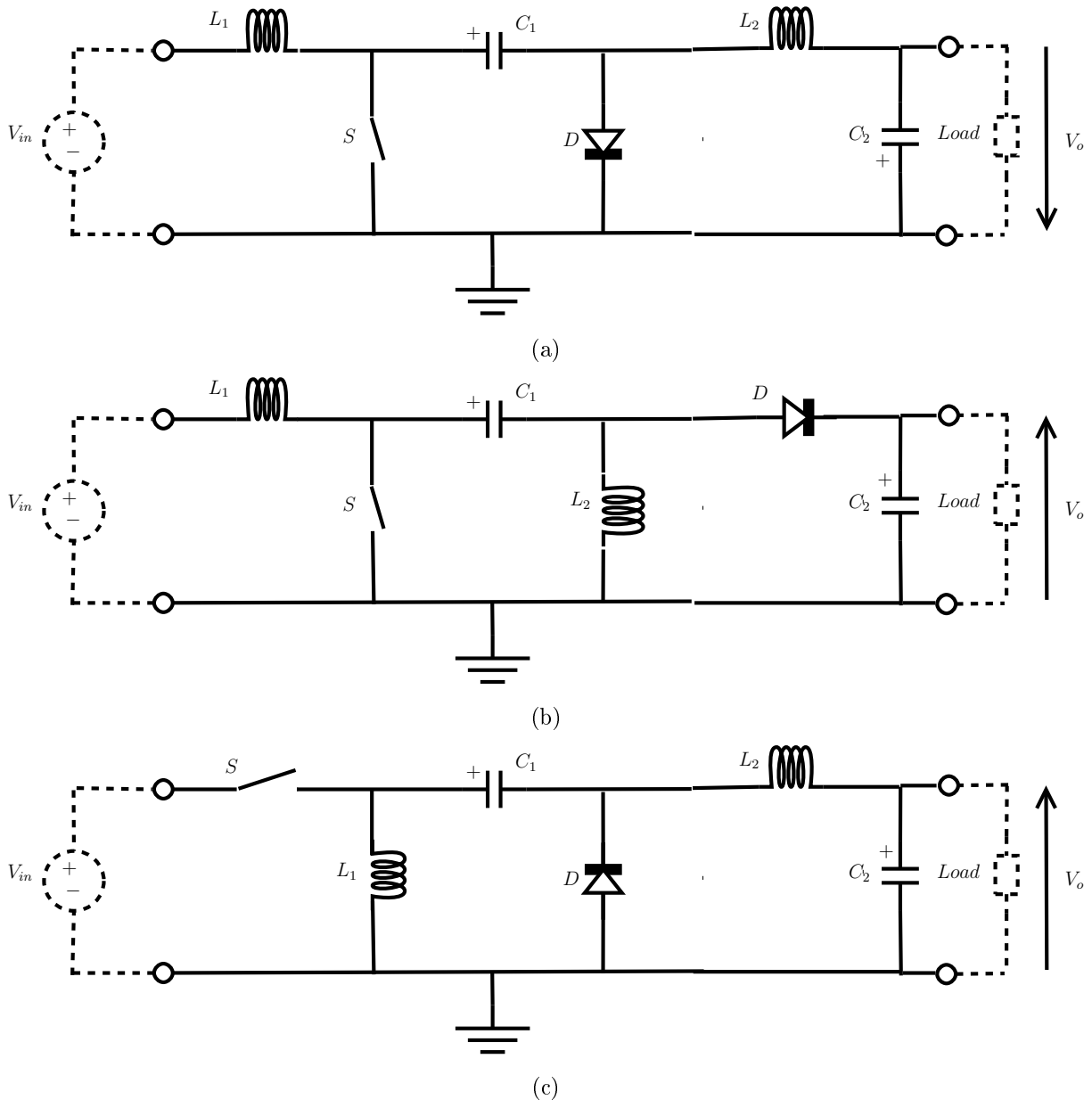

Figure 1.11: Known types of fourth-order converters with the two-inductor-two-switch cutset. (a) Cuk converter, (b) SEPIC converter, (c) Zeta converter.

converters and rectifiers, and can also sometimes occur in inverters or in other converters containing two quadrant switches [21].

The discontinuous conduction mode typically occurs with large inductor current ripple in a converter operating at light load and containing current-unidirectional switches. Since it is usually required that converters operate with their loads removed, DCM is frequently encountered. Indeed, some converters are purposely designed to operate in DCM for all loads.

The properties of converters change radically in the discontinuous conduction mode. The conversion ratio M becomes load-dependent, and the output impedance is increased. For example, the voltage conversion ratios M for the respective voltage converters when they are operating in the discontinuous inductor conduction mode are [23]:

- Voltage buck converter:
$$M = \frac{2}{1 + \sqrt{1 + \frac{4K}{D_1^2}}} \tag{1.8}$$
- Voltage boost converter:
$$M = \frac{1 + \sqrt{1 + 4\frac{D_1^2}{K}}}{2} \tag{1.9}$$
- Voltage buck-boost converter:
$$M = \frac{D_1}{\sqrt{K}} \tag{1.10}$$

with the dimensionless parameter K, defined as $K = \frac{2Lf_s}{R}$, and f_s the switching frequency. Where D_1 is the duty cycle (equivalent to D in CCM) and is a function of the turn-on time T_{on} and the period T which is the sum of turn-on and turn-off time periods, $T_{on} + T_{off}$, of the active switch S, i.e. $D_1 = \frac{T_{on}}{(T_{on}+T_{off})}$. In discontinuous conduction mode, there are now two subintervals during T_{off}. The inductor current waveforms of the two modes of switching converter operation are illustrated in Fig. 1.12.

1.2 PI stabilization of switched power converters

1.2.1 Introduction

The identification of a large class of converters that can be stabilized via adaptive PI control was shown in [39]. The work effectively exploits the key property of passivity of the nonlinear incremental model [42], first reported in [46]. More specifically, this class of switched power converters with linear capacitors and inductors, is described in the form:

$$\dot{x} = (J_0 + \sum_{i=1}^{m} J_i u_i - R)\nabla H(x) + (G_0 + \sum_{i=1}^{m} G_i u_i)E \tag{1.11}$$

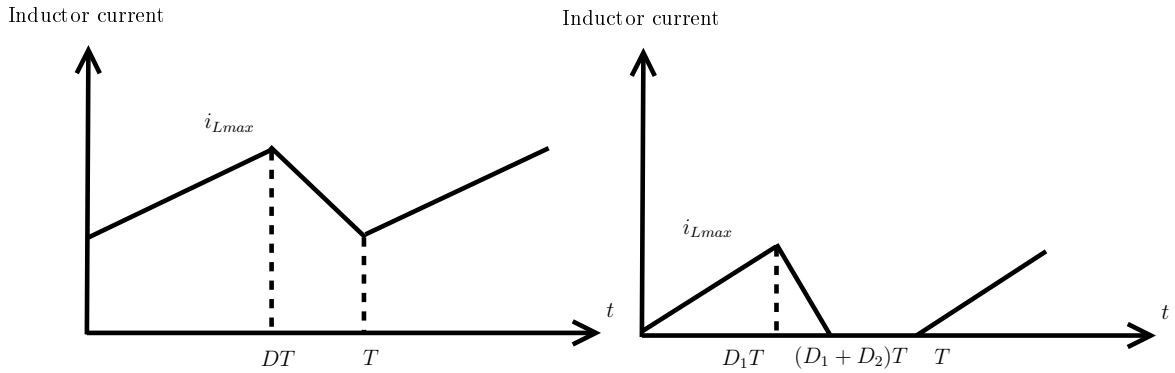

Figure 1.12: Inductor current waveforms and definitions of two modes. (a) Continuous conduction mode, (b) Discontinuous conduction mode.

where $x \in \mathbb{R}^n$, consisting of inductor fluxes and capacitor charges, is the converter state, $u \in \mathbb{R}^m$ denotes the duty ratio of the switches, the total energy stored in inductors and capacitors is

$$H(x) = \frac{1}{2} x^\top Q x, \quad Q = Q^\top > 0, \tag{1.12}$$

$\nabla = \frac{\partial}{\partial x}$, $J_i = -J_i^\top \in \mathbb{R}^{n \times n}$, $i \in \{0\} \bigcup \bar{m} := \{1, \ldots, m\}$ are the interconnection matrices, $R \in \mathbb{R}^{n \times n}$, $R = R^\top \geq 0$ is the dissipation matrix, and the vector $E \in \mathbb{R}^n$ contains the external voltage and current sources. $G_i, i \in \bar{m}$ are $n \times n$ matrices, the model contains besides the fixed sources $G_0 E$ the switching sources $\sum_{i=1}^m G_i u_i E$.

Let $x^* \in \mathbb{R}^n$ be an admissible equilibrium point of the switched power converters described in (1.11) that is x^* satisfies

$$0 = (J_0 + \sum_{i=1}^m J_i u_i^* - R) \nabla H(x^*) + (G_0 + \sum_{i=1}^m G_i u_i^*) E \tag{1.13}$$

for some $u^* \in \mathbb{R}^m$. The nonlinear incremental model of the system for the output $y = \mathcal{C}x$, where

$$\mathcal{C} = \begin{bmatrix} E^T G_1^T - (x^*)^T Q J_1 \\ \vdots \\ E^T G_m^T - (x^*)^T Q J_m \end{bmatrix} Q \in \mathbb{R}^{m \times n} \tag{1.14}$$

is passive. More precisely, the system verifies the dissipation inequality

$$\dot{V} \leq \tilde{y}^T \tilde{u} \tag{1.15}$$

where $\tilde{x} := x - x^*$, $y^* = \mathcal{C}x^*$ and the (positive definite) storage function $V : \mathbb{R}^n \to \mathbb{R}_+$ is given by

$$V(x) = \frac{1}{2} \tilde{x}^T Q \tilde{x} \tag{1.16}$$

This passivity property corresponds to the mapping $\tilde{u} \to \tilde{y}$.

1.2.2 PI stabilization

Consider a switched power converter described by (1.11) in closed loop with the PI controller

$$\begin{aligned} \dot{z} &= -\widetilde{y} \\ u &= -K_p\widetilde{y} + K_i z \end{aligned} \tag{1.17}$$

with $\tilde{y} = \mathcal{C}\tilde{x}$ and $\mathcal{C}$ given by (1.14), and $K_p = K_p^T > 0$, $K_i = K_i^T > 0$ and x^*, u^* satisfying (1.13). For all initial conditions $(x(0), z(0)) \in \mathbb{R}^{n+m}$ the trajectories of the closed loop system are bounded and such that

$$\lim_{t\longrightarrow\infty} \tilde{y}_a(t) = 0$$

where y_a is an augmented "output signal" defined as

$$\widetilde{y}_a := \begin{bmatrix} \mathcal{C} \\ RQ \end{bmatrix} \widetilde{x} \tag{1.18}$$

Moreover

$$\lim_{t\longrightarrow\infty} x(t) = x^*$$

if $\widetilde{y}_a$ is detectable, that is, if for any solution x(t) of the closed loop system the following implication is true:

$$\tilde{y}_a(t) \equiv 0 \Longrightarrow \lim_{t\longrightarrow\infty} x(t) = x^*$$

The proof is given in [39]. In this thesis (chapter 3) we will show that the I&I approach of [37] described in the next section, can be used to design an asymptotically convergent reduced order observer for a well–defined class of power converters, which is characterized by a simple linear matrix inequality (LMI). Moreover, we will prove that the I&I observer combined with the PI controller preserve the GAS properties of the closed–loop.

1.3 Immersion and invariance approach

In this section a brief introduction of the main ideas of I&I are illustrated, the I&I framework to solve stabilisation and adaptive control problems is presented after, then the observer design for general nonlinear systems based on I&I is shown [37].

1.3.1 Immersion and invariance principle

I&I is a new method for designing nonlinear and adaptive controllers for (uncertain) nonlinear systems. The method relies upon the notions of system immersion and manifold invariance, which are classical tools from nonlinear regulator theory and geometric nonlinear control, but are used in the present work from a new perspective. We call the new methodology immersion and invariance (I&I). The basic idea of the I&I approach is to

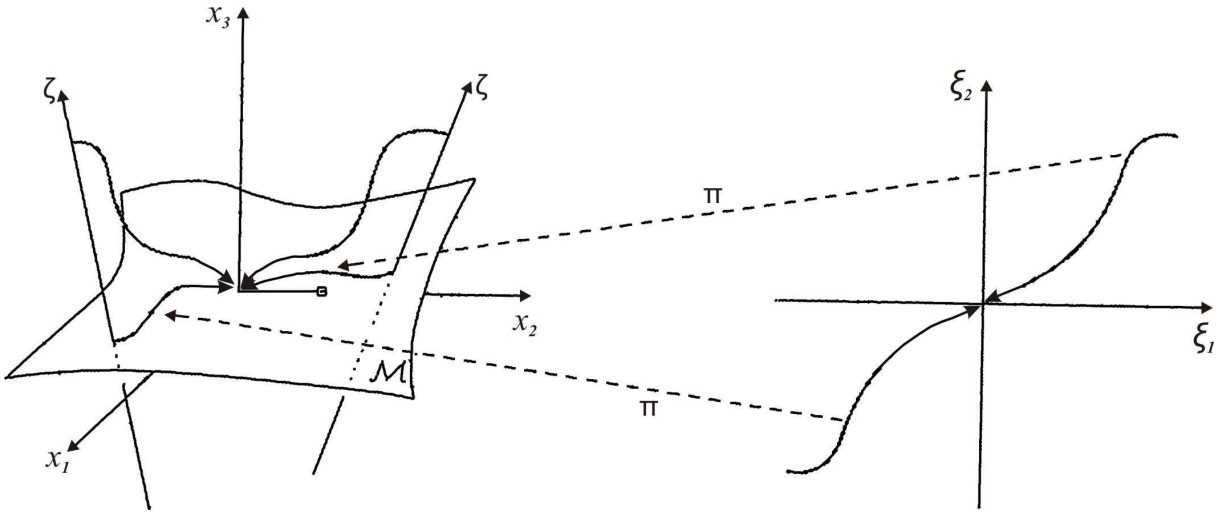

Figure 1.13: Graphical illustration of the immersion and invariance approach.

achieve the control objective by immersing the plant dynamics into a (possibly lower-order) target system that captures the desired behavior.

A graphical illustration of the I&I approach is given in Fig. 1.13. Observe that $\pi(.)$ maps a trajectory on the ξ-space to a trajectory on the x-space, which is restricted to the manifold $\mathcal{M}$ containing the origin. Moreover, all trajectories starting outside $\mathcal{M}$ converge to the origin.

The basic result for I&I stabilisation, namely a set of sufficient conditions for the construction of globally asymptotically stabilising, static, state feedback control laws for general, control affine, nonlinear systems is given in the next theorem.

Theorem 1.1. *Consider the system*

$$\dot{x} = f(x) + g(x)u \tag{1.19}$$

with $x \in \mathbb{R}^n$, $u \in \mathbb{R}^m$, and an equilibrium point $x^* \in \mathbb{R}^n$ to be stabilised. Assume that there exist smooth mappings $\alpha : \mathbb{R}^p \longrightarrow \mathbb{R}^p$, $\pi : \mathbb{R}^p \to \mathbb{R}^n$, $\phi : \mathbb{R}^n \longrightarrow \mathbb{R}^{n-p}$, $c : \mathbb{R}^p \longrightarrow \mathbb{R}^m$ and $v : \mathbb{R}^{n\times(n-p)} \longrightarrow \mathbb{R}^m$, with $p < n$, such that the following hold.

(A1) The target system

$$\dot{\xi} = \alpha(\xi) \tag{1.20}$$

with $\xi \in \mathbb{R}^p$ has a globally asymptotically stable equilibrium at $\xi^* \in \mathbb{R}^p$ and

$$x^* = \pi(\xi^*)$$

.

(A2) For all $\xi \in \mathbb{R}^p$,

$$f(\pi(\xi)) + g(\pi(\xi))c(\pi(\xi)) = \frac{\partial \pi}{\partial \xi}\alpha(\xi). \tag{1.21}$$

(A3) The set identity

$$\{x \in \mathbb{R}^n \,|\phi(x) = 0\} = \{x \in \mathbb{R}^n \,|x = \pi(\xi)\ , \xi \in \mathbb{R}^p\} \tag{1.22}$$

holds.

(A4) All trajectories of the system

$$\dot{z} = \frac{\partial \phi}{\partial x}(f(x) + g(x)v(x,z)), \tag{1.23}$$

$$\dot{x} = f(x) + g(x)v(x,z), \tag{1.24}$$

are bounded and (1.23) *has a uniformly globally asymptotically stable equilibrium at* $z = 0$. *Then* x^* *is a globally asymptotically stable equilibrium of the closed-loop system*

$$\dot{x} = f(x) + g(x)v(x,\phi(x)). \tag{1.25}$$

The proof of this theorem is given in [37].

1.3.2 Parameters estimation using I&I

Consider again the system (1.19), where the functions $f(.)$ and $g(.)$ depend on an unknown parameter vector $\theta \in \mathbb{R}^q$, and the problem of finding, whenever possible, an adaptive state feedback control law of the form

$$\begin{aligned} \dot{\hat{\theta}} &= w(x,\hat{\theta}), \\ u &= v(x,\hat{\theta}), \end{aligned} \tag{1.26}$$

such that all trajectories of the closed-loop system (1.19), (1.26) are bounded and $\lim\limits_{t\longrightarrow\infty} x(t) = x^*$. To this end, it is natural to assume that a full-information control law (that depends on θ) is known, i.e., that the following stabilisability condition holds.

Assumption 1.1. *There exists a function* $v(x,\theta)$, *where* $\theta \in \mathbb{R}^q$, *such that the system*

$$\dot{x} = f(x) + g(x)v(x,\theta) \tag{1.27}$$

has a globally asymptotically stable equilibrium at $x = x^*$. *The I&I adaptive control problem is then formulated as follows.*

Definition 1.1. *The system* (1.19) *with assumption 1.1, is said to be adaptively I&I stabilizable if there exist* $\beta(.)$ *and* $w(.)$ *such that all trajectories of the extended system*

$$\begin{aligned} \dot{x} &= f(x) + g(x)v(x,\hat{\theta} + \beta(x)), \\ \dot{\hat{\theta}} &= w(x,\hat{\theta}) \end{aligned} \tag{1.28}$$

are bounded and satisfy

$$\lim_{t\longrightarrow\infty} \Big[g(x(t))v(x(t),\hat{\theta}(t) + \beta(x(t))) - g(x(t))v(x(t),\theta)\Big] = 0. \tag{1.29}$$

Note that for all trajectories staying on the manifold

$$\mathcal{M} = \left\{ (x, \hat{\theta}) \in \mathbb{R}^n \times \mathbb{R}^q \,\middle|\, \hat{\theta} - \theta + \beta(x) = 0 \right\}$$

condition (1.28) holds. Moreover, by Definition 1.1 and Assumption 1.1, adaptive $I\&I$ stabilisability implies that

$$\lim_{t \longrightarrow \infty} x(t) = x^*. \tag{1.30}$$

1.3.3 Construction of the I&I nonlinear observer

The problem of constructing observers for nonlinear systems has received a great deal of attention due to its importance in practical applications, where some of the states may not be available for measurement. In the case of linear systems a complete theory on asymptotic (reduced-order) observers can be found in [9], while an observer with finite-time convergence has been developed in [10]. The classical approach to nonlinear observer design consists in finding a transformation that linearises the plant up to an output injection term and then applying standard linear observer design techniques. The existence of such a transformation, however, relies on a set of stringent assumptions [11], [12] which are hard to verify in practice. Lyapunov-like conditions for the existence of a nonlinear observer with asymptotically stable error dynamics have been given in [13]. An observer for uniformly observable nonlinear systems in canonical form has been developed in [14],[15],[16], based on a global Lipschitz condition and a gain assignment technique. Some extensions of this result, which avoid the transformation to canonical form and allow for more flexibility in the selection of the observer gain, have been proposed in [17]. More recently, in [18] conditions for the existence of a linear observer with a nonlinear output map have been given in terms of the local solution of a partial differential equation (PDE), thus extending LuenbergerŠs early ideas [19], [20] to the nonlinear case.

In this section the general framework for constructing globally convergent (reduced-order) observers for classes of nonlinear systems is presented. Instrumental to this development is to formulate the observer design problem as a problem of rendering invariant and attractive an appropriately selected manifold in the extended state-space of the plant and the observer.

In the $I\&I$ approach the manifold, which (as in the adaptive case) is parameterised by a function β, is rendered invariant by a nonlinear filter and attractive by a proper selection of the function β.

We consider nonlinear, time-varying systems described by equations of the form:

$$\begin{aligned} \dot{\eta} &= f_1(\eta, y, t) \\ \dot{y} &= f_2(\eta, y, t) \end{aligned} \tag{1.31}$$

where $\eta \in \mathbb{R}^n$ is the unmeasured part of the state and $y \in \mathbb{R}^m$ is the measurable part of the state. It is assumed that the vector fields $\mathrm{f}_1(.)$ and $\mathrm{f}_2(.)$ are forward complete, i.e., trajectories starting at time t_0 are defined for all times $\mathrm{t} \geq \mathrm{t}_0$.

Definition 1.2. *The dynamical system:*

$$\dot{\xi} = \alpha(\xi, y, t) \tag{1.32}$$

with $\xi \in \mathbb{R}^p$, is called an observer for the system (1.31)*, if there exist mappings $\beta : \mathbb{R}^p \times \mathbb{R}^m \times \mathbb{R} \to \mathbb{R}^p$ and $\phi : \mathbb{R}^n \times \mathbb{R}^m \times \mathbb{R} \to \mathbb{R}^p$ that are leftinvertible and such that the manifold*

$$\mathcal{M} = \{(\eta, y, \xi, t) \in \mathbb{R}^n \times \mathbb{R}^m \times \mathbb{R}^p \times \mathbb{R} \ : \ \beta(\xi, y, t) = \phi(\eta, y, t)\} \tag{1.33}$$

has the following properties.

(i) All trajectories of the extended system (1.31), (1.32) *that start on the manifold $\mathcal{M}$ remain there for all future times, i.e., $\mathcal{M}$ is positively invariant.*

(ii) All trajectories of the extended system (1.31), (1.32) *that start in a neighbourhood of $\mathcal{M}$ asymptotically converge to $\mathcal{M}$. The above definition implies that an asymptotically converging estimate of the state η is given by*

$$\hat{\eta} = \phi^L(\beta(\xi, y, t), y, t)$$

where ϕ^L denotes a left-inverse of ϕ. Note that the state estimation error $\hat{\eta} - \eta$ is zero on the manifold $\mathcal{M}$. Moreover, if the property (ii) holds for any $(\eta(t_0), y(t_0), \xi(t_0), t_0) \in \mathbb{R}^n \times \mathbb{R}^m \times \mathbb{R}^p \times \mathbb{R}$ then (1.32) *is a global observer for the system* (1.31)*.*

A general tool for constructing nonlinear (reducedorder) observers of the form given in Definition 1.2 is given:

Theorem 1.2. *Consider the system* (1.31), (1.32) *and suppose that there exist $\mathcal{C}^1$ mapping $\beta(\xi, y, t) : \mathbb{R}^p \times \mathbb{R}^m \times \mathbb{R} \to \mathbb{R}^p$ and $\phi(\eta, y, t) : \mathbb{R}^n \times \mathbb{R}^m \times \mathbb{R} \to \mathbb{R}^p$, with a left inverse $\phi^L : \mathbb{R}^p \times \mathbb{R}^m \times \mathbb{R} \to \mathbb{R}^n$, such that the following hold.*
(A1) For all y, ξ and t, $\beta(\xi, y, t)$ is left-invertible with respect to ξ and

$$det(\frac{\partial \beta}{\partial \xi}) \neq 0$$

(A2) The system

$$\begin{aligned} \dot{z} = &- \frac{\partial \beta}{\partial y}(f_2(\hat{\eta}, y, t) - f_2(\eta, y, t)) + \frac{\partial \phi}{\partial y}\Big|_{\eta=\hat{\eta}} f_2(\hat{\eta}, y, t) - \frac{\partial \phi}{\partial y} f_2(\eta, y, t) + \\ &\frac{\partial \phi}{\partial \eta}\Big|_{\eta=\hat{\eta}} f_1(\hat{\eta}, y, t) - \frac{\partial \phi}{\partial \eta} f_1(\eta, y, t) + \frac{\partial \phi}{\partial t}\Big|_{\eta=\hat{\eta}} - \frac{\partial \phi}{\partial t}, \end{aligned} \tag{1.34}$$

Then the system (1.32) *with*

$$\begin{aligned} \alpha(\xi, y, t) = &- (\frac{\partial \beta}{\partial \xi})^{-1}(\frac{\partial \beta}{\partial y} f_2(\hat{\eta}, y, t) + \frac{\partial \beta}{\partial t} - \frac{\partial \phi}{\partial y}\Big|_{\eta=\hat{\eta}} f_2(\hat{\eta}, y, t) - \\ &\frac{\partial \phi}{\partial \eta}\Big|_{\eta=\hat{\eta}} f_1(\hat{\eta}, y, t) - \frac{\partial \phi}{\partial t}\Big|_{\eta=\hat{\eta}}), \end{aligned} \tag{1.35}$$

where $\hat{\eta} = \phi^L(\beta(\xi, y, t), y, t)$ *is a (global) observer for the system* (1.31).

The proof of the theorem 1.2 is also given in [37] where $z = \beta - \phi$ represent the off-the-manifold dynamics. This theorem provides an implicit description of the observer dynamics (1.32) in terms of the mappings $\beta(.)$, $\phi(.)$ and $\phi^L(.)$ which must then be selected to satisfy (A2). (Note, however, that the function $\alpha(.)$ in (1.35) renders the manifold $\mathcal{M}$ invariant for any mappings $\beta(.)$ and $\phi(.)$.) As a result, the problem of constructing an observer for the system (1.31) is reduced to the problem of rendering the system (1.34) asymptotically stable by assigning the functions $\beta(.)$,$\phi(.)$ and $\phi^L(.)$.

Chapter 2

Robust Feedback Control of DC-DC Power Converters in Discontinuous Conduction Mode

Contents

In this chapter we are interested in the problem of voltage regulation of power converters operating in discontinuous conducting mode. Two power converters are considered: the boost converter and the buck-boost converter. The system does not admit a (continuous–time) average model approximation, hence is a *bona fide* hybrid system where the control objective is the generation of a periodic orbit and the actuator commands are switching times. Our main contribution is a simple robust algorithm that gives explicit formulas for the switching times without approximations. Simulation and experimental results that illustrate the robustness of the scheme to parameter uncertainty, as well as performance comparisons with current practice, are presented.

2.1 Introduction

Ideal switches in power converters are typically implemented using unidirectional semiconductor devices that may lead to a new operation mode generically called *discontinuous conduction mode* (DCM). The DCM arises when the ripple is large enough to cause the polarity of the signal (current or voltage) applied to the switch to reverse, violating the unidirectionality assumptions made in the realization of the switch. In classical converter topologies DCM appears very frequently in low load operating modes. More interestingly, to achieve high performance some new converters are purposely design to operate all the time in DCM [24].

The converter dynamics are significantly altered in DCM. The existing techniques for controller analysis and design, in particular, the approximations of averaging dynamics (valid under fast switching) or small ripple, are not valid anymore. With the latter approximations the converter can be treated as a continuous (possibly nonlinear) dynamical system, with the action of the switches assimilated to continuous signals ranging in some closed interval, *e.g.*, $[0, 1]$. Readers are referred to the classical reference [23] and the excellent monograph [21] for a detailed explanation of the physical phenomenon and some rules for controller design that rely on some approximations [26], [27]. Neglecting the presence ofthe ripple permits to recast the converter regulation problem as a classical equilibrium stabilization problem for which, by–now standard, nonlinear controller design techniques, *e.g.*, sliding mode [29]-[33] and passivity–based [34]-[36], are directly applicable. In most of these literatures only the CCM operation mode is considered. A method of computation of the time switching instants based on an energy balanced of the boost converter in DCM operation where the ripples are considered was proposed in [28]. In this strategy the switching instants are chosen so the total energy change is zero. The calculation needed are not simple in this strategy, and only simulation results are shown.

In DCM the converter is a *bona fide* hybrid system, which exhibits behaviors of continuous–time and discrete–time dynamical systems. Distinguishing features of converters in DCM include the following.

(i) The control is not a continuous signal, but directly the switches positions, that take values in the binary set $\{0, 1\}$, and decide the commutation among the various converter topologies.

(ii) Due to technological considerations, the activation of the switches is submitted to a minimal dwell time that has to be taken into account in the design.

(iii) Besides the commutations induced by (designer selected) switch positions, there are forced commutations due to the aforementioned violation of the unidirectionality assumption, *e.g.*, the presence of diodes.

(iv) As the ripple cannot be neglected, the control objective is not stabilization of an equilibrium but generation of a periodic orbit (with "minimal amplitude") around the desired operating point.

A burgeoning literature on hybrid systems has emerged in the control community in the last few years, see *e.g.*, [25] for a recent tutorial account. As usual in control theory, the main thrust of the research has been towards the development of general methodologies, mainly for analysis [22] but also for controller design, of classes of theoretically–motivated, hybrid dynamical systems. To the best of our knowledge, none of the existing results reported in the literature is applicable to address the problem at hand.

Motivated by this fact, in this chapter a different perspective is adopted, namely the development of a solution for a specific example of practical relevance. Towards this end, we consider a boost and a buck-boost converter operating in DCM, which exhibits the four distinguishing features discussed above. Our main contribution is a simple robust algorithm that, in contrast with current practice, gives explicit formulas for the switching times without approximations. Although the design relies on the specific topology of the boost and buck-boost converters.

2.2 Mathematical Model and Problem Formulation

Two power converters are considered in this section: the boost and the buck-boost converter given in Figs. 1.4(b), and 1.4(c). The circuits in the three topologies corresponding to the three modes of operations are depicted in Figs. 2.1, and 2.2. These modes depend on the switch position and conduction of the diode as described below. The states are the inductor current x_1 and the capacitor voltage x_2. The dynamics in both cases are described by a piece–wise affine model

$$\dot{x} = A_i x + b_i v_{in},\ i = 1, 2, 3,$$

where the pairs (A_i, b_i) are the system matrix and the input matrix, i=1,2,3 denotes the mode of operation.

In the case of the boost converter: The pairs (A_i, b_i) for the three topologies are given by

$$\Omega_1 : \qquad A_1 = \begin{bmatrix} \frac{-r_L}{L} & \frac{-1}{L} \\ \frac{1}{C} & \frac{-1}{CR_0} \end{bmatrix},\ b_1 = \begin{bmatrix} \frac{1}{L} \\ 0 \end{bmatrix} \tag{2.1}$$

$$\Omega_2 : \qquad A_2 = \begin{bmatrix} 0 & 0 \\ 0 & \frac{-1}{CR_0} \end{bmatrix},\ b_2 = \begin{bmatrix} 0 \\ 0 \end{bmatrix} \tag{2.2}$$

$$\Omega_3 : \qquad A_3 = \begin{bmatrix} \frac{-r_L}{L} & 0 \\ 0 & \frac{-1}{CR_0} \end{bmatrix},\ b_3 = \begin{bmatrix} \frac{1}{L} \\ 0 \end{bmatrix}. \tag{2.3}$$

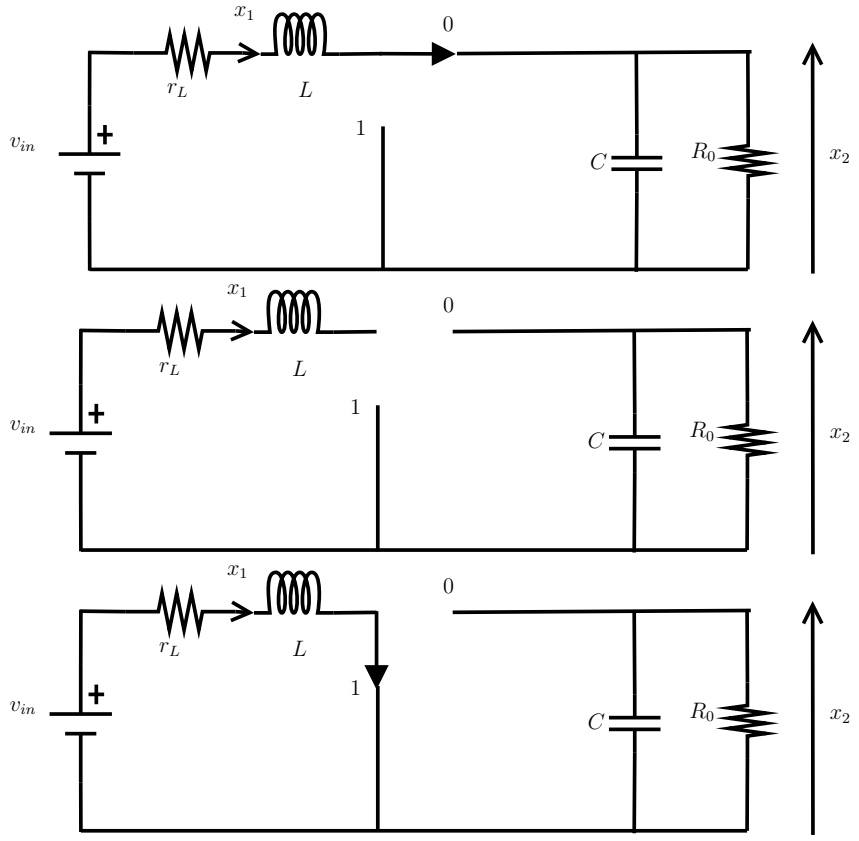

Figure 2.1: Ideal representation of the boost converter in the topologies: Ω_1 (top), Ω_2 (middle) and Ω_3 (bottom).

In the topology Ω_3, when the switch is ON, the external battery $v_{in} \in \mathbb{R}_+$ supplies magnetic energy to the (leaky) inductor L while the electric energy of the capacitor C is discharged in the load, represented here by a resistance R_0. When the switch is OFF and the diode is ON the circuit takes the topology Ω_1, then the energy flows from the inductor to the capacitor, building up its voltage x_2 and achieving the desired amplification. The topology Ω_2 represent the discontinuous conduction mode.

In the case of the buck-boost converter: The pairs (A_i, b_i) for the three topologies are given by

$$\Omega_1 : \qquad A_1 = \begin{bmatrix} \frac{-r_L}{L} & \frac{-1}{L} \\ \frac{1}{C} & \frac{-1}{CR_0} \end{bmatrix}, \; b_1 = \begin{bmatrix} 0 \\ 0 \end{bmatrix} \tag{2.4}$$

$$\Omega_2 : \qquad A_2 = \begin{bmatrix} 0 & 0 \\ 0 & \frac{-1}{CR_0} \end{bmatrix}, \; b_2 = \begin{bmatrix} 0 \\ 0 \end{bmatrix} \tag{2.5}$$

$$\Omega_3 : \qquad A_3 = \begin{bmatrix} \frac{-r_L}{L} & 0 \\ 0 & \frac{-1}{CR_0} \end{bmatrix}, \; b_3 = \begin{bmatrix} \frac{1}{L} \\ 0 \end{bmatrix}. \tag{2.6}$$

In the buckboost conveter Fig.2.2, the inductor gains energy in the topology Ω_3 and the

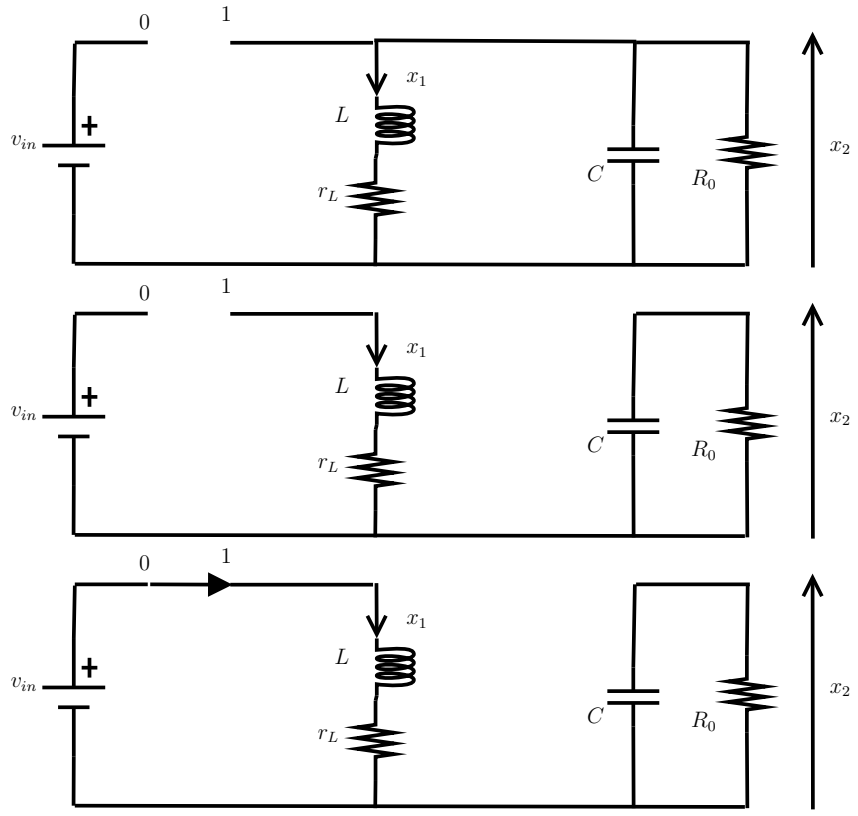

Figure 2.2: Ideal representation of the buck-boost converter in the topologies: Ω_1 (top), Ω_2 (middle) and Ω_3 (bottom).

capacitor loses its energy in the topologies Ω_3 and Ω_2. In the topology Ω_1 the inductor supplies energy to the capacitor.

Both systems evolves in the set $\{x_1 > 0, x_2 > 0\} =: \mathbb{R}^2_+$ for the topologies Ω_1 and Ω_3, while for the topology Ω_2, trajectories are restricted to the set $\{x_1 = 0, x_2 > 0\}$.[1] A typical trajectory in the phase plane $x_1 - x_2$ is shown in Fig. 2.3, where the $t_i \in \mathbb{R}_+$, $i = 1, 2, 3$, denote the time *spent* on each of the topologies.

Due to technological considerations, a minimal dwell time, denoted $t_D \in \mathbb{R}_+$, is imposed to the switch. If t_D is large, with respect to the time constant of the R_0C tank, the inductor current x_1 becomes zero and a forced transition from Ω_1 to Ω_2 is induced. On the other hand, the transitions from Ω_2 to Ω_3 and from Ω_3 to Ω_1, determined by the switch position, are decided by the controller. Of course, these switching transition times should respect the minimal dwell time constraint.

Given t_1—the time it takes for the current to go to zero—the designer has to decide

[1] The possibility of total discharge of the capacitor, *e.g.*, $x_2 = 0$, is ruled out because below a critical value of x_2 the diode starts conducing again commuting to the topology Ω_1 and driving the trajectory inside the positive quadrant.

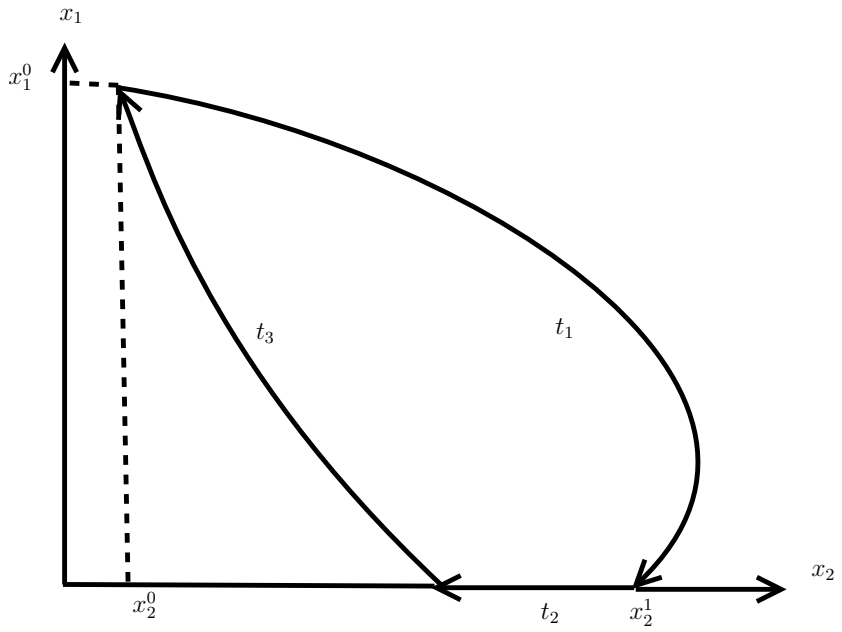

Figure 2.3: Typical periodic orbit in the phase plane.

the switching times t_2 and t_3, which should satisfy the dwell time constraints

$$t_3 \geq t_D, \quad t_1 + t_2 \geq t_D. \tag{2.7}$$

The control objective is to generate an attractive limit cycle (of period $t_1 + t_2 + t_3$) contained in the band

$$x_2(t) \in [x_2^* - \epsilon_1, x_2^* + \epsilon_2],$$

where $x_2^* \in \mathbb{R}_+$ is the desired average value for x_2 and—to minimize the voltage ripple—the constants $\epsilon_i \in \mathbb{R}_+$ are as small as possible. Although the range of values of $x_1(t)$ is not the main concern, for practical reasons, this current is also restricted to satisfy an upperbound $x_1(t) \leq x_1^M$. As discussed below, in the standard approximated algorithms [23, 21], x_1^M is fixed to some given value.

2.3 A Robust Switching Algorithm

The objective of the note is to propose a switching algorithm that guarantees the existence of the desired periodic orbit. That is, the derivation of a rule to compute the switching instants t_3 and t_2.[2] To ensure robustness it should be a feedback strategy—that is, based on measurements of the system state—and should not be very sensitive to variations of the system parameters.

[2] As shown in Section 3.4 this is equivalent to computing the duty ratios for operation in a synchronous mode with a fixed sampling time—as done in [23, 21].

An obvious procedure to compute the switching times relies on the solution of the differential equations along the periodic orbit, which leads to a set of nonlinear algebraic equations that are very hard, if at all possible, to solve. Unfortunately, the implementation of the numerical algorithm is extremely time–consuming, which renders its application practically unfeasible. As explained later in Section 2.9, to obtain explicit formulas in practice the state transition matrices of the LTI systems are approximated by a linear function, that is, $e^{A_i t} \approx I_2 + A_i t$. The approximation induces an error that, in high performance applications, may be inadmissible and, as shown in a simulation below, may even lead to instability. Instrumental to this end are the following key computations, which are carried out along a closed trajectory.

Computation of $t_2 + t_3$. Define the time interval $\mathcal{I}_1 := [t_1, t_1 + t_2 + t_3]$. For all $t \in \mathcal{I}_1$ the capacitor voltage evolves according to

$$\dot{x}_2 = -\frac{1}{CR_0} x_2, \tag{2.8}$$

whose solution is

$$x_2(t) = e^{-\frac{1}{CR_0}(t-s)} x_2(s), \quad \forall t \geq s, \ \forall t, s \in \mathcal{I}_1.$$

Hence, along the orbit depicted in Fig. 2.3 and from Fig. 2.4, one has

$$x_2^0 = e^{-\frac{1}{CR_0}(t_2+t_3)} x_2^1,$$

yielding

$$t_2 + t_3 = R_0 C \ln\left(\frac{x_2^1}{x_2^0}\right). \tag{2.9}$$

Since $x_2^1 > x_2^0$ we have that $t_2 + t_3 > 0$. Furthermore, since x_2^0 is the smallest value of $x_2(t)$ along the periodic orbit, it should be selected to satisfy $x_2^0 < x_2^*$.

Computation of t_3. Define the time interval $\mathcal{I}_2 := [t_1 + t_2, t_1 + t_2 + t_3]$. For all time $t \in \mathcal{I}_2$ the inductor current evolves according to

$$\dot{x}_1 = -\frac{r_L}{L} x_1 + \frac{v_{in}}{L},$$

whose solution with zero initial conditions is

$$x_1(t) = \left(1 - e^{-\frac{r_L}{L} t}\right) \frac{v_{in}}{r_L}, \quad \forall t \in \mathcal{I}_2.$$

Hence, fixing $x_1(t_3) = x_1^0$—again referring to Figs. 2.3 and 2.4—and solving for t_3 yields

$$t_3 = -\frac{L}{r_L} \ln\left(1 - \frac{r_L x_1^0}{v_{in}}\right). \tag{2.10}$$

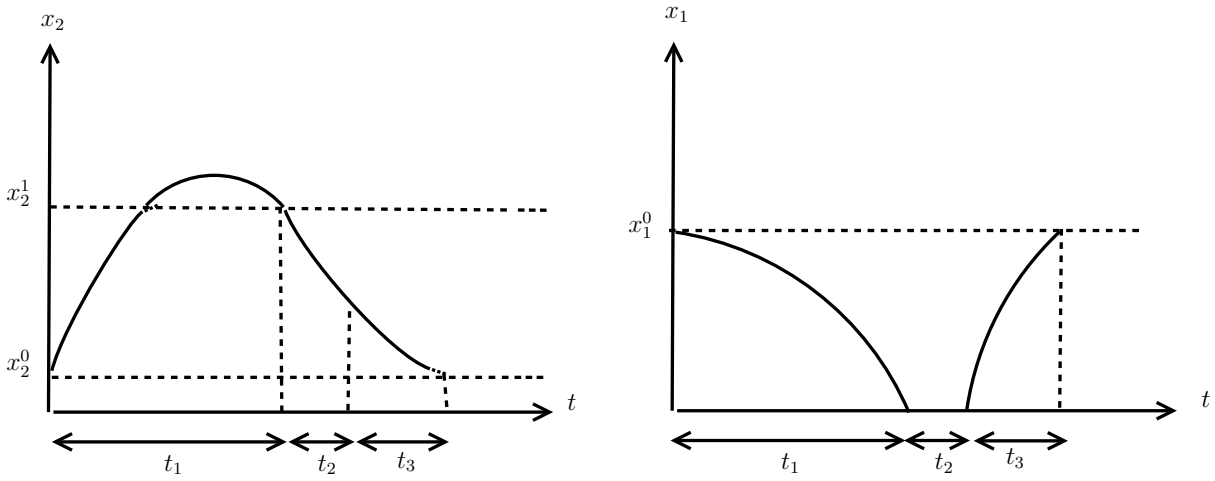

Figure 2.4: Time evolution of $x_1(t)$ and $x_2(t)$ along a periodic orbit.

The time t_3 is also positive, because

$$0 < 1 - \frac{r_L x_1^0}{v_{in}} < 1.$$

Indeed, $x_1^0 > 0$ ensures the upper bound. On the other hand, recall that the equilibrium associated to this topology is $(\frac{v_{in}}{r_L}, 0)$, which is only reached at infinity, hence $x_1^0 < \frac{v_{in}}{r_L}$.

The computations above lead naturally to the following control algorithm.

Step 1. Fix a point $(x_1^0, x_2^0) \in \mathbb{R}^2_+$, such that t_3 in (2.10) yields $t_3 \geq t_D$ and $x_2^0 < x_2^*$.
Step 2. At a time $t_0 \geq 0$ when $x(t_0) = (x_1^0, x_2^0)$ switch from $u = 0$ to $u = 1$.
Step 3. Wait (in mode Ω_1) until $x_1(t) = 0$ and measure the corresponding x_2^1.
Step 4. Compute $t_2 + t_3$ from (2.9). If $t_2 > 0$ go to Step 5, else define $t_2 := t_D - t_1$, then go to Step 5.
Step 5. Wait (in mode Ω_2) for t_2 units of time and then switch from $u = 1$ to $u = 0$.
Step 6. Wait (in mode Ω_3) for t_3 units of time and then measure the state, call it (x_1^0, x_2^0). Check whether, for the new (x_1^0, x_2^0), (2.10) yields $t_3 \geq t_D$ and $x_2^0 < x_2^*$. If so, go to Step 2, else wait for a longer time until the state meets the requirements, then assign the value t_3 to this new time and go to Step 2.

As indicated in the introduction, in normal operation the circuit operates in DCM, hence Step 3 will, in general, yield $t_2 > 0$. Also, it is clear that, in ideal conditions, when the parameters are exactly known and there are no disturbances, the point (x_1^0, x_2^0) obtained in Step 6 will coincide with the initial point. However, in practice there will be a discrepancy, hence the need to recompute the switching times as a function of the measurements. Finally, regarding Step 6, in the topology Ω_3, $x_2(t)$ decreases (tending

to converge to zero) and $x_1(t)$ increases towards $\frac{v_{in}}{r_L}$—both evolutions being monotonic. Consequently, there is indeed a (sufficiently long) time such that the new values of the state guarantee that (2.10) yields $t_3 \geq t_D$ and $x_2^0 < x_2^*$.

2.4 Estimation of the Time Constants

The computations involved in (2.9) and (2.10) are extremely simple, and can be programmed with a few lines of code. Moreover, they only depend on the input voltage, which is reasonable to assume known, and the time constants $\frac{r_L}{L}$ and CR_0. The algorithm can be robustified *vis–à–vis* uncertainty in the time constants incorporating an adaptation stage.

Let us illustrate a simple way to estimate the parameter CR_0. As explained above, during the interval $\mathcal{I}_1$, $x_2(t)$ satisfies (2.8). Discretizing this equation with a (fast) sampling time[3] T_f yields the difference equation

$$x_2(k) = \theta x_2(k-1), \quad \theta := e^{-\frac{1}{CR_0}T_f},$$

where the standard notation

$$x_2(k) = x_2(t), \quad \forall\, t \in ((k-1)T_f, kT_f],$$

with $k \in \mathbb{Z}_+$, is used. Now, sample $x_2(t)$ with the sampling rate $T_f \in \mathbb{R}_+$ and take N samples, where $N := \lfloor \frac{t_2+t_3}{T_f} \rfloor$, with $\lfloor \cdot \rfloor$ the floor operator that takes the largest previous integer. Define the N–dimensional vectors

$$X_2 := \mathrm{col}(x_2(1), \ldots, x_2(N)), \quad \Phi := \mathrm{col}(x_2(0), \ldots, x_2(N-1)).$$

Since $X_2 = \theta\Phi$, it is clear that θ can be computed from

$$\theta = \frac{1}{|\Phi|^2}\Phi^\top X_2, \tag{2.11}$$

with $|\cdot|$ the Euclidean norm. Note that $|\Phi|$ is bounded away from zero because $x_2(t) \in \mathbb{R}_+$. From the knowledge of θ the time constant CR_0 is directly obtained.

Since Φ is a shifted version of X_2 the rule (2.11) can be easily implemented in firmware. The parameter estimation algorithm need not be repeated in every period, but only when performance degradation is detected. Finally, it is obvious that a similar procedure is possible to estimate the second time constant $\frac{r_L}{L}$, and eventually also v_{in}, but they are omitted for brevity.

[3] Clearly, T_f should be selected much smaller that $t_2 + t_3$.

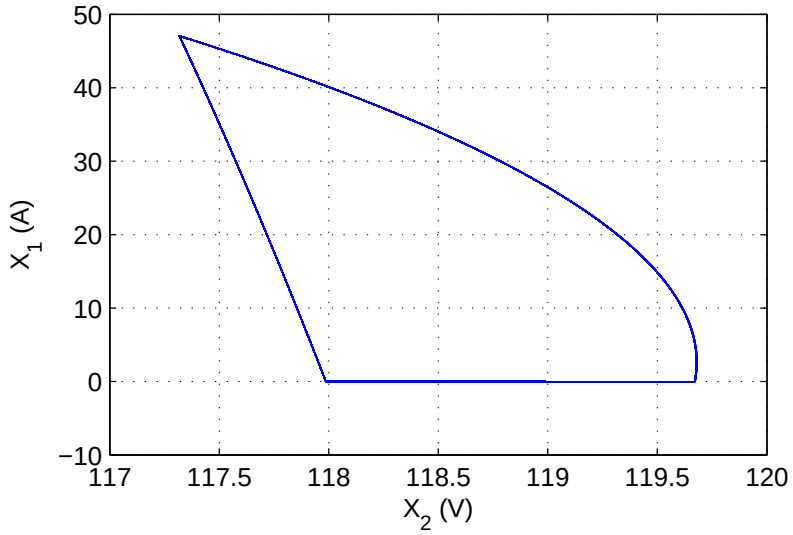

Figure 2.5: The periodic orbit in the phase plane with $R_0 = 45.5\Omega$.

2.5 Simulations Results

The usefulness of the proposed control scheme was evaluated through numerical simulations. The considered circuit parameters for the boost converter are:

$$L = 0.00015H,\ R_0 = 45.5\Omega,\ r_L = 0.066\Omega,\ C = 0.00077F$$

Simulations were developed in Matlab using the circuit toolbox Simpower systems. In Fig. 2.5 the periodic orbit obtained via the application of the algorithm is depicted. The same simulation was repeated with a 100% change the in the load resistance—whose behavior is depicted in Fig. 2.6. In this case the algorithm generates a shifted periodic orbit.

Figs. 2.7 shows the result of the simulation when a *step* in the value of the load resistance R_o occur in the nonadaptive case. Notice that the value of the regulated voltage exhibits an undesirable shift. On the other hand, in Figs. 2.8 we show the behavior of the adaptive algorithm, which estimates (almost instantaneously) the new value of R_o. It is observed that the output voltage exhibits an overshoot, but it quickly settles around the value of x_2^*. The application of the adaptive algorithm, detect the change in the value of R_o and correct the performance degradation.

For the buk-boost converter the simulations are done with these circuit parameters: $L = 0.000047H$, $R_0 = 100\Omega$, $r_L = 0.05\Omega$ and $C = 0.0000033F$. Similarly, figs. 2.9 shows the result of the simulation when a *step* in the value of the load resistance R_o occur in the nonadaptive case and figs. 2.10 shows the behavior of the adaptive algorithm, which estimates (almost instantaneously) the new value of R_o.

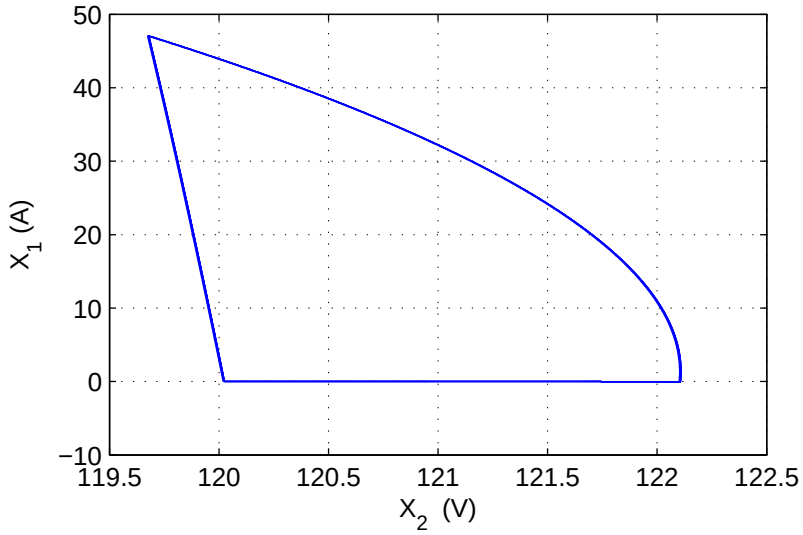

Figure 2.6: The shifted periodic orbit in the phase plane in the case of load change to $R_0 = 91\Omega$.

2.6 Experimental system

In order to test the proposed control strategy, an experimental system was built with the boost converter. Experiments were carried out in a setup located in the universitat Politècnica de Catalunya UPC. Boost converter was designed and tested using the following system parameters:

$$L = 0.00015H,\ R_0 = 45.5\Omega,\ r_L = 0.066\Omega,\ C = 0.00077F$$

The experimental card was assembled using low cost commercial electronic elements placed on a card designed in the laboratory. In Fig. 2.11 we show the diagram of the experimental set-up, consisting of the boost circuit card that receives control signals from the Digital Signal Processor (DSP) TMS320-F28335 from Texas Instruments. The DSP card acquires, using an analog to digital converter integrated in the chip, the capacitor voltage and inductor current signals previously conditioned from the boost converter. Two DC power supplies are necessary to operate the whole system, one to provide energy to the system, and the other one to feed the electronic parts of the card.

2.7 Experimental Results

Tests were performed in order to evaluate the usefulness of the proposed control scheme. Waveforms were captured using a DL1640 YOKOGAWA model oscilloscope.

Fig.2.12(a) shows the evolution of the voltage and the current via the application of the algorithm with $R_o = 45.5\ \Omega$. Three traces were captured where the upper trace

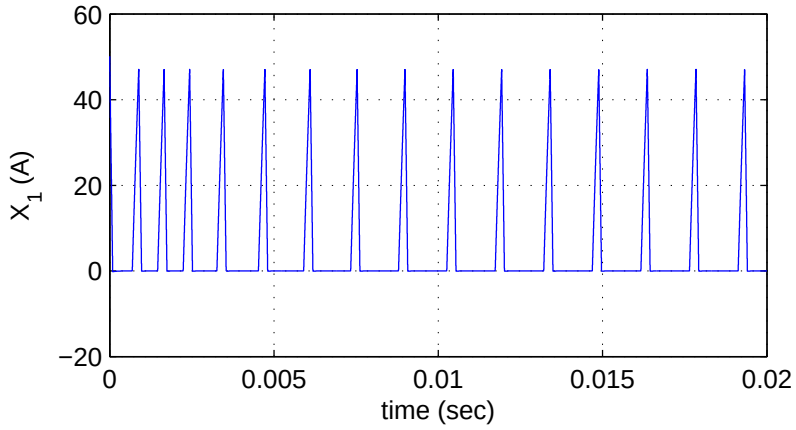

(a)

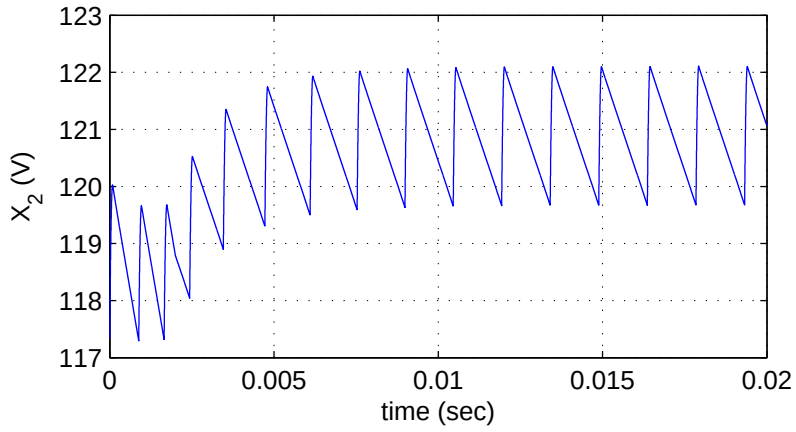

(b)

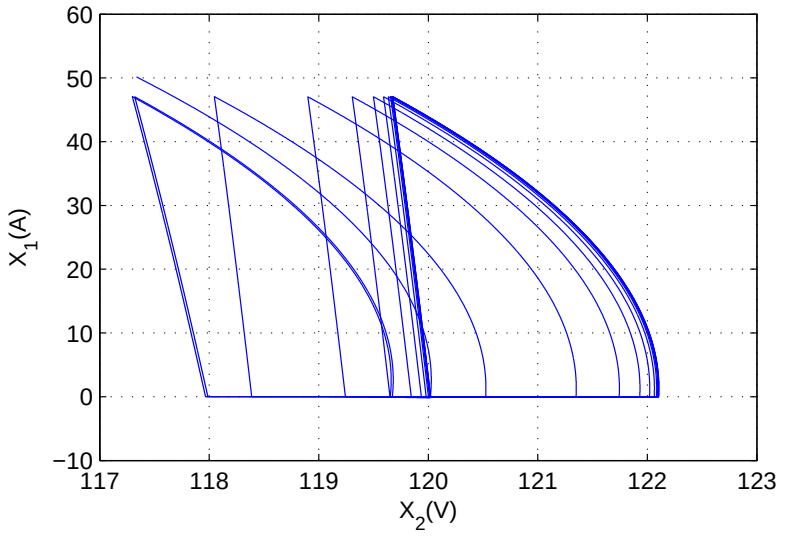

(c)

Figure 2.7: (a) Time evolution of $x_1(t)$ for the simulation with a step variation in R_0, (b) The corresponding time evolution of $x_2(t)$, (c) The corresponding orbit in the phase plane.

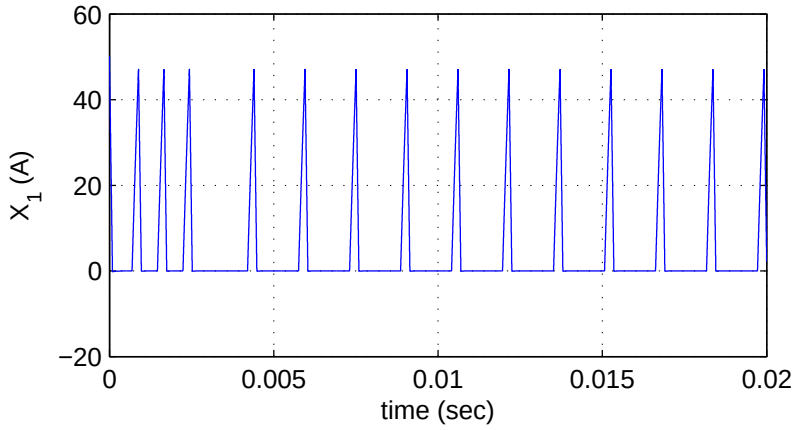

(a)

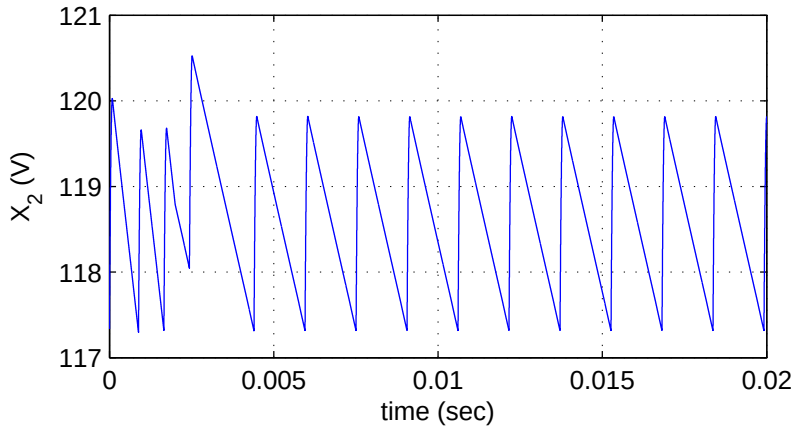

(b)

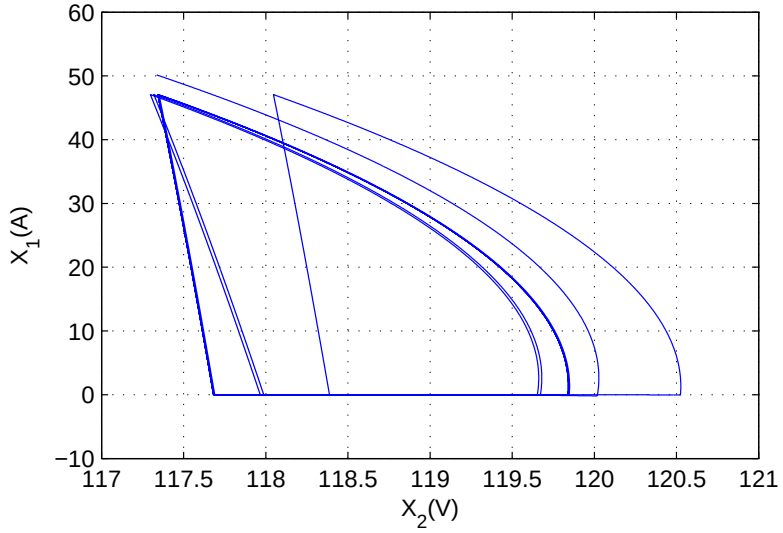

(c)

Figure 2.8: (a) Time evolution of $x_1(t)$ for the simulation in the case of the adaptive algorithm, (b) The corresponding time evolution of $x_2(t)$, (c) The corresponding orbit in the phase plane.

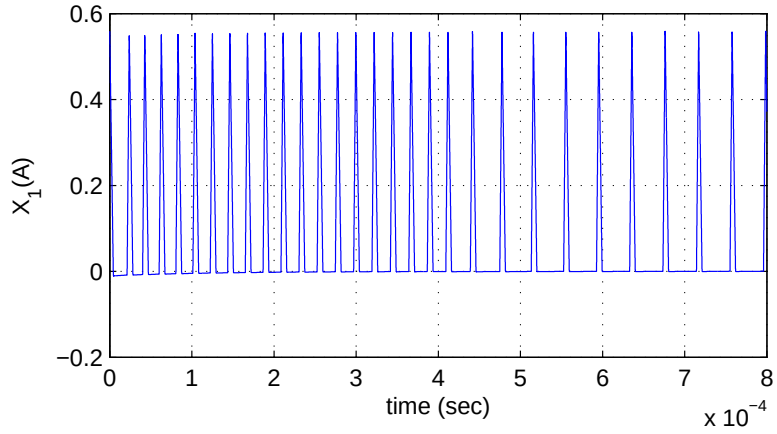

(a)

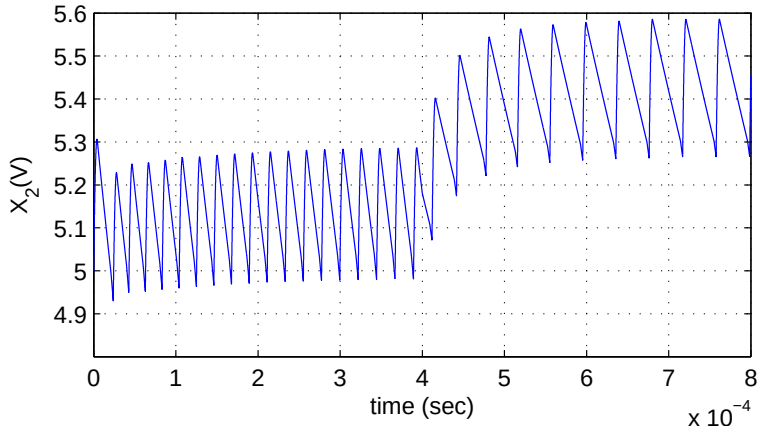

(b)

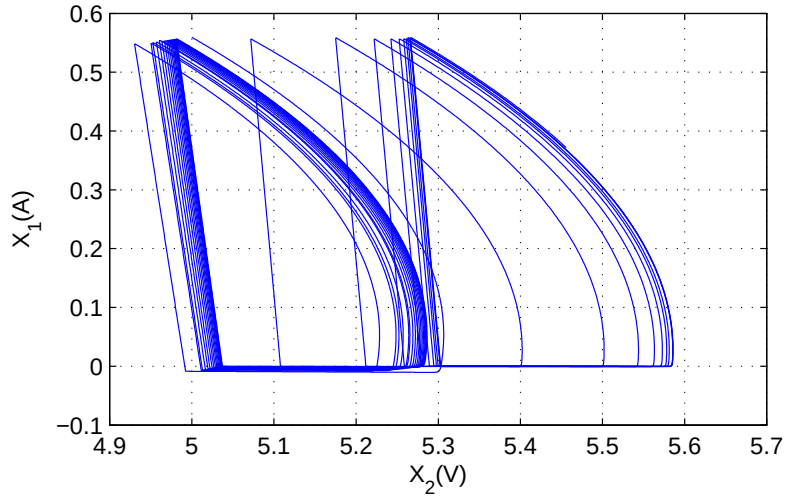

(c)

Figure 2.9: (a) Time evolution of $x_1(t)$ for the simulation with a step variation in R_0, (b) The corresponding time evolution of $x_2(t)$, (c) The corresponding orbit in the phase plane.

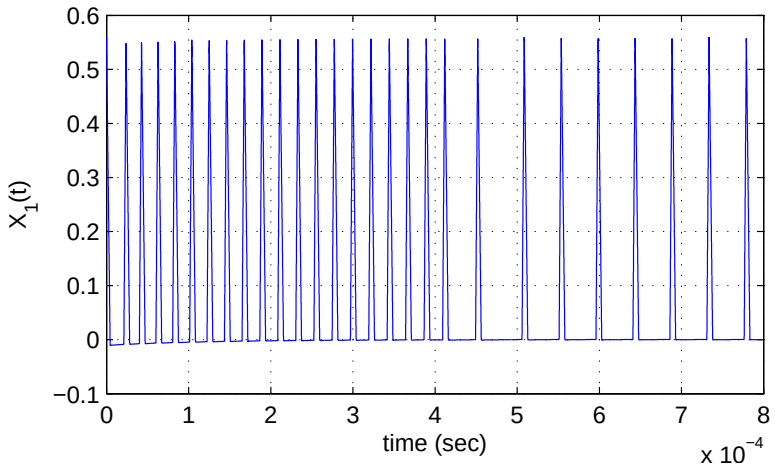

(a)

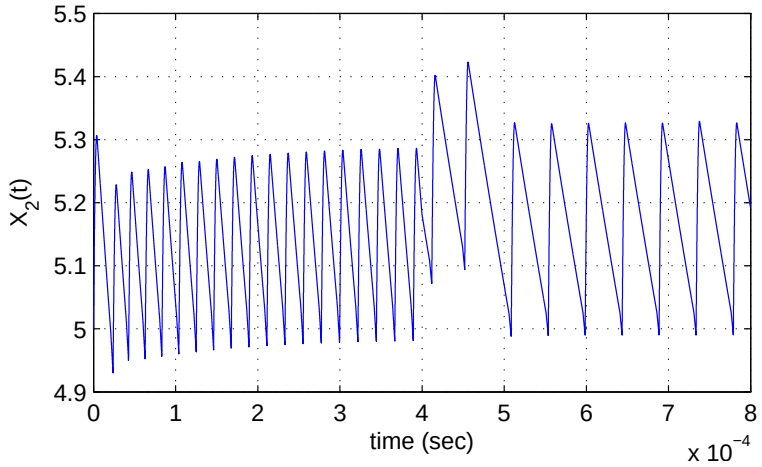

(b)

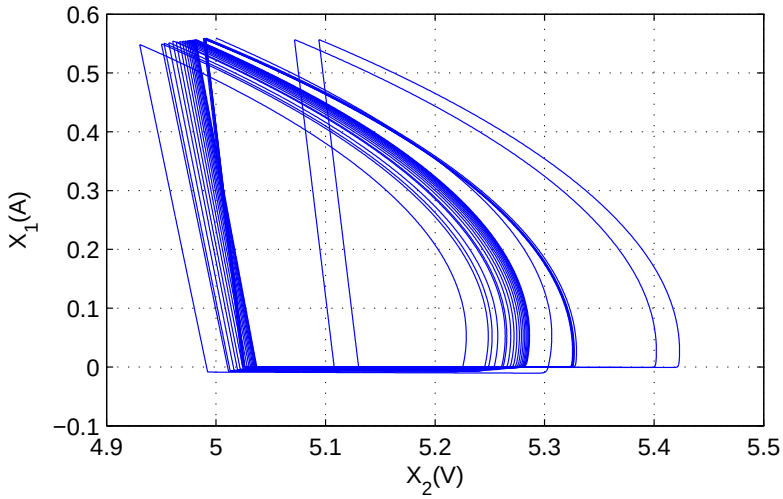

(c)

Figure 2.10: ((a) Time evolution of $x_1(t)$ for the simulation in the case of the adaptive algorithm, (b) The corresponding time evolution of $x_2(t)$, (c) The corresponding orbit in the phase plane.

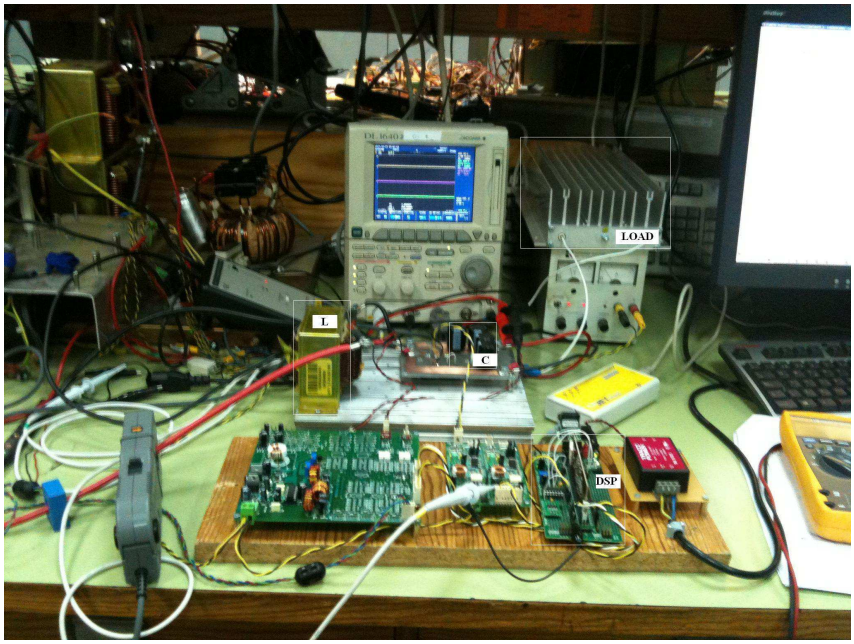

Figure 2.11: Experimental prototype of a boost converter

represented $x_2(t)$ in dc mode followed down by $x_2(t)$ in ac mode, and ending with the last trace that presents the the inductor current $x_1(t)$. In Fig. 2.12(b) the desired periodic orbit obtained with $R_o = 45.5\ \Omega$ is depicted. Fig.2.13(a) shows the time evolution of the voltage and the current obtained with $R_o = 91\ \Omega$. In Fig. 2.13(b) the corresponding shifted periodic orbit is depicted.

To test the robustness of the algorithm, the same experiment was repeated with a step change the in the load resistance from $R_o = 45.5\ \Omega$ to $R_o = 91\ \Omega$ whose behavior is depicted in Fig. 2.14. Notice that the value of the regulated voltage exhibits an undesirable shift. On the other hand, in Figs. 2.15 we show the behavior of the adaptive algorithm, which estimates (almost instantaneously) the new value of R_o, avoiding the performance degradation. A step change the in the load resistance from $R_o = 91\ \Omega$ to $R_o = 45.5\ \Omega$ is shown in Figs. 2.16. Fig. 2.17 present the behavior of the adaptive algorithm in this case. The estimation of the value of R_o is depicted in Fig. 2.18.

2.8 Approximation method

In the approximate method of [23] the equations for the three topologies of the boost, namely,

$$\begin{cases} \dot{w} = A_1 w + b_1 v_{in} & 0 \le t \le t_1 \\ \dot{y} = A_2 y + b_2 v_{in} & t_1 \le t \le t_1 + t_2 \\ \dot{z} = A_3 z + b_3 v_{in} & t_1 + t_2 \le t \le t_1 + t_2 + t_3 \end{cases}$$

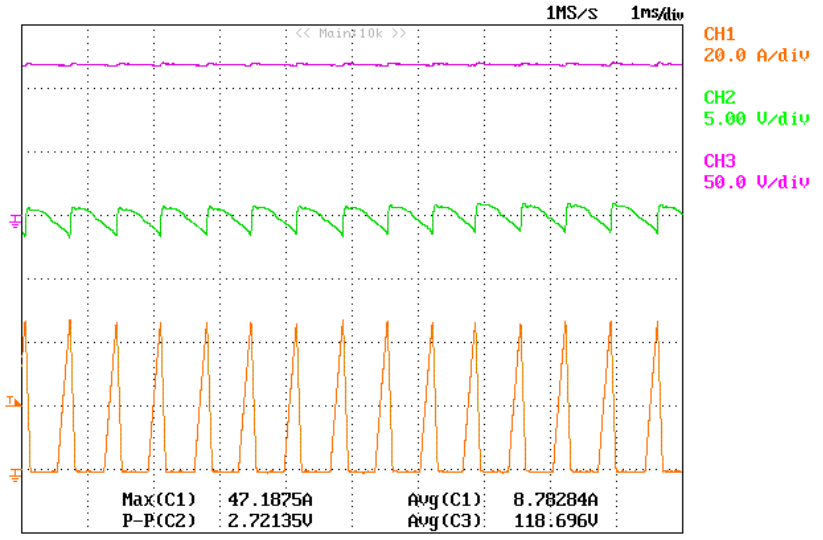

(a)

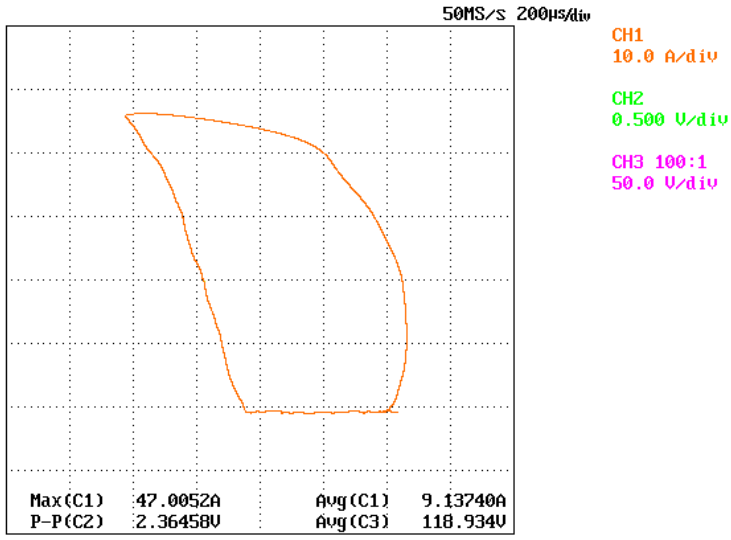

(b)

Figure 2.12: Operation with R_o= 45.5 Ω: (a) $x_2(t)$ in dc mode (top), $x_2(t)$ in ac mode (middle) and $x_1(t)$ (bottom), (b) The periodic orbit in the phase plane.

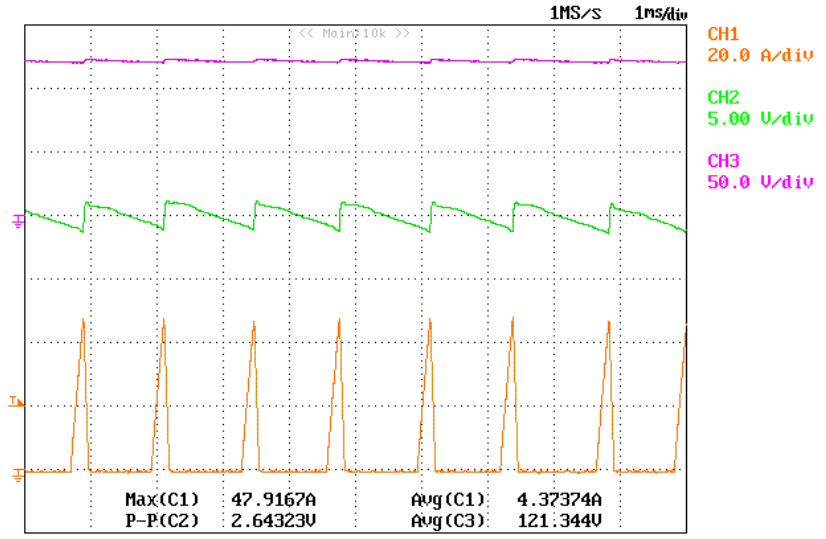

(a)

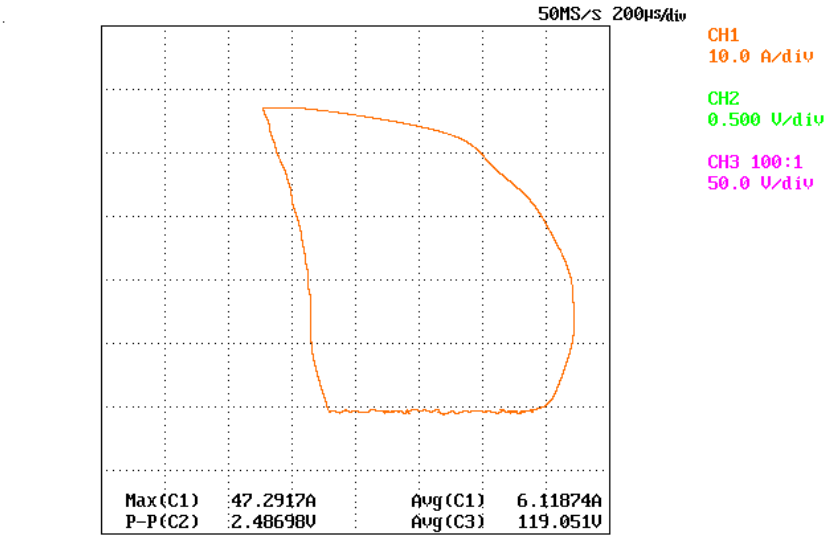

(b)

Figure 2.13: Operation with R_o= 91 Ω: (a) $x_2(t)$ in dc mode (top), $x_2(t)$ in ac mode (middle) and $x_1(t)$ (bottom), (b) The periodic orbit in the phase plane.

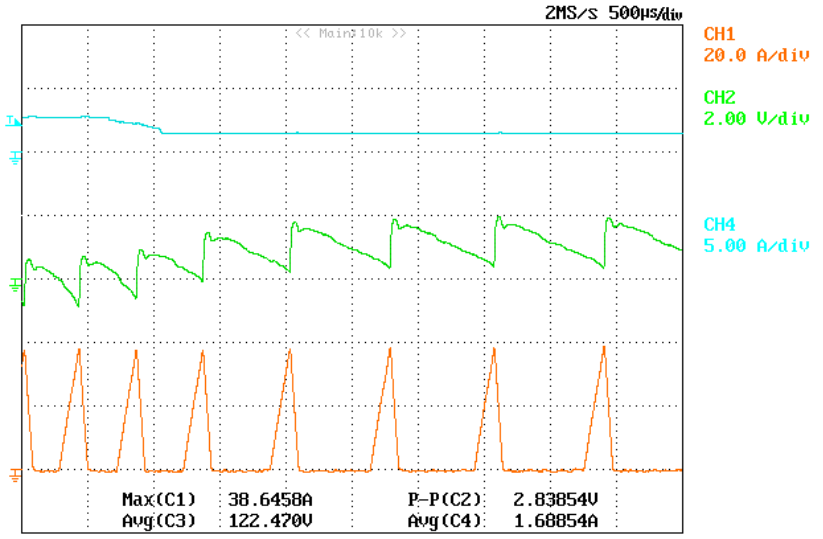

(a)

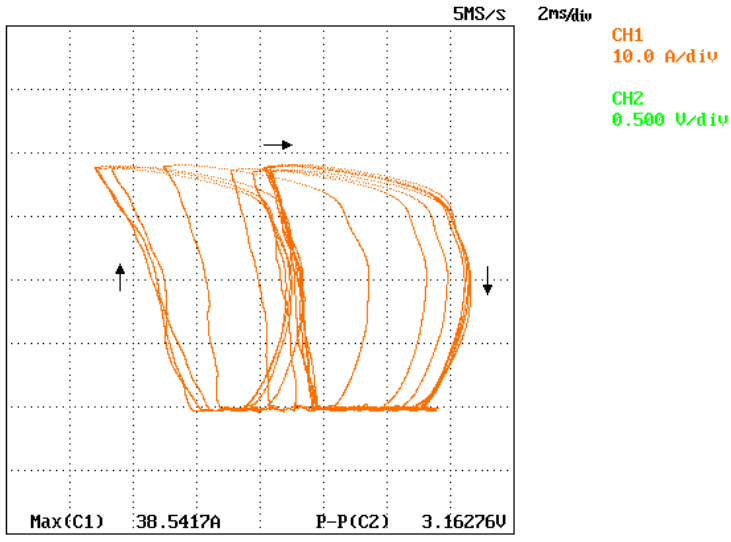

(b)

Figure 2.14: Load change from R_o= 45.5 to 91 Ω without estimation: (a) i_R (top), $x_2(t)$ in ac mode (middle) and $x_1(t)$(bottom), (b) The corresponding orbit in the phase plane.

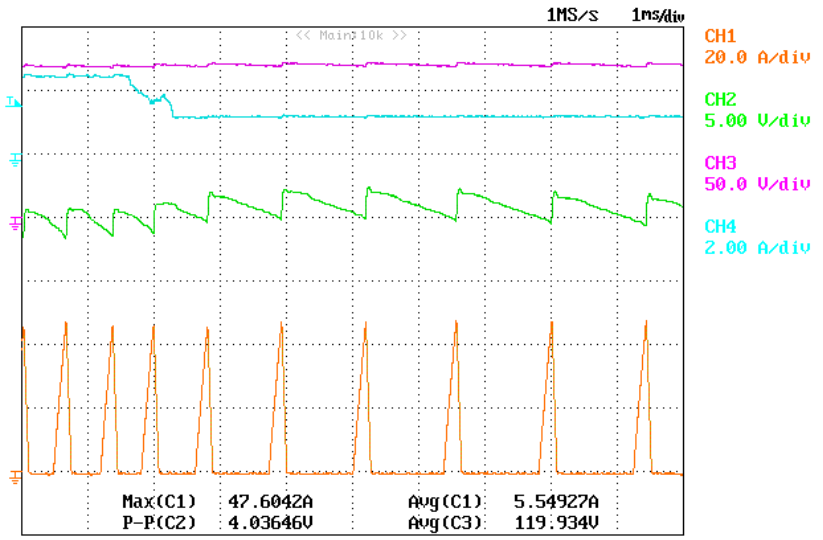

(a)

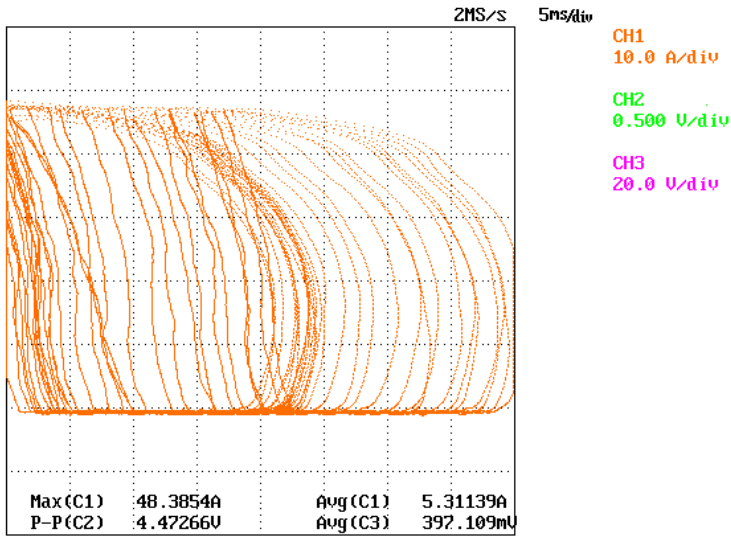

(b)

Figure 2.15: Load change from R_o= 45.5 to 91 Ω, the adaptive case: (a) From top to bottom: $x_2(t)$ in dc mode, i_R, $x_2(t)$ in ac mode and $x_1(t)$, (b)The corresponding orbit in the phase plane.

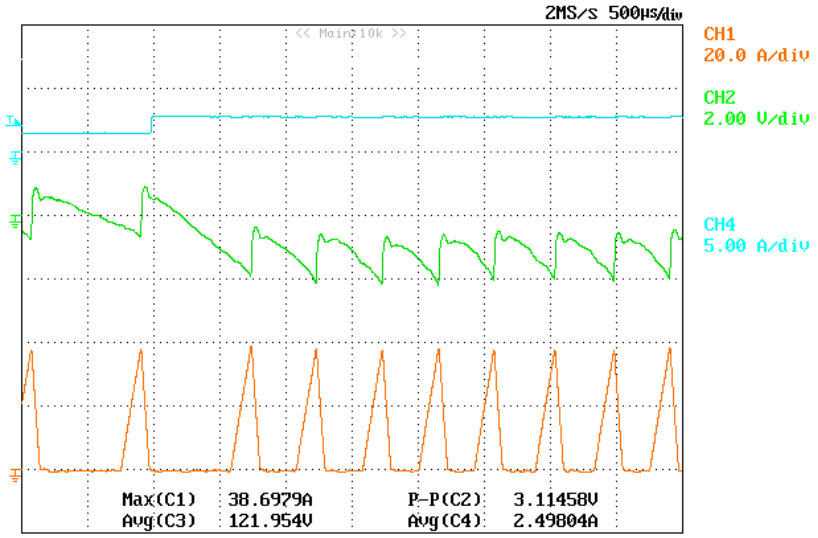

(a)

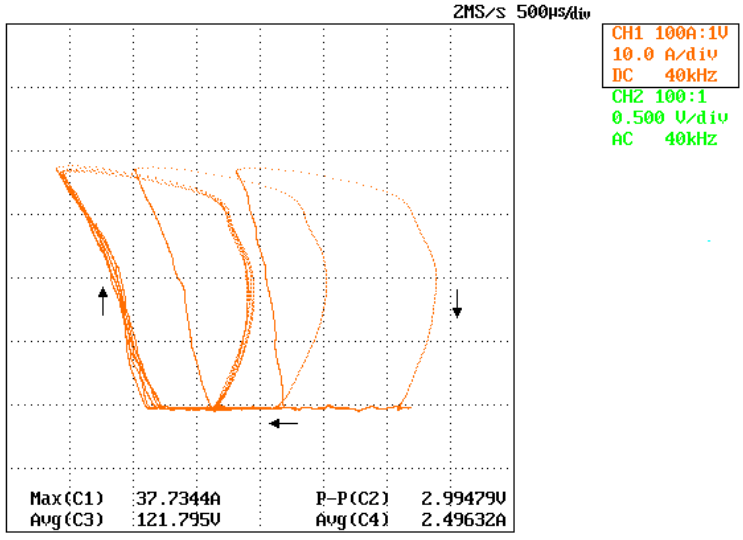

(b)

Figure 2.16: Load change from R_o= 91 to 45.5 Ω without estimation: (a) i_R (top), $x_2(t)$ in ac mode (middle) and $x_1(t)$(bottom), (b) The corresponding orbit in the phase plane.

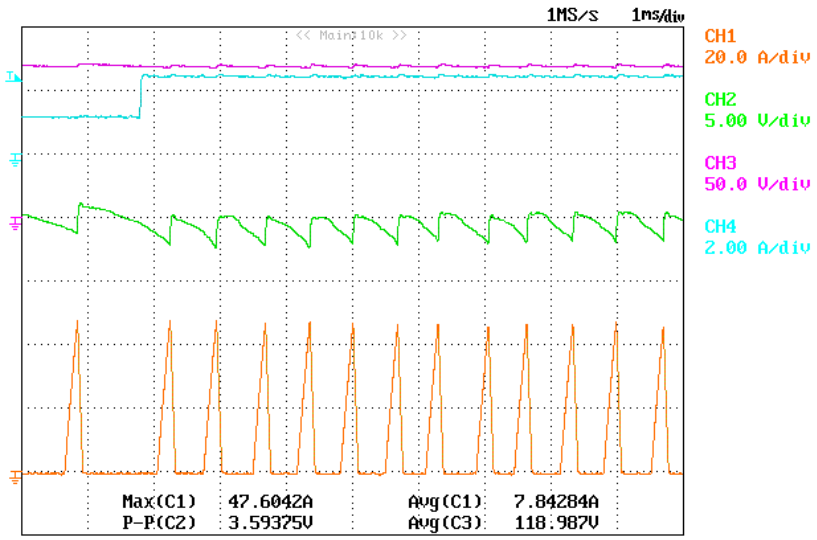

(a)

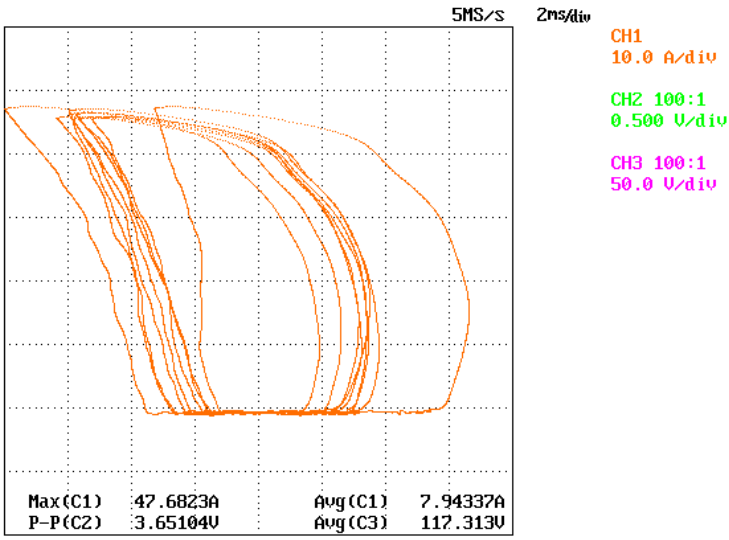

(b)

Figure 2.17: Load change from R_o= 45.5 to 91 Ω, the adaptive case: (a) From top to bottom: $x_2(t)$ in dc mode, i_R, $x_2(t)$ in ac mode and $x_1(t)$, (b)The corresponding orbit in the phase plane.

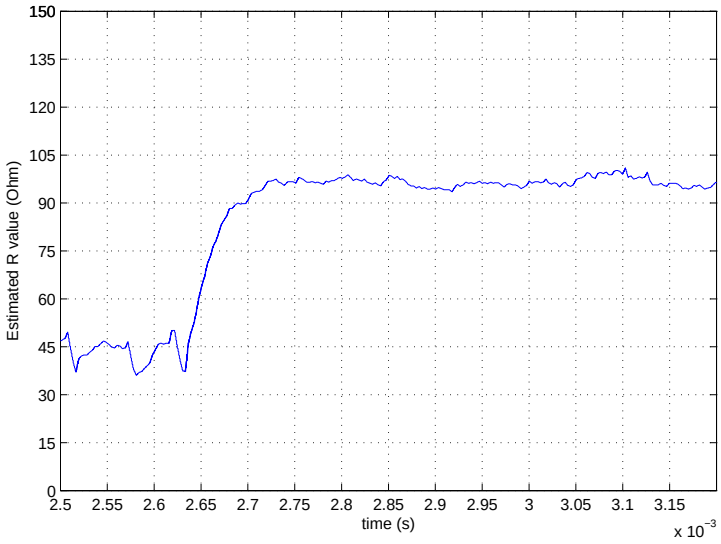

Figure 2.18: Estimation of R_o.

are solved, yielding

$$\begin{cases} w(t_1) = e^{A_1 t_1} w(0) + B_1(t_1) b_1 v_{in} \\ y(t_1 + t_2) = e^{A_2 t_2} y(t_1) + B_2(t_2) b_2 v_{in} \\ z(t_1 + t_2 + t_3) = e^{A_3 t_3} z(t_1 + t_2) + B_3(t_3) b_3 v_{in} \end{cases}$$

where $B_i(t) := \int_0^t e^{A_i \tau} d\tau$. Imposing the boundary conditions

$$w(t_1) = y(t_1),\ y(t_1 + t_2) = z(t_1 + t_2),$$

using the linear approximations $e^{A_i t_i} \approx I_2 + A_i t_i$, and after retention of only first order terms yields

$$z(t_1 + t_2 + t_3) = (I + A) w(0) + b v_{in},$$

where we have defined

$$A := A_1 t_1 + A_2 t_2 + A_3 t_3,\ b := t_1 b_1 + t_2 b_2 + t_3 b_3.$$

In a closed cycle we have $z(t_1 + t_2 + t_3) = w(0)$, hence

$$A w(0) + b v_{in} = 0. \tag{2.12}$$

Using the expressions of A_i and b_i, with the practical consideration that $r_l = 0$, yields

$$A = \begin{bmatrix} 0 & -\frac{t_1}{L} \\ \frac{t_1}{C} & -\frac{T}{RC} \end{bmatrix},\ b = \begin{bmatrix} \frac{t_1 + t_3}{L} \\ 0 \end{bmatrix} \tag{2.13}$$

where $T := t_1 + t_2 + t_3$, is assumed fixed a priori. Replacing (2.13) in (2.12) defines a set of two algebraic equations

$$\begin{aligned} -t_1 x_2^0 + (t_1 + t_3) v_{in} &= 0 \\ R t_1 x_1^0 - T x_2^0 &= 0, \end{aligned} \tag{2.14}$$

where we have adopted our notation $w(0) = (x_1^0, x_2^0)$. The first equation can be rewritten as

$$(M-1) t_1 = t_3, \tag{2.15}$$

where we have defined $M := \frac{x_2^0}{v_{in}}$. Since x_2^0 is the smallest value of the capacitor voltage and, in normal operation, this should be larger than v_{in}, it is reasonable to assume that $M > 1$. At this step, another practical consideration is made, namely, to fix x_1^0, which corresponds to the largest value of the inductor current along the cycle, to

$$x_1^0 = \frac{v_{in} t_3}{2L}. \tag{2.16}$$

This value is obtained assuming that in the interval t_3 the current grows as a ramp of slope $\frac{v_{in}}{L}$, which is indeed the case if $r_l = 0$, and taking half of the peak value.

Replacing (2.15) and (3.10) in the second equation of (2.14) yields, after some simple manipulations,

$$t_1 = \sqrt{\frac{2LTM}{R(M-1)}},\ t_3 = \sqrt{\frac{M(M-1)2LT}{R}},$$

l which are, precisely, the expressions (38) and (39) derived in [23].

Finally, the simulations showing that the approximate method of [23] may lead to instability were performed, and are shown in Fig. 2.19, and the experiments are shown in Figs. 2.20, and 2.21.

2.9 Conclusion

The switching times may, in principle, be derived integrating the differential equations describing the system along the periodic orbit. Unfortunately, due to the "coupled dynamics" in topology Ω_1, this leads to a complicated set of nonlinear algebraic equations that is difficult, if at all possible, to solve. The key observation that allows to obtain explicit solutions is that the existence of the periodic orbit can be guaranteed without the computation of the flow associated to topology Ω_1, but just looking at the intervals $\mathcal{I}_1$ and $\mathcal{I}_2$, where the inductor and capacitor dynamics are decoupled. This fact, of course, stems from the basic operation principle of the boost converter, where magnetic energy is stored in the inductor while electric energy of the capacitor is transferred to the load. In the DCM no magnetic energy is added to the inductor, but the capacitor continues its discharge—with the same time constant. This principle of operation is the same for the buck-boost converter also.

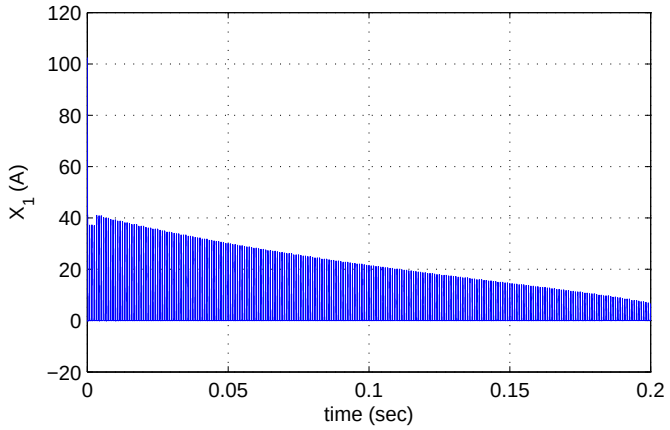

(a)

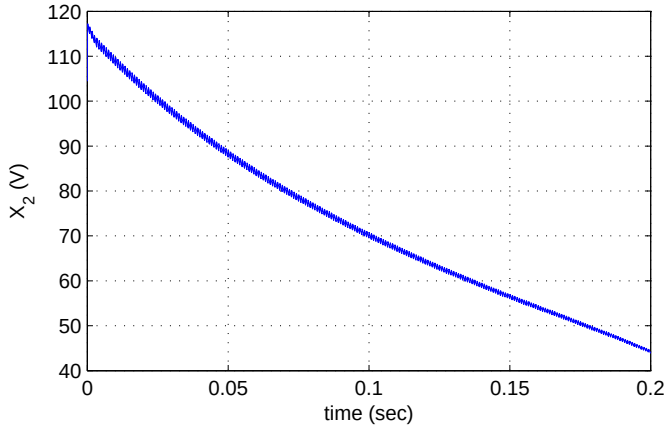

(b)

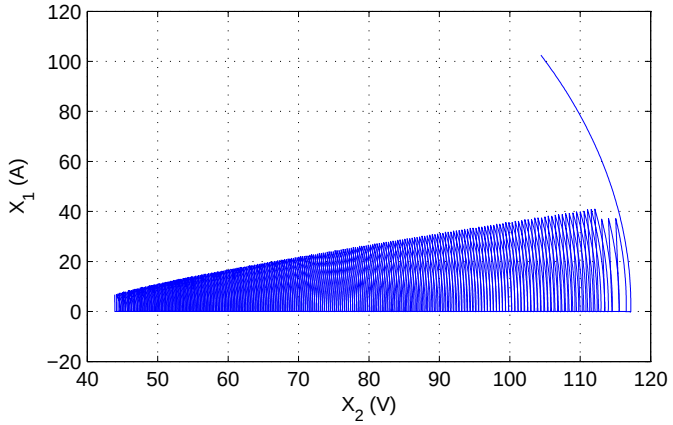

(c)

Figure 2.19: (a) Time evolution of $x_1(t)$ for the simulation in the case of using MId Cuk approximations, (b) The corresponding time evolution of $x_2(t)$, (c) The corresponding orbit in the phase plane.

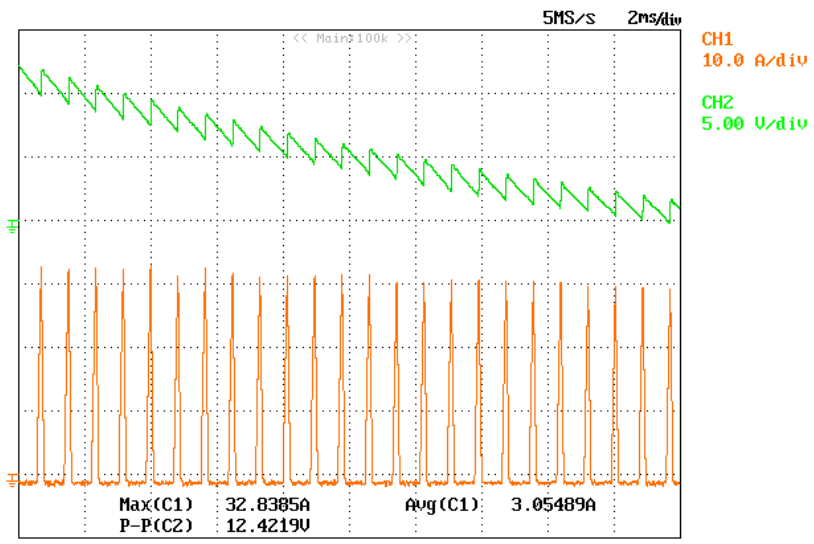

(a)

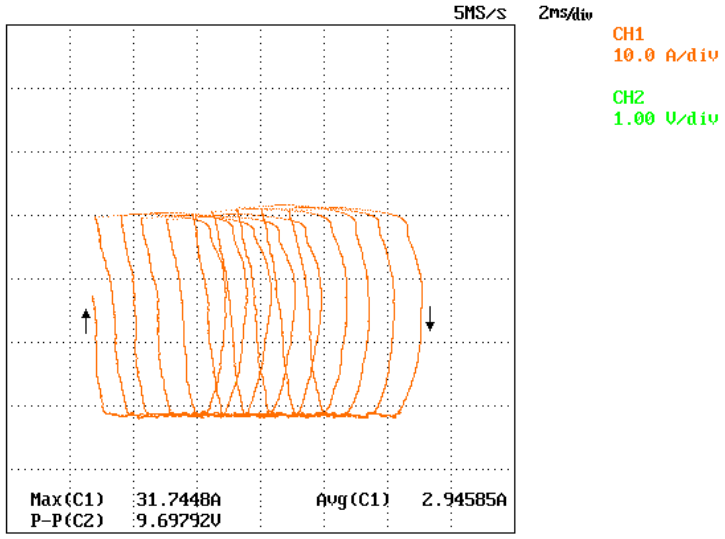

(b)

Figure 2.20: Unstable behavior using the approximate method of Cuk and Middlebrook (1976): (a) v_{in} in ac mode (top) and $x_1(t)$ (bottom), (b) The corresponding orbit in the phase plane.

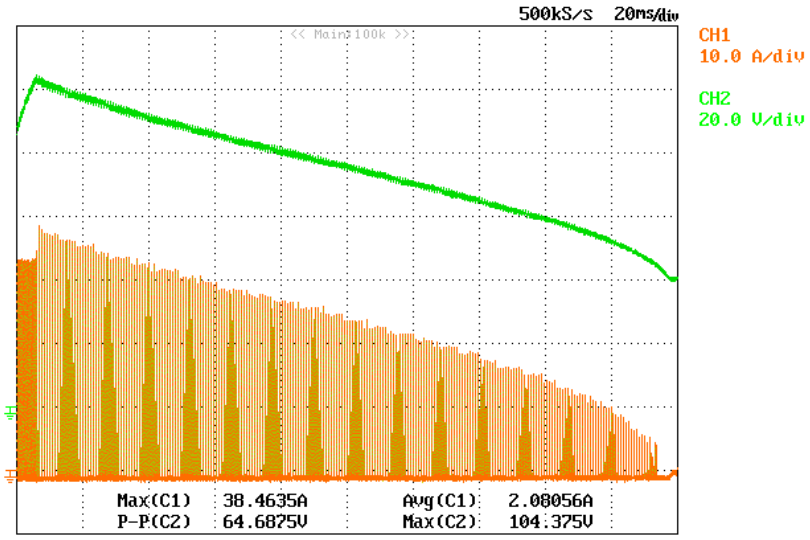

(a)

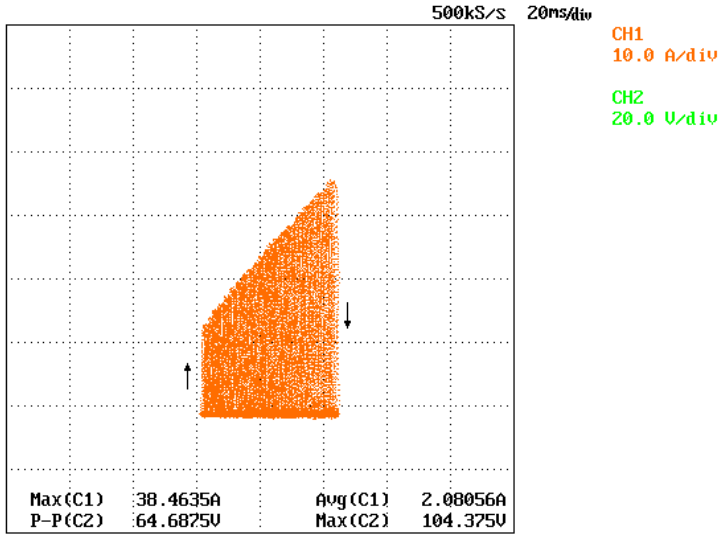

(b)

Figure 2.21: Unstable behavior using the approximate method of Cuk and Middlebrook (1976): (a) v_{in} in dc mode (top) and $x_1(t)$ (bottom), (b) The corresponding orbit in the phase plane.

Chapter 3

PI Stabilization of Power Converters with Partial State Measurements

Contents

In chapter. 1 the procedure to design globally asymptotically stabilizing linear proportional plus integral controllers for switched power converters proposed by [39] was shown. The construction requires the measurement of the full state of the system, which is often unavailable in practice. In this chapter we identify a class of converters for which an asymptotically convergent reduced order observer, preserving the aforementioned stability property of the closed–loop, can be designed. The class is characterized by a simple linear matrix inequality. The new controller is illustrated with the widely–popular, and difficult to control, single–ended primary inductor converter, for which simulation and experimental results are presented.

3.1 Introduction

In chapter. 1, it was shown that a large class of switched power converters can be globally asymptotically stabilized (GAS) with linear proportional plus integral (PI) controllers. The work effectively exploits the key property of passivity of the nonlinear incremental model [42], first reported in [46]. Unfortunately, to generate the output, with respect to which incremental passivity is established, full measurement of the state is typically required. For economic and technological reasons it is desirable to avoid the need of sensors in power converters, particularly current sensors, hence the need to reconstruct the unmeasurable part of the state.

The main contribution of this chapter is to show that the I&I approach of [37] can be used to design an asymptotically convergent reduced order observer for a well–defined class of power converters, which is characterized by a simple linear matrix inequality (LMI). Moreover, it is proven that the I&I observer can be combined with the PI controller proposed in [39] preserving the GAS properties of the closed–loop. The new (certainty–equivalent) controller is applied to regulate the voltage of the widely–popular, and difficult to control, single–ended primary inductor converter (SEPIC), for which experimental results are presented.

3.2 Observer Design

We consider the class of switched power converters with linear capacitors and inductors, described in port-Hamiltonian form [38][1]

$$\dot{x} = \left(J_0 + \sum_{i=1}^{m} J_i u_i - R \right) \nabla H(x) + E \tag{3.1}$$

where $x \in \mathbb{R}^n$, consisting of inductor fluxes and capacitor charges, is the converter state, $u \in \mathbb{R}^m$ denotes the duty ratio of the switches, the total energy stored in inductors and capacitors is

$$H(x) = \frac{1}{2} x^\top Q x, \quad Q = Q^\top > 0, \tag{3.2}$$

$\nabla = \frac{\partial}{\partial x}$, $J_i = -J_i^\top \in \mathbb{R}^{n \times n}$, $i \in \{0\} \bigcup \bar{m} := \{1, \ldots, m\}$ are the interconnection matrices, $R \in \mathbb{R}^{n \times n}$, $R = R^\top \geq 0$ is the dissipation matrix, and the vector $E \in \mathbb{R}^n$ contains the external voltage and current sources. The reader is referred to [38] for further details on this model, which is obtained applying Kirchhoff's laws to the switching topologies, as well as the motivation to select fluxes and charges as state variables instead of, the more standard, voltages and currents.

The state observer problem is formulated as follows. Assume

$$y_m = Cx \in \mathbb{R}^p,$$

[1] In [39] a more general class of converters—including switched sources—is considered.

with $p < n$ and $C \in \mathbb{R}^{p\times n}$ full rank, is available for measurement. To reconstruct the state x we define a matrix $S \in \mathbb{R}^{(n-p)\times n}$ such that the square matrix

$$T := \left[\begin{array}{c} S \\ C \end{array}\right] \in \mathbb{R}^{n\times n} \tag{3.3}$$

is full rank and consider the change of coordinates

$$\left[\begin{array}{c} \eta \\ y_m \end{array}\right] = Tx.$$

The problem is then to generate an estimate for the vector $\eta \in \mathbb{R}^{n-p}$, say $\hat{\eta} \in \mathbb{R}^{n-p}$, to define the observed state as

$$\hat{x} := T^{-1}\left[\begin{array}{c} \hat{\eta} \\ y_m \end{array}\right] = \left[\begin{array}{cc} D_1 & D_2 \end{array}\right]\left[\begin{array}{c} \hat{\eta} \\ y_m \end{array}\right], \tag{3.4}$$

where, for future reference, we introduced the matrices $D_1 \in \mathbb{R}^{n\times(n-p)}$ and $D_2 \in \mathbb{R}^{n\times p}$.

A class of power converters for which the observer problem is solvable is characterized by the following LMI.

Assumption 3.1. *Given*

$$J_0, \cdots, J_m, R, Q \in \mathbb{R}^{n\times n},$$

$$S \in \mathbb{R}^{(n-p)\times n},\ D_1 \in \mathbb{R}^{n\times(n-p)}, \quad C \in \mathbb{R}^{p\times n}.$$

Define

$$\begin{aligned} F_0 &:= S(J_0 - R)QD_1 \\ F_i &:= SJ_iQD_1, \quad i \in \bar{m} \\ G_0 &:= C(J_0 - R)QD_1 \\ G_i &:= CJ_iQD_1, \quad i \in \bar{m}. \end{aligned} \tag{3.5}$$

There exists

$$Z \in \mathbb{R}^{(n-p)\times p}, \quad P = P^\top \in \mathbb{R}^{(n-p)\times(n-p)}$$

solution of the LMI

$$\begin{aligned} P &> 0 \\ sym\{PF_0 + ZG_0\} &< 0 \\ sym\{PF_i + ZG_i\} &= 0,\ i \in \bar{m}, \end{aligned} \tag{3.6}$$

where sym$\{\cdot\}$ denotes the symmetric part.

Proposition 3.1. *Consider the power converter* (3.1), (3.2) *verifying Assumption 1. Define the mapping*

$$\begin{aligned} A &: \mathbb{R}^m \to \mathbb{R}^{n\times n} \\ A(u) &:= (J_0 - R)Q + \sum_{i=1}^{m} J_i Q u_i, \end{aligned} \tag{3.7}$$

where $u := col(u_1, \dots, u_m)$. *The* $(n-p)$*–dimensional I&I observer*

$$\begin{aligned} \dot{\xi} &= (S + \Gamma C)[A(u)((D_2 - D_1\Gamma)y_m + D_1\xi) + E] \\ \hat{\eta} &= \xi - \Gamma y_m \end{aligned} \tag{3.8}$$

where

$$\Gamma = P^{-1}Z \in \mathbb{R}^{(n-p)\times p} \tag{3.9}$$

with P *and* Z *the solution of the LMI* (3.6), *ensures global exponential convergence of the observation error. That is, for all initial conditions* $x(0) \in \mathbb{R}^n, \xi(0) \in \mathbb{R}^{n-p}$, *and controls* $u(t)$, *such that the system is forward complete, there exist* $\alpha, k \in \mathbb{R}_+$ *such that*

$$|\hat{\eta}(t) - \eta(t)| \leq ke^{-\alpha t}|\hat{\eta}(0) - \eta(0)|,$$

for all $t \geq 0$, *where* $|\cdot|$ *is the Euclidean norm.*

Proof. To establish the result we follow *verbatim* the I&I procedure [37]. Define the $(n-p)$–dimensional vector

$$z = \eta - \xi + \beta(y_m)$$

where the mapping $\beta : \mathbb{R}^p \to \mathbb{R}^{n-p}$ is to be designed. The objective in I&I is to select $\dot{\xi}$ and β to ensure an asymptotically stable dynamics for z. In this way, an estimate of η is given by

$$\hat{\eta} = \xi - \beta.$$

Differentiating z, and recalling that $\eta = Sx$ and $y_m = Cx$, one gets

$$\begin{aligned} \dot{z} &= S(A(u)x + E) - \dot{\xi} + \nabla\beta C(A(u)x + E) \\ &= (S + \Gamma C)[A(u)x + E] - \dot{\xi} \end{aligned}$$

where, to get the second identity, we have selected

$$\beta = \Gamma y_m.$$

Now, using

$$x = \begin{bmatrix} D_1 & D_2 \end{bmatrix} \begin{bmatrix} \eta \\ y_m \end{bmatrix}, \tag{3.10}$$

and selecting $\dot{\xi}$ as in (3.8), yields

$$\dot{z} = (S + \Gamma C)A(u)D_1 z. \tag{3.11}$$

The remaining problem is to show that Γ, given in (3.9), ensures an exponentially stable dynamics for z.

Towards this end, notice that with the definitions (3.5) and

$$Z := P\Gamma$$

the LMI (3.6) becomes

$$\begin{aligned} \text{sym}\{P(S + \Gamma C)(J_0 - R)QD_1\} &< 0 & (3.12)\\ \text{sym}\{P(S + \Gamma C)J_i QD_1\} &= 0, & (3.13) \end{aligned}$$

for $i \in \bar{m}$. Now, recalling the definition of $A(u)$ in (3.7) the z dynamics may be written as

$$\dot{z} = (S + \Gamma C)[(J_0 - R)QD_1 + \sum_{i=1}^{m} J_i QD_1 u_i]z.$$

Consider the Lyapunov function candidate

$$V(z) = \frac{1}{2} z^\top P z,$$

whose derivative, using (3.13) to cancel the u_i–dependent terms, and (3.12), verifies the bound

$$\begin{aligned} \dot{V} &\leq -\alpha_0 |z|^2 \\ &\leq -\frac{2\alpha_0}{\lambda_{\max}\{P\}} V, \end{aligned} \tag{3.14}$$

for some $\alpha_0 \in \mathbb{R}_+$. The proof is completed noting that

$$z = \hat{\eta} - \eta \tag{3.15}$$

and doing some standard bounding [44].
□□□

Remark 3.1. *As usual in observer design the proposed I&I observer relies on the exact knowledge of the system dynamics. Indeed, the construction of the observer* (3.8) *contains the matrix* $A(u)$ *defined in* (3.7) *and the vector* E*. In the case of uncertainty on these parameters, the dynamics of the off–the–manifold coordinate* (3.11) *is perturbed by an additive term. For instance, uncertainty in the resistance matrix* R*—that is a common situation, because the load resistance is usually unknown—yields*

$$\begin{aligned} \dot{z} &= (S + \Gamma C)A(u)D_1 z - \\ &\quad -(\hat{R} - R)Q[(D_2 - D_1\Gamma)Cx + D_1\xi], \end{aligned}$$

where $\hat{R}$ is the (constant) estimated resistance matrix. The stability analysis of the overall perturbed dynamics, with state (x, ξ, z), is a complicated task. Interestingly, the simulation and experimental results presented in Section 3.5 show that this parametric error does not destabilize the system, but it introduces a steady–state error in the observation. Moreover, we also present in Section 3.5 the implementation of the I&I adaptive scheme of [39], which estimates on–line the load resistance and overcomes this problem—alas, no complete stability analysis of this adaptive observer is available as yet. See [40] for further details.

Remark 3.2. *Although the LMI* (3.6) *gives only sufficient conditions for observer convergence, the simulation and experimental results presented in Section 3.5 show that they may not be far from being necessary. Indeed, if the algebraic condition* (3.13) *is satisfied and the inequality* (3.12) *"changes sign", that is, if*

$$sym\{P(S + \Gamma C)(J_0 - R)QD_1\} > 0,$$

the z–dynamics is unstable.

3.3 A GAS Output–Feedback PI Controller

In this section we prove that the I&I observer proposed in the previous section can be used, in a certainty equivalent way, with the PI controller of [39], preserving GAS of the closed–loop. To streamline our presentation a slight variation of the main results reported in chapter. 1 is first recalled below.

Proposition 3.2. *Consider a switched power converter described by (3.1). Let $x^\star \in \mathbb{R}^n$ be an admissible equilibrium point, that is, it satisfies*

$$0 = \left(J_0 + \sum_{i=1}^{m} J_i u_i^* - R \right) Q x^\star + E, \tag{3.16}$$

for some $u^\star \in \mathbb{R}^m$. Define the incremental input

$$\tilde{u} := u - u^\star,$$

and the output signal

$$y = \mathcal{C} x,$$

where

$$\mathcal{C} := - \begin{bmatrix} (x^\star)^\top Q J_1 Q \\ \vdots \\ (x^\star)^\top Q J_m Q \end{bmatrix} \in \mathbb{R}^{m \times n}. \tag{3.17}$$

1. *The mapping $\tilde{u} \to y$ is passive. More precisely, the system verifies the dissipation inequality*

$$\dot{H} \leq y^\top \tilde{u}, \tag{3.18}$$

with storage function

$$\begin{aligned} H &: \mathbb{R}^n \to \mathbb{R}_+ \\ H(\tilde{x}) &= \frac{1}{2}\tilde{x}^\top Q \tilde{x}, \end{aligned} \tag{3.19}$$

where $\tilde{x} := x - x^\star$.

2. *The power converter in closed loop with the PI controller*

$$\begin{aligned} \dot{w} &= y \\ u &= -K_p y - K_i w, \end{aligned} \tag{3.20}$$

with $K_p = K_p^\top > 0, K_i = K_i^\top > 0$ ensures that the equilibrium

$$(x, w) = (x^\star, -K_i^{-1} u^\star),$$

is GAS if y is detectable. *That is, if for any solution $(x(t), w(t))$ of the closed–loop system the following implication is true:*

$$y(t) \equiv 0 \quad \Rightarrow \quad \lim_{t\to\infty} x(t) = x^\star, \lim_{t\to\infty} w(t) = -K_i^{-1} u^\star. \tag{3.21}$$

We are in position to present the main result of this section.

Proposition 3.3. *Consider a switched power converter described by (3.1), verifying Assumption 1, with an assignable equilibrium state $x^\star$ and corresponding input $u^\star$. Assume* (3.21) *of Proposition 3.2 holds. The observer–based PI controller*

$$\begin{aligned} \dot{w} &= \mathcal{C}\hat{x} \\ u &= -K_p \mathcal{C}\hat{x} - K_i w \end{aligned} \tag{3.22}$$

with $\hat{x}$ the estimate of the state generated via (3.4), (3.7), (3.8) *and* (3.9), *ensures that the equilibrium*

$$(x, w, z) = (x^\star, -K_i^{-1} u^\star, 0)$$

is GAS.

Proof. From (3.4) and (3.10) we see that the observation error can be expressed as

$$\hat{x} - x = D_1 z.$$

Hence, we can write the control (3.22) in the perturbed form

$$\begin{aligned} \dot{w} &= y + \mathcal{C}D_1 z \\ u &= -K_p y - K_i w - K_p \mathcal{C} D_1 z \end{aligned} \tag{3.23}$$

To carry out the proof we write the overall system as a cascade interconnection of the observer error subsystem and the full state-feedback dynamics, which takes the form

$$\begin{aligned} \begin{bmatrix} \dot{\tilde{x}} \\ \dot{\tilde{w}} \end{bmatrix} &= f(\tilde{x}, \tilde{w}) + g(\tilde{x}) z \\ \dot{z} &= -A(u) z \end{aligned} \tag{3.24}$$

where

$$\tilde{w} := w + K_i^{-1} u^\star$$

and $f : \mathbb{R}^n \times \mathbb{R}^m \to \mathbb{R}^{n+m}, g : \mathbb{R}^n \to \mathbb{R}^{n+m}$ are some suitably defined mappings. Proposition 3.2 shows that the system with $z = 0$ is GAS. To establish the claim we invoke the fundamental result of [47], see also [48], and see that the proof will be completed if we can establish boundedness of the trajectories $(\tilde{x}(t), \tilde{w}(t))$. Towards this end, we follow closely the derivations in [45] and construct a function $W_3(\tilde{x}, \tilde{w}, z)$ whose boundedness implies boundedness of the state and that satisfies a bound

$$\dot{W}_3 \leq c|z| W_3,$$

for some $c \in \mathbb{R}_+$. Since z is clearly an *integrable* function, invoking the Comparison Lemma [44], we immediately conclude boundedness of W_3 and, consequently, boundedness of the trajectories as desired.

Consider the function

$$W_1(\tilde{x}, \tilde{w}) = H(\tilde{x}) + \frac{1}{2} \widetilde{w}^T K_i \widetilde{w},$$

where H is defined in (3.19).[2] Computing the time derivative along the trajectories of (3.24) we get the bounds

$$\begin{aligned} \dot{W}_1 &\leq -\alpha_1 |y|^2 + (c_1 |y| + c_2 |\widetilde{w}|) |z| \\ &\leq \frac{c_1^2}{4\alpha_1} |z|^2 + c_2 |\widetilde{w}| |z|, \end{aligned}$$

where we defined the constants

$$\alpha_1 := \lambda_{\min}\{K_p\},\ c_1 := \|K_p \mathcal{C} D_1\|,\ c_2 := \|K_i \mathcal{C} D_1\|,$$

with $\|\cdot\|$ the 2–norm, and we have used

$$|y| |z| \leq \frac{\alpha_1}{c_1} |y|^2 + \frac{c_1}{4\alpha_1} |z|^2$$

[2] See the proof of Proposition 2 in [39] for further details on this, rather standard, derivation.

to get the second inequality. Consider, now, the function

$$W_2(\tilde{x}, \tilde{w}, z) = W_1(\tilde{x}, \tilde{w}) + \frac{c_1^2}{4\alpha_1\alpha_0} V(z),$$

whose derivative, in view of (3.14), satisfies the bound

$$\begin{aligned} \dot{W}_2 &\leq c_2 \, |\tilde{w}| \, |z| \\ &= \left(c_2 \, |\widetilde{w}| \, |z|^{\frac{1}{2}} \right) |z|^{\frac{1}{2}} \\ &\leq \frac{c_2^2}{2} \, |\widetilde{w}|^2 \, |z| + \frac{1}{2} \, |z| \, , \end{aligned}$$

where, to get the last inequality, we have applied $2ab \leq a^2 + b^2$ to the factors in the second equation.

Now, from (3.14) it follows that

$$\frac{d}{dt} V^{\frac{1}{2}}(z) \leq -\frac{\alpha_0 \lambda_{\min}^{\frac{1}{2}}\{P\}}{\sqrt{2}\lambda_{\max}\{P\}} |z|.$$

Consequently, to cancel the term $\frac{1}{2}|z|$, define the function

$$W_3(\tilde{x}, \tilde{w}, z) = 2W_2(\tilde{x}, \tilde{w}, z) + \frac{\sqrt{2}\lambda_{\max}\{P\}}{\alpha_0 \lambda_{\min}^{\frac{1}{2}}\{P\}} V^{\frac{1}{2}}(z),$$

whose derivative clearly yields

$$\begin{aligned} \dot{W}_3 &\leq c_2^2 \, |\widetilde{w}|^2 \, |z| \\ &\leq \frac{c_2^2}{\lambda_{\min}\{K_i\}} \, |z| \, W_3, \end{aligned} \tag{3.25}$$

where we have used the bound

$$W_3 \geq 2W_1 \geq \lambda_{\min}\{K_i\} \, |\widetilde{w}|^2 \, ,$$

to get the last equation. In view of the argument above, the inequality (3.25) completes the proof.
□□□

Remark 3.3. *Of course, the interesting feature of Proposition 3.3—that is a consequence of exploiting a passivity property—is that GAS is ensured* for all *positive values of the PI gains, considerably simplifying the controller tuning procedure.*

3.4 Application to the SEPIC

The SEPIC is a DC–to–DC power electronic device that has found wide application in industry because is relatively simple and can operate both in step–up and step–down

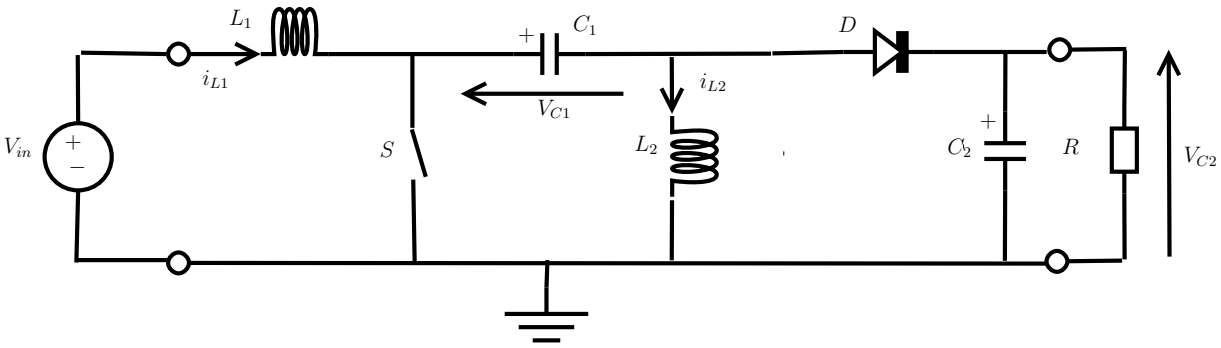

Figure 3.1: Schematic of the SEPIC with a resistive load.

modes [49]. In spite of its similarity with the well–known Cuk converter, it is widely recognized that designing a controller to achieve a high performance behavior is a major open problem. The interested reader is referred to [40], and references therein for further details on the SEPIC model and control problem.

A schematic representation of the SEPIC, feeding a purely resistive load, is depicted in Fig. 3.1. Assuming continuous conduction mode, its average model, can be expressed in the Port–Hamiltonian form (3.1) with $n = 4$ and the definitions

$$x = \text{col}(\phi_1, \phi_2, q_1, q_2),\ E = \text{col}(V_{in}, 0, 0, 0)$$

$$R = \text{diag}\left\{r_{L_1}, r_{L_2}, 0, \frac{1}{r}\right\}$$

$$Q = \text{diag}\left\{\frac{1}{L_1}, \frac{1}{L_2}, \frac{1}{C_1}, \frac{1}{C_2}\right\}$$

$$J_0 = \begin{bmatrix} 0 & 0 & -1 & -1 \\ 0 & 0 & 0 & 1 \\ 1 & 0 & 0 & 0 \\ 1 & -1 & 0 & 0 \end{bmatrix}$$

$$J_1 = \begin{bmatrix} 0 & 0 & 1 & 1 \\ 0 & 0 & -1 & -1 \\ -1 & 1 & 0 & 0 \\ -1 & 1 & 0 & 0 \end{bmatrix}$$

where ϕ_i are the fluxes in the inductors, q_i the charges in the capacitors, u is the modulation index, V_{in} is the constant direct supply voltage, L_i, C_i, r_{L_i}, are the SEPIC parameters and r is the load resistance.

The relationship between the elements of x, and the signals indicated in Fig. 3.1 is:

$$i_{L1} = \frac{x_1}{L_1}, i_{L2} = \frac{x_2}{L_2}, V_{c1} = \frac{x_3}{C_1}, V_{c2} = \frac{x_4}{C_2}.$$

The control objective is the regulation of the output voltage to a given constant value $V^\star$, *i.e.*, the regulation of the charge x_4 to a desired reference $x_4^\star > 0$ where $C_2 V^\star = x_4^\star$. It is assumed that the only variable available for measurement is the output voltage, that is, $p = 1$, and

$$C = (0\ 0\ 0\ 1).$$

The proposition below that—via Proposition 3.1 establishes the existence of a GAS I&I observer—is the main result of this section. Direct application of Proposition 3.3 proves then that an output–feedback PI controller renders the SEPIC GAS.

Proposition 3.4. *Fix $P_{13} > 0$ and set*

$$P_{22} = \frac{1}{r_{L_2}} P_{13} + K \tag{3.26}$$

$$P_{33} = (r_{L_2} + \frac{L_2}{C_1 r_{L_2}}) P_{13} + \frac{L_2}{C_1} K. \tag{3.27}$$

There exists $K_{min} > 0$ such that, for all $K \geq K_{min}$ the matrices

$$P = \begin{bmatrix} \frac{L_2}{L_1} P_{22} & 0 & P_{13} \\ 0 & P_{22} & P_{13} \\ P_{13} & P_{13} & P_{33} \end{bmatrix}$$

and

$$Z = \begin{bmatrix} -P_{13} \\ -P_{13} \\ L_2(\frac{P_{22}}{C_1} - \frac{P_{33}}{L_1}) \end{bmatrix}.$$

solve the LMI of Assumption 1 for the SEPIC model.

Proof. From (3.3) and (3.4), we have that

$$T = I_4,\ S = [I_3 \mid 0] = D_1^\top,\ D_2 = e_4,$$

where I_3 is the 3×3 identity matrix. Now, use (3.5) to compute

$$F_0 = \begin{bmatrix} -\frac{r_{L_1}}{L_1} & 0 & -\frac{1}{C_1} \\ 0 & -\frac{r_{L_2}}{L_2} & 0 \\ \frac{1}{L_1} & 0 & 0 \end{bmatrix}$$

$$F_1 = \begin{bmatrix} 0 & 0 & \frac{1}{C_1} \\ 0 & 0 & -\frac{1}{C_1} \\ -\frac{1}{L_1} & \frac{1}{L_2} & 0 \end{bmatrix}$$

$$G_0 = \begin{bmatrix} \frac{1}{L_1} & -\frac{1}{L_2} & 0 \end{bmatrix},\ G_1 = \begin{bmatrix} -\frac{1}{L_1} & \frac{1}{L_2} & 0 \end{bmatrix}.$$

To simplify the derivations set the $(1,2)$–element of the matrix P equal to zero, that is, $P_{12}=0$. Direct replacement proves that, under this condition, the equality condition

$$\operatorname{sym}\{PF_1+ZG_1\}=0.$$

is satisfied if and only if

$$P_{11}=\frac{L_2}{L_1}P_{22},\ P_{13}=P_{23},$$

and

$$Z=\begin{bmatrix} -P_{13} \\ -P_{13} \\ L_2(\frac{P_{22}}{C_1}-\frac{P_{33}}{L_1}) \end{bmatrix}.$$

Now, define

$$Q_0:=-\operatorname{sym}\{PF_0+ZG_0\}.$$

The remaining task is to select the elements of P, which is of the form

$$P=\begin{bmatrix} \frac{L_2}{L_1}P_{22} & 0 & P_{13} \\ 0 & P_{22} & P_{13} \\ P_{13} & P_{13} & P_{33} \end{bmatrix},$$

that, preserving $P>0$, ensure that $Q_0>0$. Replacing P and Z above in Q_0 yields

$$Q_0=\begin{bmatrix} \frac{2r_{L_1}L_2}{L_1^2}P_{22} & \frac{-1}{L_2}P_{13} & \frac{r_{L_1}}{L_1}P_{13} \\ * & K & \frac{1}{C_1}P_{22}-\frac{1}{L_2}P_{33}+\frac{r_{L_2}}{L_2}P_{13} \\ * & * & \frac{2}{C_1}P_{13} \end{bmatrix}$$

where we have defined

$$K:=\frac{2r_{L_2}}{L_2}P_{22}-\frac{2}{L_2}P_{13}.$$

To simplify the positivity test set the $(2,3)$ term to zero, that is,

$$\frac{1}{C_1}P_{22}-\frac{1}{L_2}P_{33}+\frac{r_{L_2}}{L_2}P_{13}=0$$

This yields

$$Q_0=\begin{bmatrix} \frac{2r_{L_1}L_2}{L_1^2}P_{22} & \frac{-1}{L_2}P_{13} & \frac{r_{L_1}}{L_1}P_{13} \\ \frac{-1}{L_2}P_{13} & K & 0 \\ \frac{r_{L_1}}{L_1}P_{13} & 0 & \frac{2}{C_1}P_{13} \end{bmatrix}.$$

A Schur complement analysis shows that $P>0$ if and only if

$$P_{22}>0,\quad P_{33}P_{22}>P_{13}^2(1+\frac{L_1}{L_2})$$

Replacing P_{22} and P_{33} by (3.26) and (3.27) gives the first condition that K must satisfy, namely,

$$\frac{1}{4r_{L_2}^3 C_1}\frac{L_2^4}{L_1}K^2 + (\frac{1}{2r_{L_2}}\frac{L_2}{L_1} + \frac{1}{r_{L_2}^3 C_1}\frac{L_2^3}{L_1})KP_{13} +$$
$$(\frac{1}{r_{L_2}L_1} + \frac{1}{r_{L_2}^3 C_1}\frac{L_2^2}{L_1} - \frac{1}{r_{L_2}}\frac{L_2}{L_1} - \frac{1}{r_{L_2}})P_{13}^2 > 0. \tag{3.28}$$

On the other hand, a Schur complement analysis shows that $Q_0 > 0$ if and only if

$$\frac{2r_{L_1}L_2}{L_1^2}P_{22} > P_{13}^2(\frac{1}{KL_2^2} + \frac{C_1 r_{L_1}^2}{2L_1^2 P_{13}})$$

which, upon replacement of P_{22}, gives the second condition that K must satisfy

$$\frac{r_{L_1}}{r_{L_2}}\frac{L_2^2}{L_1^2}K^2 + (2\frac{r_{L_1}}{r_{L_2}}\frac{L_2}{L_1^2} - \frac{r_{L_1}^2}{L_1^2}\frac{C_1}{2})P_{13}K - \frac{1}{L_2^2}P_{13}^2 > 0. \tag{3.29}$$

Since the coefficients of K^2 in the right hand sides of (3.28) and (3.29) are positive, it is clear that, for any fixed P_{13}, there exists $K > 0$ such that both inequalities hold. This completes the proof. □□□

3.5 Simulation and Experimental Results of the SEPIC

In this section simulation and experimental results of the observer–based PI controller for the SEPIC presented in Section 3.4 are given. The parameters of the converter, used in both cases, are given by

$$V_{in} = 20V, L_1 = 2.3 \times 10^{-3}H, L_2 = 330 \times 10^{-6}H$$

$$C_1 = C_2 = 190 \times 10^{-6}F, r_{L_1} = 1.7\Omega, r_{L_2} = 0.5\Omega.$$

The load resistance was originally set to $r = 22\Omega$, but it was later changed to test the robustness of the controller. The voltage reference $V^\star$ is initially set equal to $20V$, with a pulse change of $2V$ introduced later.

3.5.1 Simulations

Simulations were first performed in MATLAB® Simulink®. A first set of simulations was carried out to show the effect of the tuning gains P_{13} and K of Proposition 3.4 on the performance of the observer. The initial conditions were taken as $x(0) = 0$, $w(0) = 0$ and $(\hat{x}_1(0), \hat{x}_2(0), \hat{x}_3(0)) = \text{col}(1.9550 \times 10^{-7}, 1.9550 \times 10^{-7}, -2.2 \times 10^{-8})$. The gains of the PI were set to $K_p = 0.001$ and $K_i = 5$.

In Fig. 3.2 the observation error $\hat{x}_1 - x_1$ for $P_{13} = 0.5$ and several values of $K \geq K_{min} = 4545$ is shown.[3] In Fig. 3.3 the error is shown for $K = 1$ and values of $P_{13} \leq 0.0001$ that satisfy the conditions of Proposition 3.4. As indicated by (3.14), the transient performance improves with increasing K and decreasing P_{13}. Notice the vertical scale.

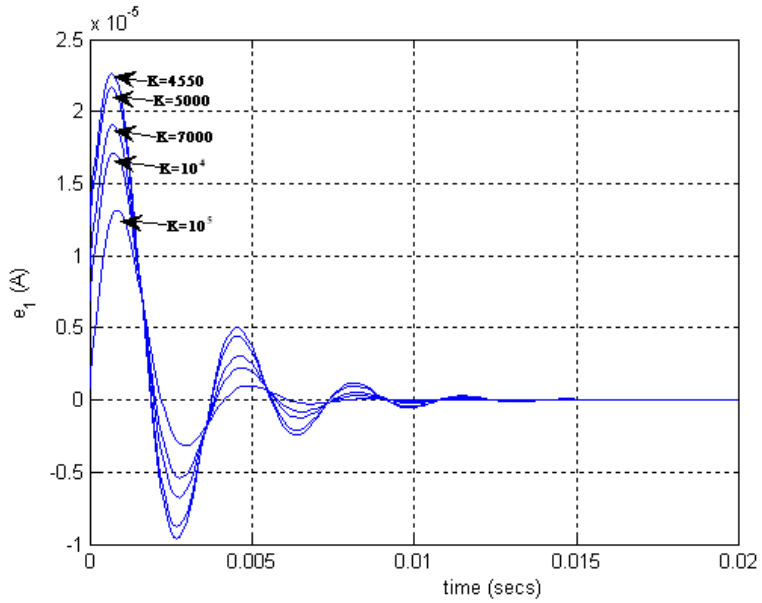

Figure 3.2: State observation error $\frac{(\hat{x}_1 - x_1)}{L_1}$ for $P_{13} = 0.5$ and admissible $K \geq K_{min} = 4545$.

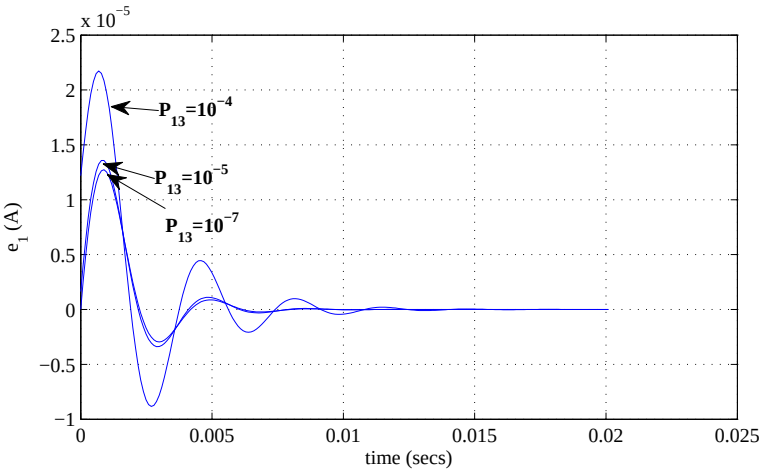

Figure 3.3: State observation error $\frac{(\hat{x}_1 - x_1)}{L_1}$ for $K = 1$ and admissible $P_{13} \leq 0.0001$.

To illustrate Remark 3.2, that is, how close from being necessary are the sufficient conditions given in the proposition, in Fig. 3.4 we show that the observer becomes unstable

[3]The other observation errors show a similar pattern, hence they are omitted for brevity.

if K is taken outside the admissible range. A similar instability phenomenon was observed for $K = 1$ and $P_{13} = 0.0002 > 0.0001$.

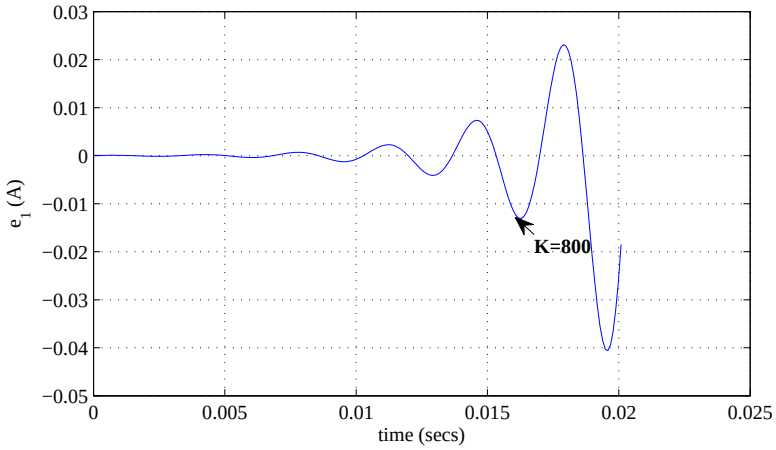

Figure 3.4: State observation error $\frac{(\hat{x}_1 - x_1)}{L_1}$ for $P_{13} = 0.5$ and inadmissible $K = 800 < K_{min} = 4545$.

Fig. 3.5 shows the response of the output voltage, with $P_{13} = 0.5$, $K = 4550$, and various values of K_p and K_i. As predicted by the theory, the overall system exponentially converges with a zero steady state error. It was observed that the parameter that more strongly influences the transient behavior is K_p.

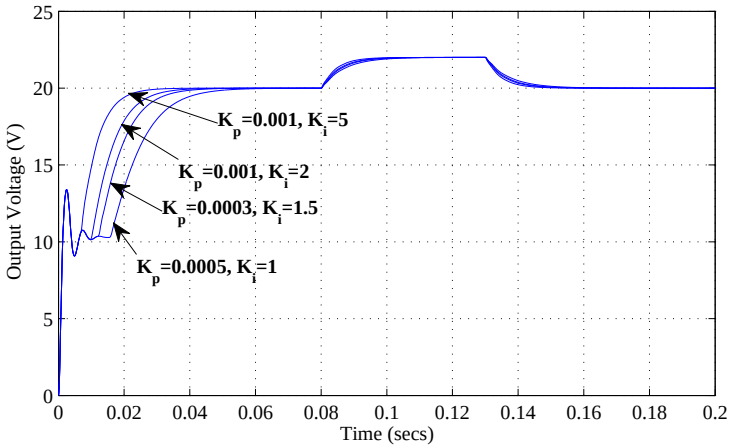

Figure 3.5: Output voltage $\frac{x_4}{C_2}$ for different tunings of the PI gains.

As explained in Remark 3.1, the observer is sensitive to parameter uncertainty. To illustrate this point a 100% pulse change of the load resistance r—from 22Ω to 44Ω—was introduced.[4] Fig. 3.6 shows the performance of the observation errors that, in spite of the very large parameter variation, remain bounded but exhibit a steady–state error. As

[4]This corresponds to a power change from $9W$ to $18W$, that might occur in applications.

a consequence of the observation error the output voltage also has a constant bias, as shown in Fig. 3.7

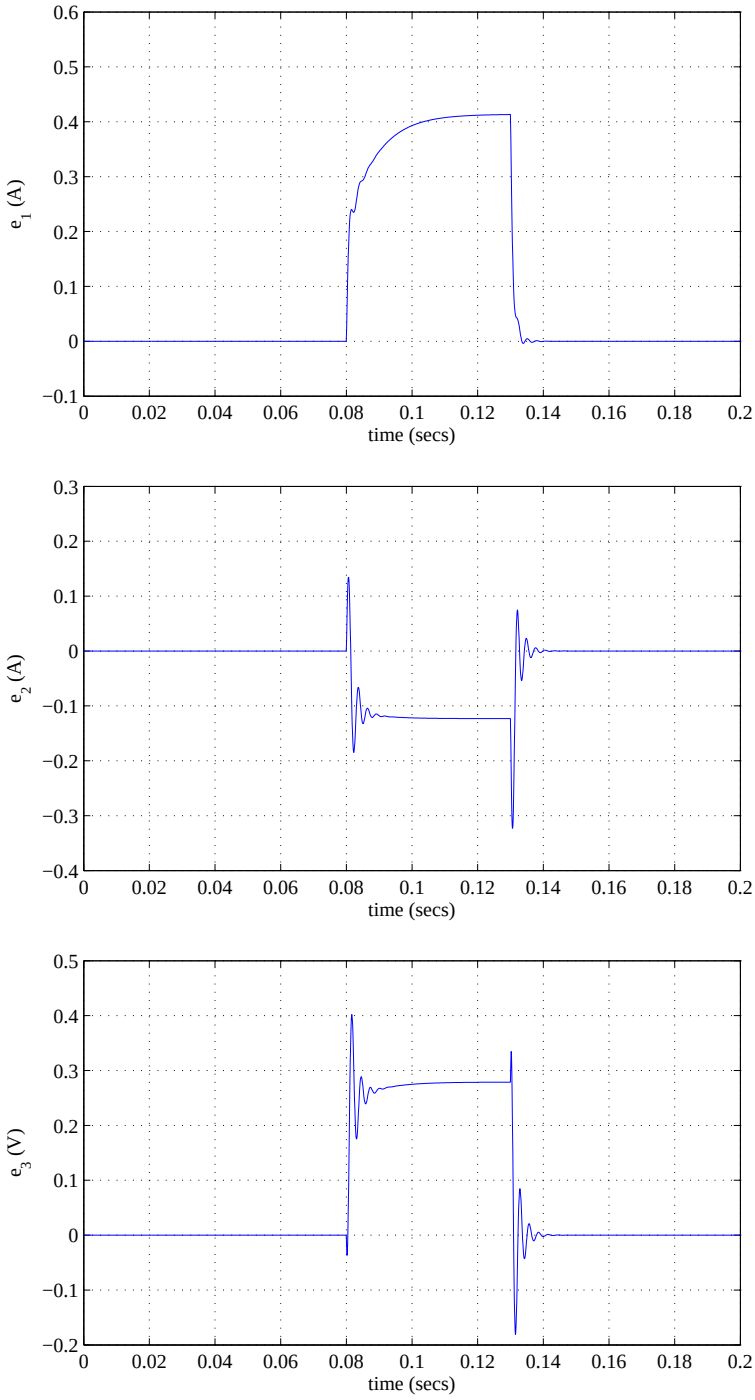

Figure 3.6: Behavior of the observation errors, $\frac{(\hat{x}_i - x_i)}{L_i}, i = 1, 2$ and $\frac{(\hat{x}_3 - x_3)}{C_1}$, in the face of a 100% load resistance pulse change.

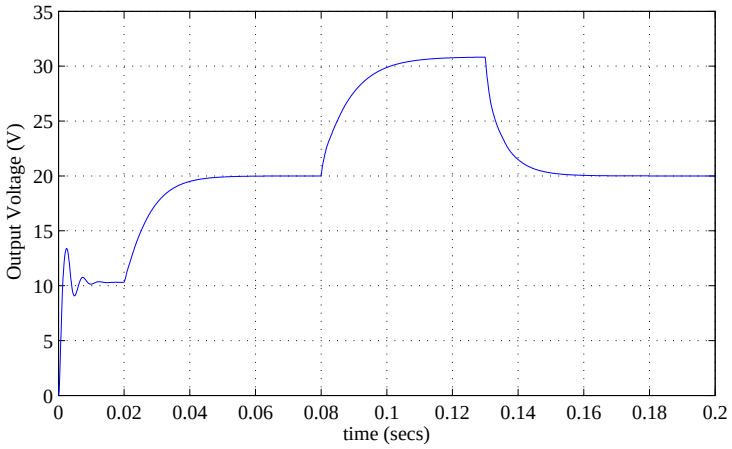

Figure 3.7: Behavior of the output voltage in the face of a 100% load resistance pulse change.

3.5.2 Experiments

The performance of the observer–based PI controller has then been experimentally validated on the laboratory test bench prototype shown in Fig. 3.8. It operates at a constant switching frequency of $20kHz$ and includes a load variation kit, a "dSpace®" acquisition card, used to interface data transfer (measured output voltage and calculated duty ratio) between the converter and a PC, where the control law and observer are implemented using the Real-Time Windows Target Simulink® Library. The "Control Desk®" software environment is used as a graphical user interface.

Figure 3.8: SEPIC prototype (right) with load variation kit (left).

The response of the output voltage for the pulse reference voltage change is given in Fig. 3.9, which was obtained using the same observer and controller settings as in the simulation. Besides a steady–state error, which is due to sensor bias, it closely matches the simulated one.

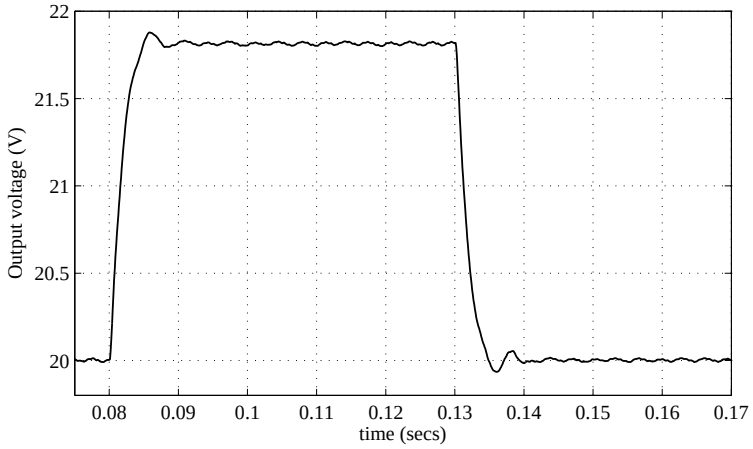

Figure 3.9: Experimental response of the output voltage $\frac{x_4}{C_2}$ to a pulse in the voltage reference.

The behavior for a pulse change in the load resistance was also very similar to the one shown in Fig. 3.7—that is, exhibiting a large steady–state error. On the other hand, as indicated in Remark 3.1, the observer can be combined, in an *ad–hoc* basis, with the I&I load estimator proposed in [39]. See [41] for details. Interestingly, the overall scheme performs remarkably well because, as shown in Fig. 3.10, the estimator closely tracks the parameter variations. Fig. 3.11 shows the behavior of the output voltage of the adaptive observer–based PI controller, in simulation and experiments, when the voltage reference and the load resistance change. As seen in the figure, the similarity between the simulation and the experiment is remarkable.

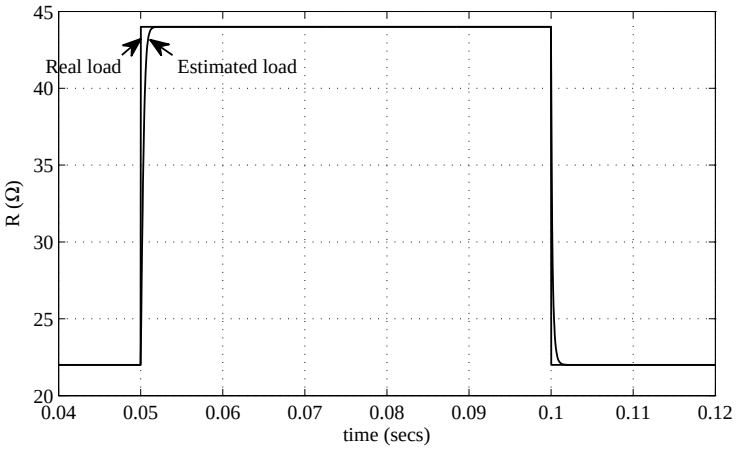

Figure 3.10: Load resistance variation and its estimated value.

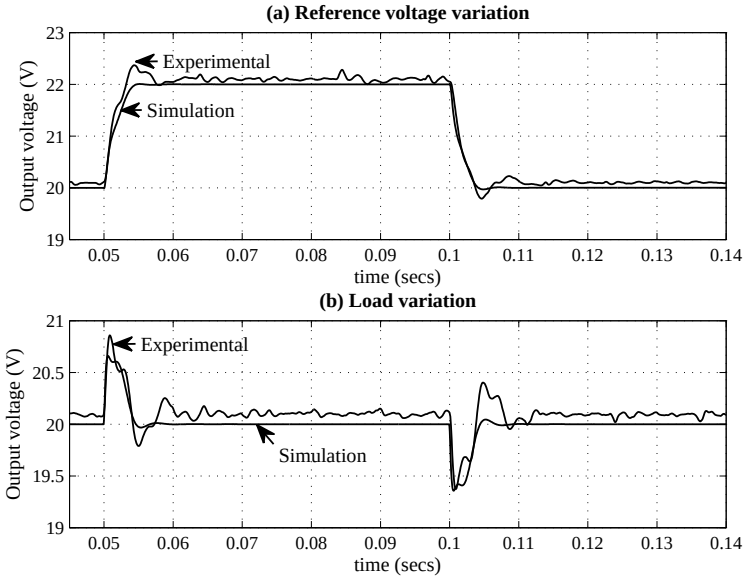

Figure 3.11: Behavior of the output voltage to reference (top) and load resistance (bottom) variations, in simulation and experiments.

3.6 Conclusions

A class of power converters that can be globally stabilized with an output–feedback PI controller has been identified. The characterization is given in terms of an LMI that can be easily verified with standard computational tools. Instrumental for the establishment of the result is the construction of an observer that uses the new I&I techniques proposed in [37].[5] In order to get simple designs, we have taken here the basic version of I&I —defining the manifold via separable functions and taking a linear function β. Some preliminary calculations show that considering a larger class of functions does not lead to possible extensions.

The approach adopted in the observer design is to "eliminate" the input–dependent terms in the Lyapunov function derivative. This lead to a conservative design that clearly reduces the admissible class of converters. Since the control is a duty ratio, that is bounded by definition, an alternative is to add a saturation function to the control and determine intervals for the observer parameters that ensure stability of the resulting polytopic system. This approach, pursued in Chapter 8 of [37], is certainly applicable to a larger class of converters. Indeed, it can be shown that the LMI is not feasible for classical converters like the boost or Cuk—examples that are successfully treated in [37]. It is, however, applicable for the quadratic converter, that will be reported in the near future.

[5] Although it is possible to design a full–order Luenberger observer, the admissible class of systems—which is also characterized by an LMI—is extremely restrictive and does not seem to include any practical power converter topology.

As a byproduct of our derivations we have identified, via an LMI, a class of bilinear systems of the form

$$\begin{aligned} \dot{x} &= A_0 x + \sum_{i=1}^{m} u_i A_i x + E \\ y &= Cx. \end{aligned}$$

for which a globally convergent observer can be designed. To the best of our knowledge, in spite of its simplicity, this result is new.

Conclusion

This thesis contributes to provide hybrid and nonlinear control problem solutions to several types of power converters. Specifically, this thesis deals with DC-DC power converters.

The development of a solution for a specific example of practical relevance was the motivation of the chapter 2. We considered a boost and a buck-boost converter operating in DCM, which exhibits the four distinguishing features:

(i) The control is not a continuous signal, but directly the switches positions, that take values in the binary set $\{0, 1\}$, and decide the commutation among the various converter topologies.

(ii) Due to technological considerations, the activation of the switches is submitted to a minimal dwell time that has to be taken into account in the design.

(iii) Besides the commutations induced by (designer selected) switch positions, there are forced commutations due to the aforementioned violation of the unidirectionality assumption, *e.g.*, the presence of diodes.

(iv) As the ripple cannot be neglected, the control objective is not stabilization of an equilibrium but generation of a periodic orbit (with "minimal amplitude") around the desired operating point.

Our main contribution was a simple robust algorithm that, in contrast with current practice, gives explicit formulas for the switching times without approximations. Although the design relies on the specific topology of the boost and buck-boost converters. The switching times may, in principle, be derived integrating the differential equations describing the system along the periodic orbit. Unfortunately, due to the "coupled dynamics" in topology Ω_1, this leads to a complicated set of nonlinear algebraic equations that is difficult, if at all possible, to solve. The key observation common to both of converters, that allows to obtain explicit solutions, was that the existence of the periodic orbit can be guaranteed without the computation of the flow associated to topology Ω_1, but just looking at the intervals $\mathcal{I}_1$ and $\mathcal{I}_2$, where the inductor and capacitor dynamics are decoupled.

A second contribution was presented in Chapter 3. We show that the I&I approach can be used to design an asymptotically convergent reduced order observer for a well–defined

class of power converters, which is characterized by a simple linear matrix inequality (LMI). Moreover, it is proven that the I&I observer can be combined with the PI controller proposed preserving the GAS properties of the closed–loop. The new controller was applied to regulate the voltage of the widely–popular, and difficult to control, single–ended primary inductor converter (SEPIC). We have identified, via an LMI, a class of bilinear systems of the form

$$\begin{aligned} \dot{x} &= A_0 x + \sum_{i=1}^{m} u_i A_i x + E \\ y &= Cx. \end{aligned}$$

for which a globally convergent observer can be designed. To the best of our knowledge, in spite of its simplicity, this result is new.

List of Figures

Bibliography

[1] N. Mohan, T.M. Undeland, and W.P. Robbins. Power electronics. Wiley New York, 1995.

[2] A.I. Pressman, K. Billings, and T. Morey. Switching power supply design. McGraw-Hill Professional, 2009.

[3] F.Vasca, L.Lannelli, *Dynamics and control of switched electronic systems*, Springer, Advances in industrial control, 2012.

[4] S. Cuk, R.D. Middlebrook, Advances in switched-mode power conversion-part1. *IEEE Trans. Ind. Electron.* 30(1), 10-19 (1993).

[5] J.J. Jozwik, M.K. Kazimierczuk, Dual SEPIC PWM switching mode DC/DC power converter. *IEEE Tans. Ind. Electron.* 36(1), 64-70 (1989).

[6] R.P. Maasey, E.C. Synder, High voltage single-ended DC-DC cinverter. In: Proc. of the IEEE Power Electronics Specialist Conference, Orlando, Florida, USA, pp. 156-159 (1977).

[7] D. Maksimovic, S.Cuk, Switching converters with wide DC conversion range. *IEEE Trans. Power Electron.* 6(1), 151-157 (1991).

[8] R.P. Severns, G.E. Bloom, Modern DC-to-DC Switchmode Power Converter Circuits. VanNostrand Reinhold, New York (1985).

[9] D.G. Luenberger. An introduction to observers. *IEEE Trans. Automatic Control*, 16(6):596Ű602, 1971.

[10] R. Engel and G. Kreisselmeier. A continuous-time observer which converges in finite time. *IEEE Trans. Automatic Control*, 47(7):1202-1204, 2002.

[11] A.J. Krener and A. Isidori. Linearization by output injection and nonlinear observers. Systems and Control Letters, 3(1):47-52, 1983.

[12] A.J. Krener and W. Respondek. Nonlinear observers with linearizable error dynamics. SIAM J. Control and Optimization, 23(2):197-216, 1985.

[13] J. Tsinias. Further results on the observer design problem. Systems and Control Letters, 14(5):411-418, 1990.

[14] J.-P. Gauthier, H. Hammouri, and S. Othman. A simple observer for nonlinear systems applications to bioreactors. *IEEE Trans. Automatic Control*, 37(6):875-880, 1992.

[15] J.-P. Gauthier and I. Kupka. Deterministic Observation Theory and Applications. Cambridge University Press, 2001.

[16] J.-P. Gauthier and I.A.K. Kupka. Observability and observers for nonlinear systems. SIAM J. Control and Optimization, 32(4):975-994, 1994.

[17] G. Ciccarella, M. Dalla Mora, and A. Germani. A Luenberger-like observer for nonlinear systems. Int. J. Control, 57(3):537-556, 1993.

[18] N. Kazantzis and C. Kravaris. Nonlinear observer design using LyapunovŠs auxiliary theorem. Systems and Control Letters, 34(5):241-247, 1998.

[19] D.G. Luenberger. Observing the state of a linear system. *IEEE Trans. Military Electronics*, 8:74-80, 1964.

[20] D.G. Luenberger. An introduction to observers. *IEEE Trans. Automatic Control*, 16(6):596-602, 1971.

[21] R.W. Erikson and D. Maksimovic, *Fundamentals of Power Electronics*, Second Edition, Kluwer Academic Publishers.

[22] D. Liberzon,*Switching in Systems and Control*, System and Control: Foundations and Applications,Birkhauser, 2003.

[23] S. Cuk and R.D. Middlebrook, A General Unified Approach to Modelling Switching DC to DC Converters in Discontinous Conduction Mode. *PESC 76*, Rec, 1976.

[24] M. Mohr, W. T. Franke, B. Witting, F.W. Fuchs (2010), Converter Systems for Fuel Cells in the Medium Power Range - A Comparative Study. *IEEE Transactions on Industrial Electronics, 57*, 2010, pp. 2024-2032.

[25] A. Goebel, R. Sanfelice and A. Teel, Hybrid Dynamical Systems. *IEEE Control Systems Magazine*, April 2009, pp. 28-93.

[26] J. Sun, D. M. Mitchell, F. Greuel, P. T. Krein, and R. M. Bass (2009). Averaged Modeling of PWM Converters Operating in Discontinuous Conduction Mode. *IEEE Transactions on Power Electronics*, Vol. 16, No. 4, 2001, pp. 482-492.

[27] C. Qiao and J. Zhang, Control of boost type converter at discontinuous conduction mode by controlling the product of inductor voltage-second, in *Proc. IEEE PESC*, Brazil, Sep. 2005, pp. 1213-1219.

[28] P. Gupta, A. Patra, Hybrid mode-switched control of dc-dc boost converter circuits. *IEEE Transactions on Circuits and Systems*, vol. 52, no 11, november 2005.

[29] Y.B. Shtessel, A.S.Zinober and I.Shkolnikov, Boost and Buck-boost power converters control via sliding modes using dynamic sliding manifold, *IEEE conference on decision and control*, Las Vegas, Nevada USA, 2002, pp 2456-2461.

[30] M. Fadel and A. Llor. Fixed frequency sliding mode control for boost converter. *EPE-PEMC*, pages 957-960, Portoroz, 2006.

[31] S. C. Tan, Y. M. Lai, and C. K. Tse. A unified approach to the design of PWM-based sliding-mode voltage controllers for basic DC-DC converters in continuous conduction mode. *IEEE Transactions on Circuits and Systems*, 53(8) :1816-1827, 2006.

[32] J. Mahdavi, A. Emaadi, and H. A. Toliyat. Application of state space averaging method to sliding mode control of pwm dcdc converters. *IEEE Industry Applications Society Annual Mee- ting*, pages 820-827, New Orleans, Louisiana, USA, 1997.

[33] R. Venkataramanan, A. Sabonovic, and S.Cuk. Sliding mode control od dc-dc converters. *Proc. IEEE IECON*, 1985, pp 251-258.

[34] H. Sira Ramirez and R. Ortega. Passivity-based controllers for the stabilization of DC-to-DC power converters. In Conference on Decision and Control, pages 3471-3476, New Orleans, LA, USA, December 1995.

[35] Romeo Ortega, Antonio Loria, Per J Nicklasson, and Hebertt Sira-Ramirez. Passivity-based control of Euler-Lagrange systems. Mechanical, electrical and electromechanical applications. Springer-Verlag, 1998.

[36] H. Sira-Ramirez, R.A. Perez-Moreno, R. Ortega and M.Garcias-Esteban. Passivity-based controllers for the stabilization of dc-dc power converters, Automatica, vol. 33, no. 4, pp. 499-513, 1997.

[37] A. Astolfi, D. Karagiannis and R. Ortega, *Nonlinear and Adaptive Control with Applications*, Springer-Verlag, Berlin, Communications and Control Engineering, 2007.

[38] G. Escobar, A. J. van Der Schaft and R. Ortega, "A Hamiltonian viewpoint in the modeling of switching power converters", *Automatica*, Vol. 35, no. 189, pp. 445-452, 1999.

[39] M. Hernandez-Gomez, R. Ortega, F. Lamnabhi-Lagarrigue and G. Escobar, "Adaptive PI stabilization of switched power converters", *IEEE Trans.on Control Systems Technology*, Vol. 18, No. 3, pp. 688-698, 2010.

[40] A. Jaafar *et al.*, "Experimental validation with a control point of view analysis of the SEPIC converter," in *Proc. IEEE Industrial Electronics Society Conference*, Porto, Portugal, 2009, pp. 467-472.

[41] A. Jaafar *et al.*, "Passivity with Immersion and Invariance for Modelling, Control and Observation of High Order DC-DC Converters," *IET Control Theory and Applications Journal*, submitted for review.

[42] B. Jayawardhana, R. Ortega, E. Garcia-Canseco and F. Castaños, "Passivity of nonlinear incremental systems: Application to PI stabilization of nonlinear RLC circuits" *Systems and Control Letters,* Vol. 56, pp.618-622, 2007.

[43] J. Kassakian, M. Schlecht and G. Verghese, *Principles of Power Electronics*, Addison–Wesley, Reading, 1991.

[44] H. Khalil, *Nonlinear systems*, 3rd ed., Prentice Hall, Upper Saddle River, N.J, 2002.

[45] E. Panteley and A. Loria, "Growth rate conditions for stability of cascaded time-varying systems", *Automatica*, 2001, Vol. 37, No. 3, 453-460.

[46] S. Sanders and G. Verghese, "Lyapunov-based control for switched power converters", *IEEE Trans. Power Electronics.* vol. 7, No. 1, pp. 17-24, 1992.

[47] P. Seibert and R. Suarez, "Global stabilization of nonlinear cascaded systems", *Systems & Control Letters*, Vol. 14, pp. 347-352, 1990.

[48] E. D. Sontag, "A remark on the converging–input converging–output property", *IEEE Trans. Automatic Control*, Vol. 48, No. 2, pp. 313-314, Feb 2003.

[49] V. Vorperian, *Analysis of the SEPIC Converter*, 2006, Ridley Engineering Inc.